Synthesis of Transition Metal Aluminides from Elemental Powder Mixtures

Sina, Hossein

2015

HOSSEIN SINA

Synthesis of Transition Metal Aluminides from Elemental Powder Mixtures

Printed by Media-Tryck, Lund University 2015

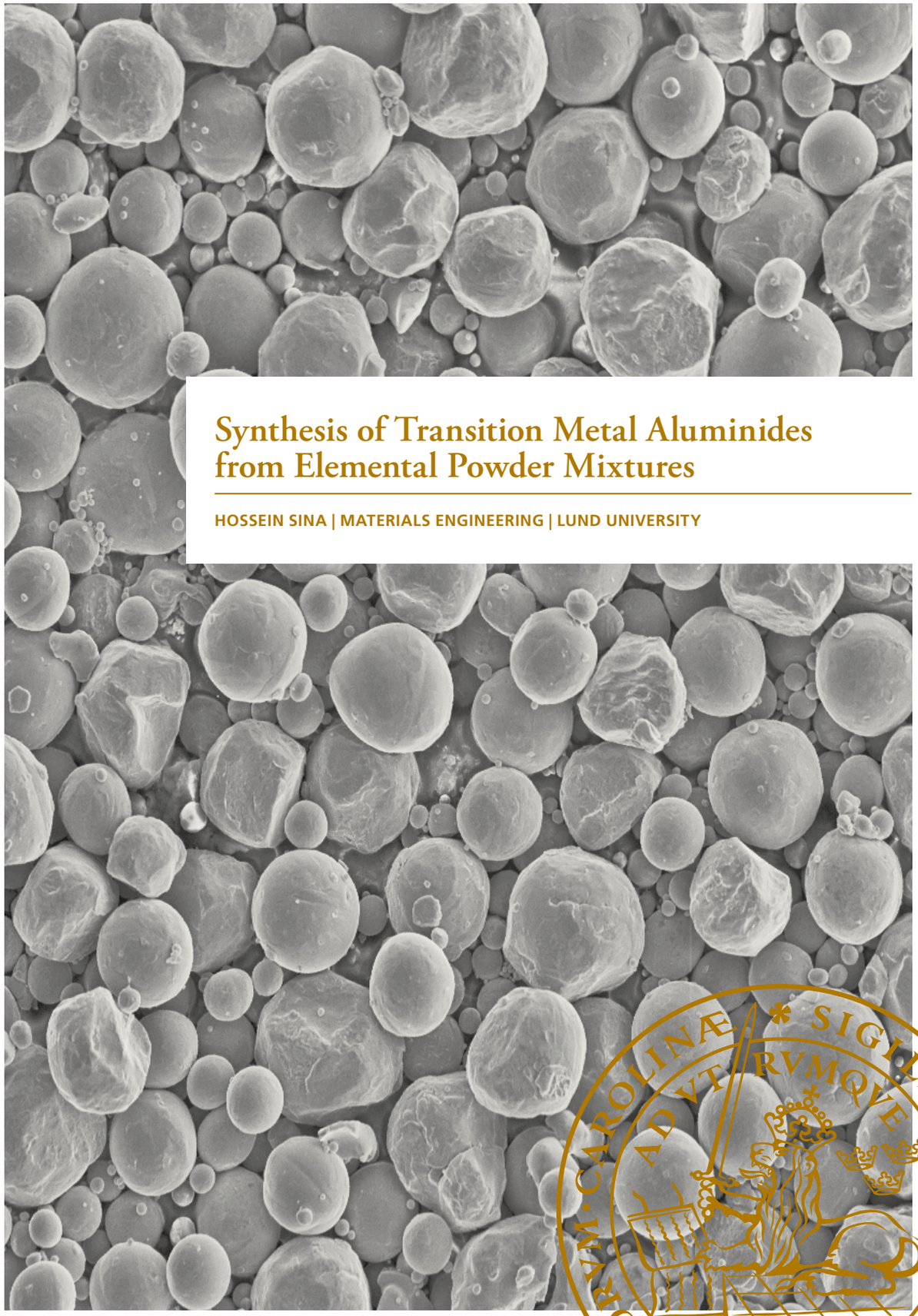

Synthesis of Transition Metal Aluminides from Elemental Powder Mixtures

HOSSEIN SINA | MATERIALS ENGINEERING | LUND UNIVERSITY

LUND UNIVERSITY
Faculty of Engineering
Division of Materials Engineering
ISBN 978-91-7623-470-9

Synthesis of Transition Metal Aluminides from Elemental Powder Mixtures

Hossein Sina

LUND
UNIVERSITY

DOCTORAL DISSERTATION

by due permission of the Faculty of Engineering, Lund University, Sweden
to be defended at lecture hall M:E (M-Building, LTH),
on 30 October 2015 at 13:00 hrs

Faculty opponent

Prof. Michael Gasik

Aalto University, Finland

Organization:
Division of Materials Engineering
Faculty of Engineering
LUND UNIVERSITY
P.O. Box 118
22100 Lund

Document name:
DOCTORAL DISSERTATION

Date of issue: October 2015

Author: Hossein Sina

Sponsoring organization

Title: Synthesis of Transition Metal Aluminides from Elemental Powder Mixtures

Abstract

Structural components such as those used in gas turbines for energy conversion applications, are subjected to high loads at elevated temperatures. In order to ensure that the components survive under these conditions for a sufficiently long time, it is imperative to select materials with good high temperature properties like strength and corrosion resistance. Such materials are usually alloys with a microstructure consisting of several phases where one or more phases have a strengthening effect. These phases are generally hard and are compounds formed from two or more metals. Current trends show an increasing interest in the use of such intermetallic compounds. The vast potential of intermetallic compounds like aluminides emerges from a combination of their attractive characteristics such as high melting point, high-temperature strength and excellent oxidation resistance. Transition metal aluminides fall into this category and the formation of these compounds from elemental powder mixtures is the focus of this thesis. Thermal effects (release and absorption of heat) have been studied during the heating of powder compacts containing aluminum and a transitional element (Ti, Fe, Nb and Ta), using a differential scanning calorimeter (DSC). The reaction behavior in samples containing two transitional elements (Ni and Ti), have also been studied. The effects of changes in sample composition, particle size and heating rate on the onset temperatures were investigated and the products obtained during various stages of reaction were characterized using scanning electron microscopy (SEM), energy dispersive spectroscopy (EDS) and X-ray diffraction (XRD).

The results from the present study show that high melting transition metal aluminides can be produced using the powder metallurgical route at relatively low temperatures. However, the synthesis of pure compounds requires careful control over critical process parameters like particle sizes of the reactants, composition, temperature and time. The knowledge obtained from studies on the evolution of phases in various powder mixtures is useful in optimizing process parameters. Studies on Al-Ni-Ti compacts have revealed the formation of ternary phases during reactive sintering, which have not been observed during conventional production.

Keywords: Aluminides, Intermetallics, Powder Metallurgy, Reactive Sintering, Combustion Synthesis, Thermal Analysis, DSC, Onset temperature, Phase evolution, SEM, EDS, XRD.

Classification system and/or index terms (if any)

Supplementary bibliographical information

Language: English

ISBN
978-91-7623-470-9 (print)
978-91-7623-471-6 (pdf)

ISSN and key title

Recipient's notes

Number of pages: 155

Price

Security classification

Signature H. Sina Date 2015/09/21

Synthesis of Transition Metal Aluminides from Elemental Powder Mixtures

Hossein Sina

DOCTORAL THESIS

2015

LUND UNIVERSITY

Division of Materials Engineering
Department of Mechanical Engineering
Sweden

Cover: Pure titanium powder with a maximum particle size of 45 microns.

Division of Materials Engineering
Department of Mechanical Engineering
Lund University, Sweden

ISBN 978-91-7623-470-9 (print)
ISBN 978-91-7623-471-6 (pdf)
ISRN LUTFD2/TFMT-15/1014-SE (1-71)

Printed in Sweden by Media-Tryck, Lund University
Lund 2015

Abstract

Structural components such as those used in gas turbines for energy conversion applications, are subjected to high loads at elevated temperatures. In order to ensure that the components survive under these conditions for a sufficiently long time, it is imperative to select materials with good high temperature properties like strength and corrosion resistance. Such materials are usually alloys with a microstructure consisting of several phases where one or more phases have a strengthening effect. These phases are generally hard and are compounds formed from two or more metals. Current trends show an increasing interest in the use of such intermetallic compounds. The vast potential of intermetallic compounds like aluminides emerges from a combination of their attractive characteristics such as high melting point, high-temperature strength and excellent oxidation resistance. Transition metal aluminides fall into this category and the formation of these compounds from elemental powder mixtures is the focus of this thesis.

This work presents differential scanning calorimeter (DSC) studies on the formation of aluminides in the Ti-Al, Fe-Al, Nb-Al, Ta-Al binary systems and extended to the ternary Al-Ni-Ti system. The synthesis of various aluminides was followed by heating the well-mixed powder mixtures to temperatures at which aluminide formation is initiated, accompanied by heat evolution. The effect of initial composition, particle size and heating rate on the onset temperatures was also studied. The products obtained during various stages of reaction were characterized using scanning electron microscopy (SEM), energy dispersive spectroscopy (EDS) and X-ray diffraction (XRD).

The results show that aluminide formation could be initiated at temperatures below the melting point of aluminum, only in the case of relatively low melting metals like iron and titanium. Onset temperatures for reactions involving niobium and tantalum were much higher and showed the importance of wetting the particle surfaces of niobium and tantalum by molten aluminum. In the Fe-Al system, with coarse iron particles, an exothermic peak was observed before the melting of aluminum, followed by a stronger peak at much higher temperatures.

In all cases, irrespective of the initial composition of the powder mixture, aluminides rich in aluminum were the first compounds to form at the onset of reaction. These compounds had the general formula MAl_3 where M represents Ti, Nb and Ta. However, the reaction between iron and aluminum particles led to the initial formation of Fe_2Al_5. In general, obtaining single phase, homogeneous products from Al-rich samples was relatively easier and did not require heating much beyond the combustion peak. A single phase product was also yielded in Fe-40 at.%Al powder compacts with fine-sized iron particles after heating to 1000°C.

A sharper reaction peak and lower onset temperatures were obtained on decreasing the aluminum content in the mixture or the particle size of the transitional element. The onset temperatures for reaction showed a tendency to increase with increasing heating rates. Multiphase, heterogeneous products were obtained at 1000°C in samples containing lower aluminum contents or those with coarse iron particles. It was relatively more difficult to homogenize multiphase products in the Ta-Al system than the rest and the easiest in the Fe-Al system. The evolution of phases during the heat treatment of the samples was followed using microstructural and X-ray diffraction studies.

Extending the studies to a ternary system, the progress of reaction in a compacted powder mixture containing two aluminide forming metals like nickel and titanium was followed using DSC. The effect of composition was studied by varying the aluminum addition (0 to 40 at.%) to nickel and titanium powders in equal proportions. The powder compacts were heated at 20°C min^{-1} up to 1200°C, in a continuous stream of pure and dry argon gas. Two main exothermic peaks were observed and for all the samples studied, the first exothermic peak was in the interval 595°-625°C. The heat release increased with increase in the aluminum content of the samples. At this stage, microstructural studies showed that Al_3Ni and Al_3Ni_2 were the major constituent phases and only a thin layer of Al_3Ti was observed around the titanium powder particles, indicating a diffusional barrier. The second exothermic peak was observed in the interval 938°-946°C which corresponds to the reaction between nickel and titanium. Titanium-rich and nickel-rich ternary compounds, in addition to some binary compounds, have been observed after this reaction in all aluminum containing samples. The formation of $AlNi_2Ti$ (τ_4) phase together with some new ternary compounds was observed in most of the Al-Ni-Ti samples after heating to 1200°C. The compositions of two of these phases, unidentified and not reported in literature so far, are close to $Al_2Ni_3Ti_5$ and $Al_{36}Ni_{28}Ti_{36}$.

The present work has shown that while transition metal aluminides can be produced through the powder metallurgy route, the synthesis of pure compounds requires careful control over critical process parameters like particle sizes of the reactants, initial composition of the powder mixture, heating temperature and time. The reactive sintering process can be optimized using the knowledge obtained from studies on the evolution of phases in various powder mixtures.

Keywords: Aluminides, Intermetallics, Powder Metallurgy, Reactive Sintering, Combustion Synthesis, Thermal Analysis, DSC, Onset temperature, Phase evolution, SEM, EDS, XRD.

Acknowledgements

This work has been carried out with financial support from the Eramus Mundus Program and the Division of Materials Engineering at Lund University, which is gratefully acknowledged. During my doctoral study, many people have supported me in different ways. First and foremost, I would like to express my gratitude to Prof. Srinivasan Iyengar who has been a great supervisor for me all these years. During our frequent discussions, I have enormously benefited from his broad knowledge and experience in the field of materials science and engineering. He was carefully tracking my progress, and I appreciate the enthusiasm and the inspiring guidance he showed throughout my study. Without his continuous support and motivation, this work would not have been accomplished.

I am also very thankful to my co-supervisor, Prof. Solveig Melin, for her valuable support and help during my study. Particular thanks go to Dr. Kumar Babu Surreddi who was not only a good friend but also a knowledgeable advisor for me. He supported me when I needed it most, especially while working on the ternary paper.

I am very grateful to Prof. Sven Lidin, Head of the Chemistry Department, for giving me access to the X-ray diffractometer, and also for his valuable time in discussing XRD data.

I appreciate all the help given by my colleagues and the staff at the department. In particular, I would like to thank Zivorad Zivkovic and Rose-Marie Hermansson for their technical and administrative assistance, respectively. I am very happy for having had very good times with my nice friends who created a pleasant working atmosphere in the department, especially during our joyful coffee breaks.

I take the opportunity to thank my beloved family, particularly my dear parents to whom I owe my whole life and success. Although they were not physically beside me, but their endless emotional and spiritual support was with me all the times. I am also very thankful to my kind sister and my conscientious brother, who have taken care of the family during my absence. I greatly appreciate my parents-in-law for their continuous encouragement and kind support.

Last but by no means least, I deeply thank my wife, Maryam, who has generously dedicated her love for my achievements. She sacrificed her ongoing doctoral study in Singapore to join me here in Sweden. During these years, she provided me incredible support and patiently inspired me to manage all those tough situations along my work. I am glad that she managed to begin a new PhD program at Lund University and I wish her the very best.

List of Publications and Author's Contribution

This thesis is based on the following papers:

Paper I **H. Sina**, S. Iyengar, "Reactive synthesis and characterization of titanium aluminides produced from elemental powder mixtures", Journal of Thermal Analysis and Calorimetry, 2015, doi: 0.1007/s10973-015-4815-6.

Paper II **H. Sina**, J. Corneliusson, K. Turba, S. Iyengar, "A study on the formation of iron aluminide (FeAl) from elemental powders", Journal of Alloys and Compounds, Vol. 636, 2015, pp. 261-269.

Paper III **H. Sina**, S. Iyengar, "Studies on the formation of aluminides in heated Nb-Al powder mixtures", Journal of Alloys and Compounds, Vol. 628, 2015, pp. 9-19.

Paper IV **H. Sina**, S. Iyengar, S. Lidin, "Reaction behavior and evolution of phases during the sintering of Ta-Al powder mixtures", Journal of Alloys and Compounds, Vol. 654, 2016, pp. 103-111.

Paper V **H. Sina**, K. B. Surreddi, S. Iyengar "Phase evolution during the reactive sintering of Al-Ni-Ti powder compacts", submitted to Journal of Alloys and Compounds, August 2015.

In each and every one of the papers listed above, the author has made major contributions in planning and executing the experimental work, analysis of data and preparing the manuscript for publication.

Other publications

The papers prepared during the doctoral study and included in the Licentiate Thesis are given below.

- **H. Sina**, S. Iyengar, S. Melin, "Sintering and Reaction Behavior in Ni-Ti Powder Mixtures", Advances in Powder Metallurgy and Particulate Materials, Nashville, USA, 2012 (ISBN: 978-0-9853397-2-2).

- **H. Sina**, S. Iyengar, S. Melin, "Ignition Temperatures for Cu-Al and Ni-Al Reactions in Elemental Powder Mixtures Using Differential Scanning calorimetry", Advances in Powder Metallurgy and Particulate Materials, Nashville, USA, 2012 (ISBN: 978-0-9853397-2-2).

List of Abbreviations

BSE	Back-Scattered Electrons
DSC	Differential Scanning Calorimetry
DTA	Differential Thermal Analysis
EDS	Energy Dispersive X-ray Spectroscopy
ESEM	Environmental Scanning Electron Microscope
P/M	Powder Metallurgy
PSD	Particle Size Distribution
SE	Secondary Electrons
SEM	Scanning Electron Microscope
SHS	Self-propagating High-temperature Synthesis
SMA	Shape Memory Alloy
TE	Thermal Explosion
TGA	Thermo-Gravimetric Analysis
VAR	Vacuum Arc Remelting
VIM	Vacuum Induction Melting
WDS	Wave-length Dispersive X-ray Spectroscopy
XRD	X-ray Diffraction

Glossary

Powder
Small sized particles (<1mm).

Powder metallurgy
Production of metal powders and their use in fabricating massive components.

Powder mixtures
Mixtures of dissimilar powders.

Compaction
Application of pressure to shape, deform and densify powder mixtures in a die.

Sintering
A thermal process which increases the strength of a powder mixture by inter-particle bonding through diffusion and related events.

Reactive sintering
A novel sintering process where an exothermic reaction occurs in a mixture of different elemental powders resulting in compound formation.

Liquid phase sintering
Formation of a liquid phase during sintering, which enhances the process kinetics.

Combustion reaction
The strong and rapid exothermic reaction which occurs between the reactant particles (solid-solid or solid-liquid) when a powder mixture is heated.

Combustion synthesis
Synthesis of products (compounds) where the combustion reaction plays a major role.

Pre-combustion reaction
A solid-state reaction which occurs between the elemental particles prior to the initiation of combustion in the sample.

SHS

A technique which keeps the process self-sustaining by utilizing the heat released by the combustion reaction between dissimilar powders. The reaction wave propagates continuously after ignition.

Thermal explosion

Heating of premixed powders to temperatures at which all the reactant particles in the powder mixture can react with each other at the same time.

Ignition temperature

A temperature above which the combustion reaction can occur in a powder mixture.

Onset temperature

A temperature corresponding to the initiation of the combustion reaction. This is usually determined as the intersection point of the tangent drawn at the leading edge of the combustion peak with the extrapolated base line of the DSC curve.

Phase evolution

Formation of various phases in the sample, at different stages of heating.

Surface coverage

The extent of contact between the reactant particles in a powder mixture.

Swelling

Increase in compact dimensions due to pore formation and /or volume expansion due to phase transformation.

Differential Thermal Analysis

Measurement of temperature and temperature difference between the sample and a reference material during heating.

Differential Scanning Calorimetry

Measurement of heat flow into or out of a sample.

Thermogravimetry

Measurement of mass changes during heating.

List of Figures

Fig. 1. Ti-Al phase diagram 5
Fig. 2. Fe-Al phase diagram 7
Fig. 3. Nb-Al phase diagram 9
Fig. 4. Al-Ta phase diagram 11
Fig. 5. Al-Ni-Ti isothermal section at 900°C 13
Fig. 6. DSC plot for the Ti-50at.%Al sample heated to 1000°C at 15°C min^{-1} 20
Fig. 7. SEM images of Ti-50at.%Al samples heated to selected temperatures at 15°C min^{-1} 21
Fig. 8. Diffractograms of Ti-50at.%Al samples heated to different temperature at 15°C min^{-1} 22
Fig. 9. DSC plot of the Fe-40at.% Al sample heated to 1000°C at 7.5°C min^{-1} 23
Fig. 10. SEM images of Fe-40at.% Al samples heated to selected temperatures at 15°C min^{-1} 24
Fig. 11. DSC plot of the Nb-33.3at.%Al sample heated to 1000°C at 7.5°C min^{-1} 26
Fig. 12. SEM images of Nb-33.3at.%Al samples heated to different temperatures at 15°C min^{-1} 27
Fig. 13. Diffractograms of Nb-33.3at.%Al samples heated to different temperatures at 15°C min^{-1} 28
Fig. 14. DSC plot of the Ta-50at.%Al sample heated to 1200°C at 15°C min^{-1} 29
Fig. 15. SEM images of Ta-50at.%Al samples heated to different temperatures at 15°C min^{-1} 30
Fig. 16. Diffractograms of Ta-50at.%Al samples heated to different temperatures at 15°C min^{-1} 31
Fig. 17. SEM images of unreacted Nb-33.3at.%Al samples with different aluminum particle sizes 33
Fig. 18. DSC peaks observed during the combustion reaction in Ta-75at.%Al samples at different heating rates 34
Fig. 19. Starink isoconversion plots for the determination of apparent activation energy of the combustion reaction in Ta-75at.%Al samples 34
Fig. 20. DSC plot of the Ni-50at.%Ti sample heated to 1200°C at 20°C min^{-1} 36
Fig. 21. SEM images of Ni-50at.%Ti samples heated to 1050° and 1200°C at 20°C min^{-1} 37
Fig. 22. DSC plot of the 25AlNiTi sample heated to 1200°C at 20°C min^{-1} 38
Fig. 23. SEM images of 25AlNiTi samples heated to 1050° and 1200°C at 20°C min^{-1} 39
Fig. 24. Diffractograms of 25AlNiTi samples heated to 1050° and 1200°C 20°C min^{-1} 40
Fig. 25. DSC plots of Al-Ni-Ti samples heated to 1200°C 41
Fig. 26. SEM images of Al-Ni-Ti samples (Ni:Ti =1) heated to 1200°C at 20°C min^{-1} 42
Fig. 27. Various phase compositions identified in the Al-Ni-Ti samples heated to 1200°C 44

List of Tables

Table 1. Metal powders used in the present work 15
Table 2. Process parameters studied in the present work 16
Table 3. Chemical compositions of various regions marked in Fig. 26 43

Contents

Abstract i
Acknowledgements iii
List of Publications and Author's Contribution v
List of Abbreviations vi
Glossary vii
List of Figures ix
List of Tables x
1. Introduction 1
1.1 Transition metal aluminides 2
1.2 Methods of synthesis 2
1.3 Objectives of the present work 4
1.4 Literature survey on chosen systems 4
1.4.1 Ti-Al 4
1.4.2 Fe-Al 6
1.4.3 Nb-Al 9
1.4.4 Ta-Al 10
1.4.5 Al-Ni-Ti 12
2. Materials and Methods 15
2.1 Differential Scanning Calorimetry (DSC) 16
2.2 Microstructural Characterization 17
2.3 X-ray Diffraction (XRD) 18
3. Results and Discussion 19
3.1 Transition metal-aluminum binary systems 19
3.1.1 Ti-Al 20
3.1.2 Fe-Al 23
3.1.3 Nb-Al 26
3.1.4 Ta-Al 29
3.1.5 Effect of process variables on reaction behavior 32
3.2 Al-Ni-Ti ternary system 35
3.2.1 Ni-Ti samples 35
3.2.2 25AlNiTi samples 37
4. Conclusions 47
References 49
Appended Papers (I-V)

1. Introduction

During the last few decades, the growing demand for finding suitable materials for high temperature applications has led to a strong interest in developing various compounds which form a distinct group of materials known as intermetallics. These compounds consist of two or more metals, but exhibit non-metallic behavior. Their mechanical properties are similar to those for ceramic compounds, and are usually very hard, stiff and brittle, particularly at ambient temperatures. They are typically characterized by a phase with its own composition, crystal structure and properties, different from those of the constituent metals [1]. They exhibit a unique combination of scientifically interesting and technologically important properties, with a wide range of applications from structural components in aircrafts to biomedical implants in the human body [2–8]. Their properties are strongly influenced by the nature of atomic bonding [9] and they are usually classified into different groups based on whether the dominant atomic bonding is ionic, covalent or metallic, or a combination of different types [10].

Most ionic and covalent compounds show high levels of ordering and are associated with large exothermic heats of formation, indicating their high stability. Ordered crystal structures usually show a tendency to disorder above a critical temperature, generally referred to as the critical ordering temperature (T_c). In a disordered structure, the constituent atoms occupy the lattice positions randomly. The stability of an ordered intermetallic compound is an important factor for high-temperature applications. The free energy of formation of an intermetallic compound is a good indicator of the stability of the compound and this is closely related to the nature of bonding.

Most ordered intermetallic compounds have low fracture toughness especially at ambient temperatures, making their fabrication difficult. However, alloying has been widely employed to overcome the brittleness problem in these compounds. Reports show that the ductility of polycrystalline Ni_3Al can be improved dramatically after microalloying with boron. Brittle intergranular fracture in the material is suppressed due to the segregation of boron at the grain boundaries. The success of achieving remarkably ductile, ordered intermetallic phases has inspired significant efforts aimed at the manufacture of monolithic components from such compounds [11].

1.1 Transition metal aluminides

Transition metal aluminides constitute a large group of intermetallic compounds which are of considerable interest due to their industrial importance. They possess a potentially attractive set of physical, chemical and mechanical properties. Many of these compounds exhibit ordered structures, and are very stable due to their strong atomic bonding. The vast potential of these materials emerges from their high melting points, good mechanical strength together with remarkable resistance to corrosion and oxidation at elevated temperatures. The continuous and adherent layer of alumina forming on the surface of aluminides protects them against corrosion. Therefore, they do not necessarily require chromium to enhance their corrosion resistance, making them more affordable as compared to most conventional steels and superalloys. Further, the protective alumina layer is thermodynamically more stable at high temperatures compared to chromium oxide [12]. Apart from this, they have lower densities relative to most of the structural alloys. They also show good chemical and thermal expansion compatibility with Al_2O_3-reinforcements, allowing the fabrication of composites with high specific-strengths [13,14].

1.2 Methods of synthesis

Intermetallic compounds can be produced through a variety of methods. However, processing and manufacturing of intermetallic compounds involve several difficulties. For example, there are limited possibilities for forming and shaping components from intermetallic compounds due to their low ductility. Intermetallic compounds such as transition metal aluminides are also difficult to cast due to the high temperatures required, high evaporation rate of aluminum as well as large differences in the melting points and densities of the constituent elements. For compounds showing a very

narrow homogeneity range, extra care must be taken to prepare the single-phase products through casting. Advanced melting techniques such as vacuum induction melting (VIM) and vacuum arc remelting (VAR) offer good control over product composition [12] and have been used to produce intermetallic compounds. However, in general, these methods have limited application due to their complexity, high cost and low productivity.

Among various other production methods, powder metallurgical techniques offer the possibility of near-net shape production, with relatively fewer limitations [7,15–17]. Most powder metallurgical routes for intermetallic compounds use pre-alloyed powders as starting materials. Although successful, these techniques involve some complex and expensive processes like hot consolidation, which are economically feasible only for a few special applications.

Reactive sintering or combustion synthesis is a technique, well-suited to produce intermetallic compounds from elemental powders. This technique has been recognized as a promising method to synthesize different groups of materials, including ceramics, intermetallic compounds and composites [18–23]. The main advantages of this process include savings in time and energy, simplicity and the possibility of obtaining a variety of products ranging from highly porous to densified materials. The method involves heating of a powder mixture to a temperature at which a combustion reaction (strongly exothermic) can be initiated. This results in the formation of intermetallic compounds as products. If the heat released during the reaction is large enough, the process can be self-sustaining. The onset temperature of the combustion reaction in most systems is considerably lower than the temperatures required for melting and casting. Besides the technological importance, reactive synthesis is of considerable scientific interest, due to the extremely fast reactions in the condensed state [18].

Reactive sintering can be classified into two types, self-propagating high-temperature synthesis (SHS) and thermal explosion (TE). In the self-propagating mode, the green compact is locally heated on one side by means of an external heating source like a heating coil or laser beam. This method generaly involves high heating rates, resulting in a combustion reaction which can propagate throughout the sample. In the thermal explosion mode, the sample is heated in a furnace at a relatively slower heating rate, and the combustion reaction occurs in the whole powder mix at the same time.

In general, the products obtained through reactive synthesis are porous, making them unsuitable for structural applications. However, this could be beneficial in the manufacture of products such as filters, catalysts and medical implants [7,24,25].

Dense products can also be obtained through the application of pressure during sintering [26] and post-processing.

1.3 Objectives of the present work

In order to produce products with desired properties, it is essential to optimize parameters influencing reaction behavior during the synthesis. This is all the more important in processes like reactive synthesis involving high reaction rates at elevated temperatures. A large number of investigations on the reactive synthesis of intermetallic compounds like aluminides have been reported in literature. However, the systems studied are not yet fully characterized. For example, even in the case of systems like Fe-Al and Ti-Al which have been studied extensively, there are only a few studies on the influence of processing parameters such as particle sizes of the reactants, heating rate, composition of the powder mixture and also the evolution of phases at various stages of reaction. Work on the formation of aluminides of refractory transition metals is also limited and studies on the formation of ternary aluminides are very few. More work is needed in these areas to improve the understanding of reaction behavior in systems involving aluminum and transition metals. This is the motivation behind the present study on the formation of aluminides and other intermetallic compounds in binary systems involving Ti, Fe,Nb and Ta, as well as the ternary Al-Ni-Ti system.

1.4 Literature survey on chosen systems

In this section, a brief description is given for each system studied in the present work, followed by a general overview of the reactions occurring during high temperature processing of powder mixtures.

1.4.1 Ti-Al system

The low density of titanium aluminides together with their high melting points, good strength and corrosion resistance at elevated temperatures make them attractive materials for advanced applications in vehicles and aircrafts [27–30]. Despite limited fracture toughness, Ti_3Al and TiAl show good potential for enhanced performance at high temperatures. Because of slower diffusion rates than in conventional titanium alloys, titanium aluminides exhibit improved high temperature features such as

strength retention and creep resistance. Typical applications include light-weight structural airframes, compressor blades, rotors, and many other components in automobiles or aircrafts [11,31]. It may be noted that, in oxidizing atmospheres, titanium aluminides show a strong tendency to form TiO_2 rather than the protective Al_2O_3 at elevated temperatures, which needs to be considered in high-temperature applications [11].

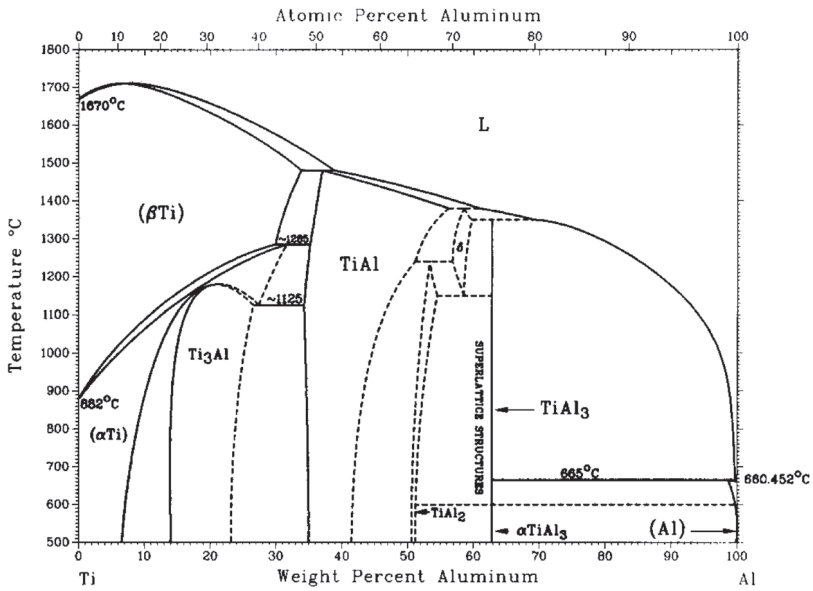

Fig. 1. Ti-Al phase diagram [32a]*.

Fig. 1 shows the Ti-Al binary phase diagram which is characterized by a number of stable intermetallic compounds such as Ti_3Al (α_2), TiAl (γ), $TiAl_2$ and $TiAl_3$ [32,33]. TiAl and Ti_3Al play a prominent role in strengthening titanium alloys for structural applications at elevated temperatures, and they are the most extensively studied phases among Ti-Al compounds and their alloys [34]. TiAl (γ) phase has a $L1_0$ face-centered tetragonal ordered structure with a relatively small *c/a* ratio, which tends towards fcc with a decrease in aluminum content [33,35]. This compound has a high melting point (1460°C), and exhibits high elastic modulus and good structural stability. These properties primarily originate from the strong bonding which retains the ordered

structure up to temperatures close to the melting point [11,36,37]. As compared to conventional titanium alloys, TiAl has a lower density and better corrosion resistance due to the higher aluminum content.

Ti_3Al (α_2) exhibits a $D0_{19}$ hexagonal ordered structure and a wide range of compositional stability (22-39 at.% Al). The compound, with an aluminum content of 32 at.%, is congruently transformed to α-phase at a temperature of 1180°C, while the stoichiometric composition (25 at.% Al) is stable up to about 1090°C [11,38]. $TiAl_3$ phase has a relatively simple crystal structure ($D0_{22}$ tetragonal). This compound is brittle, but otherwise attractive as a high-temperature material due to its low density, relatively high melting point (1340°C) and good oxidation resistance [34].

Titanium aluminides can be produced using reactive synthesis, through both propagating as well as thermal explosion modes. However, due to the relatively low exothermicity of the reactions involved [39], the thermal explosion mode is more suitable, particularly for industrial applications [27].

Previous studies [38–42] have shown that the combustion reaction occurs between aluminum melt and titanium particles, which results in the formation of $TiAl_3$ as the major product. However, pre-combustion products were also observed to form through solid-state diffusion reactions [43]. During the ignition process, inter-diffusion of the reactant species through the product layer ($TiAl_3$) is generally considered to be the rate-determining step [44,45]. It has been reported that mechanical activation of the powder mixture and relatively fine titanium powder can enhance the combustion reaction [39,41]. Higher heating rates were also observed to increase the density of the end product [38,41].

The formation of a dominant and single-phase $TiAl_3$ product was also observed in Ti-Al diffusion couples [46–51]. This observation was mainly attributed to the higher diffusivity of aluminum ions in $TiAl_3$ in comparison with other aluminides, which in any case may be formed in small amounts [50]. The growth of $TiAl_3$ layer on the titanium side of the diffusion couple, together with the movement of markers proved that aluminum is the dominant diffusing specie [44,48,49,52–54]. However, diffusion of titanium has also been reported as significant by some workers [55,56].

1.4.2 Fe-Al system

Iron aluminides, particularly Fe_3Al and FeAl, possess excellent resistance to oxidation and sulfidation at high temperatures. The corrosion rates of iron aluminides in oxidizing environments have been found to be lower than those observed for

chromia-forming commercial alloys [57]. Iron aluminides are also associated with higher specific strength and stiffness than many other structural materials like stainless steels and superalloys [12,58]. These characteristics make them suitable materials for high-temperatures applications in corrosive environments [12,59,60]. However, they exhibit poor ductility and environmental embrittlement at ambient temperatures. This is attributed to the interaction of aluminum with water vapor in the atmosphere [12].

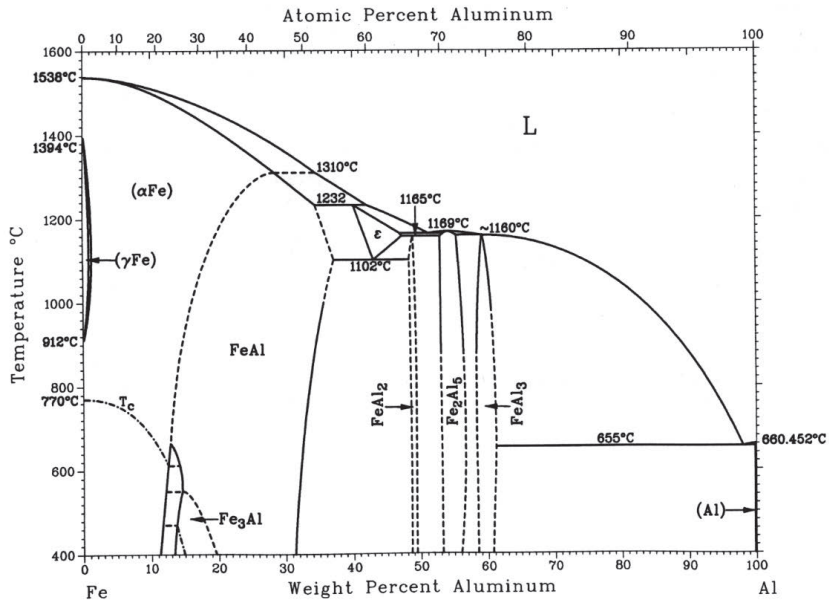

Fig. 2. Fe-Al phase diagram [32b] *.

Fig. 2 shows the binary phase diagram for the Fe-Al system which contains several intermetallic compounds. The phase Fe_3Al has a $D0_3$ crystal structure and is stable within the composition range 23-36 at.% Al. The region of stability of Fe_3Al decreases with increase in temperature, after a maximum of 26.8 at.% Al at 550°C [32,58]. Above 550°C, it transforms to an imperfectly ordered B2 structure, which ultimately changes to a disordered solid solution α-Fe. The phase FeAl exhibits a B2-type crystal structure within a composition range of 35-50 at.% Al, while it transforms to α-Fe at temperatures above 1100°C [12]. Both B2 and $D0_3$ structures are perfectly ordered only if they have stoichiometric compositions [58]. The high magnetic permeability

* Reprinted with permission of ASM International. All rights reserved. www.asminternational.org

of Fe_3Al is beneficial for soft magnetic applications. Relative to Fe_3Al, FeAl has a lower density and a better oxidation resistance, which is due to higher aluminum content [61]. Additionally, it exhibits relatively high electrical resistivity which allows it to serve as a heating element [62,63].

Iron aluminides have been produced by various processing techniques such as melting and casting [62,64], as well as mechanical alloying [65–67]. Powder metallurgical processes are attracting increasing interest, in particular reactive sintering which offers several advantages like better microstructural control, low cost, and near-net-shape production.

Several studies have been carried out on the reactive synthesis of iron aluminides, showing the formation of aluminides during different stages of heating. Aluminum-rich compounds like Fe_2Al_5 have been found to form initially as the product of solid-state reactions. This is followed by a combustion reaction at higher temperatures resulting in the formation of some other compounds like FeAl [63,68,69]. The formation of intermetallic phases has also been reported in Fe-Al diffusion couples, where aluminide formation is more significant at the grain boundaries in iron, highlighting the diffusion of aluminum into iron grains [70]. Although thermodynamic data indicate the formation of $FeAl_3$ before Fe_2Al_5, in general, Fe_2Al_5 forms as the major phase at the interface between elemental particles due to kinetic factors [71–73]. It may also be noted that the growth parameter is much larger for Fe_2Al_5 relative to FeAl [72,74,75].

The reactive sintering of Fe-Al powder mixtures is associated with an extensive volume expansion in the sintered products, mainly due to the formation of Fe_2Al_5 phase [63,76]. This has been attributed to the large solubility of aluminum in iron, large differences in melting points and diffusion rates of the reactants [69,77,78]. In general, pore evolution can occur during various stages, including the initial compaction of the sample, solid-state reactions, the combustion reaction between aluminum melt and iron particles, and phase transformations at higher temperatures [68]. The rapid release of heat due to exothermic reactions occurring simultaneously within the material is also believed to cause large thermal expansions [76]. The amount of swelling depends on various processing parameters such as the powder mixture composition, particle sizes of the reactants and the heating rate. Generally, lower aluminum contents, smaller particle sizes and higher heating rates minimize porosity [26,78,79]. Further, highly densified products of FeAl and Fe_3Al can be obtained through pressure-assisted synthesis [26,63].

1.4.3 Nb-Al system

Niobium aluminides have been considered as structural materials which can be used beyond the service temperature of the conventional high-temperature alloys. Niobium aluminides are preferred over many refractory metal compounds because of their low densities, high melting points, high elastic modulus and excellent oxidation resistance [20,21]. Fig. 3 shows three intermetallic compounds, namely Nb_3Al, Nb_2Al and $NbAl_3$, in the Nb-Al binary phase diagram [32]. Nb_3Al and Nb_2Al phases are stable over a broad composition range, but $NbAl_3$ is stable over a small range around the stoichiometric composition.

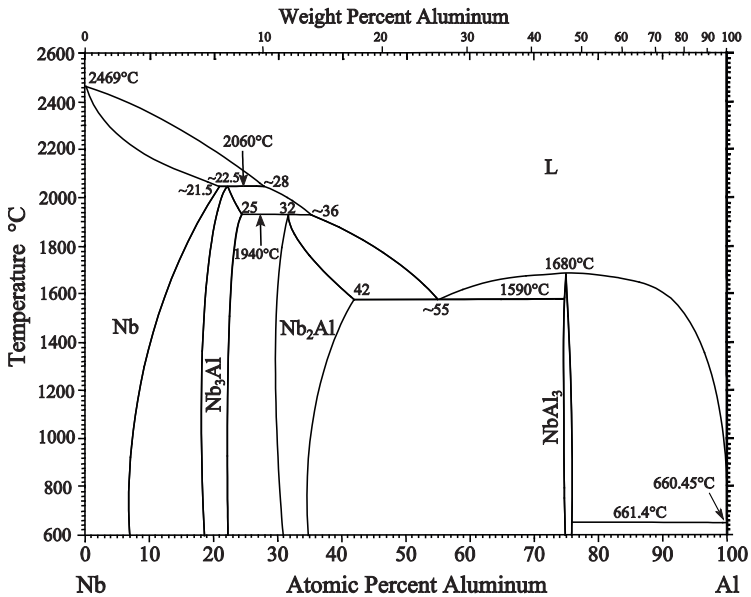

Fig. 3. Nb-Al phase diagram [32c] [*].

Nb_3Al and Nb_2Al have A15 and σ-type close packed ordered structures which decompose peritectically at 1940° and 2060°C, respectively [80,81]. Good creep resistance and superconductivity are exhibited by Niobium-rich compounds in general and Nb_3Al in particular. This makes them attractive for use in high-field and large-scale magnetic applications such as nuclear fusion reactors and high-energy particle accelerators [82,83]. The complex A15 crystal structure of Nb_3Al is responsible for its high temperature strength, and also the extreme susceptibility to

[*] Reprinted with permission of ASM International. All rights reserved. www.asminternational.org

brittle fracture at room temperature. However, the ductility and fracture toughness of Nb_3Al at room temperature can be improved by introducing a ductile niobium-rich solid-solution phase in the microstructure [21]. $NbAl_3$ has a face-centered tetragonal $D0_{22}$ ordered crystal structure with attractive properties. These include a relatively low density (4.54 g cm^{-3}), a high melting point (1680°C), good chemical and thermal expansion compatibility with alumina-fibers, enabling the fabrication of light-weight and creep-resistant composites. Moreover, $NbAl_3$ exhibits good resistance to sulfidation and oxidation at high temperatures, which is due to the formation of protective niobium sulfide and alumina scales, respectively [13].

The combustion reaction in the Nb-Al system has been reported to occur at temperatures considerably above the melting point of aluminum [81,84–86]. This observation differs from the general understanding that melt formation during the heating of powder mixtures triggers the combustion reaction due to enhanced contact between the reactants. Surface oxidation and poor wettability of niobium particles and the low solubility of niobium in liquid aluminum are the reasons attributed to this behavior [81,86,87]. However, an increase in temperature has been observed to increase the solubility of niobium in liquid aluminum [84]. When the aluminum melt is saturated with niobium, formation of aluminides is initiated through precipitation on the surfaces of niobium particles [81,85,86]. $NbAl_3$ has been confirmed as the first phase to form during the reaction of niobium with solid as well as liquid aluminum [46,84–89]. It has been suggested that the diffusion of aluminum is the dominant mechanism in the formation of aluminides, resulting in aluminum-rich compounds [90]. Mechanical activation of the powder particles has also been observed to decrease the ignition time and temperature significantly [13,85,88]. The particle size of niobium has a direct influence on ignition temperature as well as the grain size of the product. Nanostructured $NbAl_3$ has been obtained by heating a heavily milled Nb+3Al powder mixture [85].

1.4.4 Ta-Al system

Tantalum aluminides show good potential for high-temperature structural applications due to their high melting points and excellent resistance to corrosion and oxidation at elevated temperatures [4,91,92]. Of these compounds, Al_3Ta is an almost stoichiometric (24-25at.%Ta) phase [91,93,94] with a tetragonal $D0_{22}$ crystal structure and melts incongruently at 1541°C, as shown in the phase diagram (Fig. 4). In addition to Al_3Ta, a non-stoichiometric σ-phase has also been identified in the Al-Ta system [91,93–97]. According to a recent study [97], the σ-phase is stable over a composition range of 65-81 at.%Ta [94]. This phase has a topologically close packed

structure with a tetragonal unit cell [95,97], and has been mainly designated as $AlTa_2$ [91,93–96,98]. However, deviations in phase composition and stability range for this phase have been noted in some studies [95,96,98].

As seen in the Al-Ta phase diagram (Fig. 4), the σ-phase is in equilibrium with phase φ which is stable, close to the equiatomic composition (52.2 to 57.3 at.% Ta) [94]. In some references, this phase has been designated as AlTa [95,98,99] and is considered to be a line compound at lower temperatures [97]. It has been suggested that phase φ has a complex monoclinic unit cell representing a topologically close-packed structure [95].

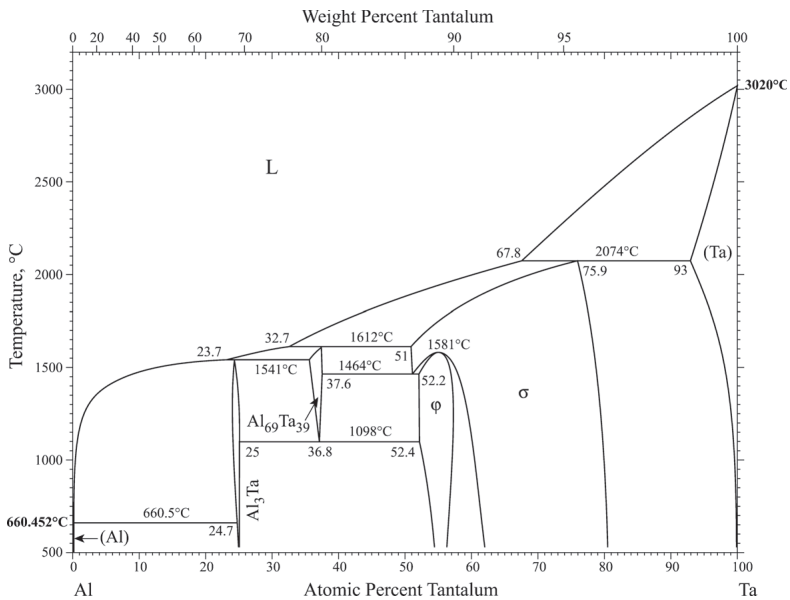

Fig. 4. Al-Ta phase diagram [94]*.

According to the Al-Ta phase diagram, the σ phase decomposes to φ (AlTa) and an intermediate phase which was initially reported as Al_3Ta_2 or Al_2Ta [97,98]. However, further studies [100] revealed that this intermediate phase corresponds to $Al_{69}Ta_{39}$ compound, exhibiting a face centered cubic structure, with a giant unit cell. The eutectoid transformation at 1098°C [97] leads to the decomposition of $Al_{69}Ta_{39}$ phase into φ and Al_3Ta phases.

Several researchers [46,50,51] have studied the formation of tantalum aluminides through reactions proceeding through solid-state diffusion. In these experiments, Al_3Ta was observed to form as the first phase at temperatures below the melting point of aluminum [46,50,51]. A non-parabolic growth has been reported for the Al_3Ta compound, which has been attributed to the selective penetration of diffusing species through the grain boundaries [50]. It has been suggested that high melting compounds like Al_3Ta exhibit parabolic growth during annealing [50] and a lower lattice diffusivity compared to those with relatively lower melting points. Thermal stabilities of tantalum aluminides have also been found to increase with tantalum content [101].

Tantalum aluminides have been prepared using combustion synthesis. However, studies on the synthesis of these compounds from elemental powder mixtures are very limited. Thermite-based combustion synthesis [102] has been used to produce various tantalum aluminides from tantalum oxide (Ta_2O_5) and aluminum powder mixtures. Alumina-tantalum carbide composites have also been synthesized using a thermite-based combustion process [22]. Similar to the Nb-Al system, the formation of aluminides through the reaction between tantalum particles and aluminum melt initiates at temperatures well above the melting point of aluminum. At these temperatures, the solubility of tantalum in molten aluminum increases [84], leading to the precipitation of an aluminum-rich product on tantalum particles.

1.4.5 Al-Ni-Ti system

Al-Ni-Ti system is characterized by several binary and ternary intermetallic compounds, which have been the subject of great interest due to their attractive physical and mechanical properties [103–109]. Of the binary compounds, nickel aluminides are known to strengthen structural alloys [109,110], titanium aluminides are corrosion-resistant at high temperatures [34,111], and nickel-titanium alloys are widely used as shape memory materials for functional applications [6,112,113]. Recent investigations [103,107,109,114–117] have confirmed the existence of five stable ternary intermetallic phases in the Al-Ni-Ti system. These ternary phases are designated as $Al_{13}Ni_2Ti_5$ (τ_1), Al_2TiNi (τ_2), Al_3NiTi_2 (τ_3), $AlNi_2Ti$ (τ_4) and $Al_{65}Ni_{20}Ti_{15}$ (τ_5). It has been reported that τ_1, τ_2 and τ_5 melt incongruently at 1347°C, 1225°C, and 1107°C, while τ_3 and τ_4 phases melt congruently at 1289°C and ~1500°C, respectively [104]. Fig. 5 shows an isothermal section of Al-Ni-Ti ternary phase diagram at 900°C [118] where several binary and ternary compounds coexist.

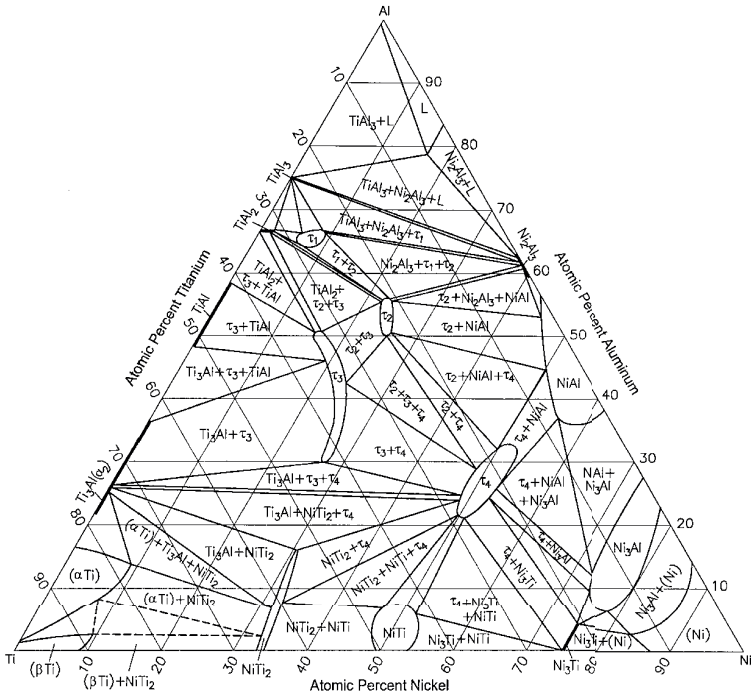

Fig. 5. Al-Ni-Ti isothermal section at 900 °C [118] [*].

Investigations concerning the reactive sintering of Al-Ni-Ti powder mixtures are very rare in literature. However, extensive work has been done on the related binary systems. In nickel-titanium powder mixtures, the combustion reaction initiates at temperatures close to eutectic melting at 942°C [119–122]. However, compounds including Ti_2Ni, NiTi and Ni_3Ti are reported to form due to solid-state reactions at lower temperatures [120,121]. NiTi exhibits the most promising shape memory behavior, while Ni_3Ti is suitable for high temperature applications [7,15,123]. It has been reported that the addition of aluminum to equiatomic Ni-Ti powder mixtures improves the hardness and corrosion resistance of the product, followed by a decrease in porosity [119]. However, in these studies, aluminum additions were limited to a maximum of 10 at.% [108,119,124].

Studies on reactive sintering of Al-Ni powder mixtures show the formation of several nickel aluminides during various stages of heating [110,125–127]. It has been

[*] Reprinted with permission of Springer Science + Business Media. All rights reserved. www.link.springer.com

reported that solid-state reactions between the elemental particles in the temperature interval 550° to 600°C, result in the formation of aluminum-rich compounds such as Al_3Ni and Al_3Ni_2 [110,128]. The combustion reaction occurs upon further heating to about 640°C, where eutectic melting is expected to occur, according to the Al-Ni phase diagram. In the Al-Ni system, NiAl and Al_3Ni are two important aluminides having the highest melting points. Ni_3Al is well known as the strengthening phase in nickel and nickel-iron based superalloys. Large heats of formation are associated with both Ni_3Al and NiAl phases, which show thermal stability due to their strong bonds and ordered structures [110,129,130]. It has been suggested that the addition of titanium to NiAl improves the creep strength due to a relatively large atomic mismatch as well as the precipitation of other intermetallic phases like $AlNi_2Ti$ [131]. It may be noted that Ni_3Al dissolves up to 15 at.% Ti and forms a non-equilibrium phase $Ni_3(Al,Ti)$ in which aluminum is partially replaced by titanium [109]. It is of scientific and industrial importance to study the reactive sintering and phase evolution in the Al-Ni-Ti ternary system in which various intermetallic compounds can form through mutual as well as combined interactions between aluminum, titanium and nickel.

2. Materials and Methods

Table 1 presents the details of the elemental powders used in this work. In each system, the metal powders were thoroughly mixed in proportions indicated in Table 2. Compacted discs (4 mm in diameter, ~1 mm in thickness) were prepared by uniaxially pressing the powder mixtures in a tool-steel die. In addition to the powder compacts, loose powder samples were also used in the present study. A set of calorimetric studies have been made using a differential scanning calorimeter (DSC), in which the samples were heated to temperatures where the combustion reaction could be initiated. The effect of various processing parameters including the initial composition of the sample, reactants particle size and heating rate on the onset temperature of the combustion reaction was studied in each system, as described in Table 2.

Table 1. Metal powders used in the present work

Powder [a]	Max. Particle size (μm)	Purity (%)
Aluminum (fine)	15	99.0
Aluminum (coarse)	60	99.9
Titanium	45	99.5
Iron (fine)	6-8[b]	>99.0
Iron (coarse)	60	>99.0
Nickel	45	99.5
Niobium	74	99.85
Tantalum (fine)	1-3[b]	99.9
Tantalum (coarse)	75	99.9

[a] Supplied by Goodfellow (UK), [b] Average.

Table 2. Process parameters studied in the present work

System	Particle size combination	Sample composition (Al at.%)	Heating rate (°C min^{-1})
Ti-Al	Ti Al (coarse)	25, 50, 75	7.5, 15
Fe-Al	Fe (fine, coarse) Al (fine, coarse)	40	7.5, 15
Nb-Al	Nb Al (fine, coarse)	25, 33.3, 75	7.5, 15
Ta-Al	Ta (fine, coarse) Al (fine, coarse)	33.3, 50, 75	7.5, 10, 15, 20, 30, 40
Al-Ni-Ti	Ni, Ti, Al (coarse)	0-40 (Ni:Ti=1)	20

2.1 Differential Scanning Calorimetry (DSC)

Differential scanning calorimetry (DSC), which allows the measurement of heat flow into or out of a sample while it is being heated, can be used to determine onset temperatures and enthalpies of the reactions and phase transformations. This can be done using the power-compensated approach or the heat flux method. In the power compensated method, the sample and reference are heated at a constant rate using two separate furnaces. The temperatures of the sample and the reference material are kept identical by regulating the power applied to one or both the furnaces. The amount of power required to maintain the same temperature is directly proportional to the thermal changes in the sample. A heat flux differential scanning calorimeter consists of a furnace to heat both the sample and the reference material, together with a set of thermocouples in contact with the sample and reference crucibles. This allows continuous monitoring of the temperature difference between them which generates the signal corresponding to the heat flow. The increase in temperature follows a linear trend during heating at a constant rate, until the sample undergoes a reaction or phase transformation which is associated with a thermal effect. This causes a difference in temperature between the sample and the reference which continues to show a linear increase in temperature. This results in an exothermic or endothermic peak in the DSC plot, representing a reaction during which heat is evolved or absorbed.

Calorimetric analysis can be integrated with thermogravimetry (TG) where both heat flow and mass changes in a sample can be measured as a function of temperature or time. In a simultaneous TG-DSC unit, the mass of the sample is continuously recorded. Such a heat-flux type instrument (Netzsch F3-Jupiter STA) with alumina

crucibles was used in this work to perform the calorimetric study. The DSC unit was calibrated for temperature (with an accuracy of ±0.1°C) and heat sensitivity using pure metal standards. Baseline correction was done using data from heating cycles with empty crucibles. In order to minimize the presence of air and avoid the oxidation of samples during heating, the DSC chamber was evacuated and flushed with pure argon gas at least three times prior to running the experiments and a constant flow of the gas (70 ml min^{-1}) was maintained during the measurements. The gas was dried by passing through towers containing drying agents like anhydrous calcium chloride and molecular sieve 4Å, before entering the DSC chamber. Thermogravimetric data was monitored carefully to check whether there was any mass change in the sample during heating. Netzsch Proteus software (version 6.1) was used to analyze DSC data.

2.2 Microstructural Characterization

Scanning electron microscopy is used extensively for high resolution imaging and characterization of microstructures in various types of materials. An electron microscope consists of an electron gun and a set of magnetic lenses assembled in an evacuated column. In general, the sample chamber is also highly evacuated, unless the microscope is designed to operate at low vacuum. An accelerated electron beam is produced at the top of the column, which passes through different apertures. This gives rise to a highly focused beam which impinges on the sample surface. The electron beam scans the surface in a raster pattern and its interaction with the specimen surface generates signals which are used to create an image of the sample surface. Secondary electrons have energies less than about 50 eV, and are the best source of high resolution images. Back-scattered electrons, with energies from 50 eV to the maximum acceleration voltage (for example, 30 kV), contribute to enhanced image contrast for large differences in atomic number between the constituent elements. Further, characteristic X-rays are emitted when high-energy electrons collide with the sample, which can be used to make quantitative analysis of the sample or phase composition. The intensity of the characteristic X-rays can be measured using either a wavelength-dispersive spectrometer (WDS), or an energy dispersive spectrometer (EDS).

In this study, heat treated samples were examined using a scanning electron microscope (Philips, XL-30 ESEM). Energy dispersive spectroscopy was used to analyze the phase compositions in the sample. For this purpose, a liquid nitrogen cooled Si(Li) detector (EDAX) was utilized. The detector had a super ultra-thin polymer window, providing a resolution of 127.4 eV (with reference to Mn-K_α). The

distribution of various elements in the microstructure was checked using X-ray mapping and line scanning. Quantification analysis was made using the Genesis software (version 5.21), based on ZAF correction and standardless calibration. The results from EDS analysis were verified at different accelerating voltages and spot sizes to minimize the effect of signals from adjacent areas. The consistency of these data was checked by numerous measurements.

2.3 X-ray Diffraction (XRD)

X-ray powder diffraction technique, which is probably the most widely-used phase characterization method, covers various investigations such as qualitative and quantitative phase analysis, determination of crystalline structures and lattice parameters. In general, this method employs monochromatic radiation (for example, Cu-K_α) to characterize the powder sample. A significant feature of the X-ray powder diffraction method is to provide general-purpose qualitative and quantitative information regarding crystalline phases present in an unknown mixture. The identification of phases is based on a comparison of the unknown pattern with the standard powder diffraction files collected in crystallographic databases, which may show a variation in d-spacing and intensities reported for a particular phase. In such cases, the accuracy of experimentally collected data used as the reference in the database needs to be carefully checked in order to perform an accurate analysis. The stability of the beam generator, X-ray tube and counting electronics is also important to obtain precise results. In this technique, peak broadening can occur in the diffraction pattern due to various reasons like the presence of very small sized crystallites, micro-stresses, and inhomogeneous solid solutions in the sample. This problem can be minimized by a mild annealing treatment of the sample prior to the measurement.

In the present study, X-ray powder diffraction analysis was made in order to confirm the phases formed during the experiments. A vertical Stoe Stadi MP machine was used, equipped with a Germanium monochromator (Johan geometry), a copper tube and a linear PSD as the detector with transition setup. Sintered specimens were crushed to get the samples in powder form. The instrument was calibrated using a standard sample of silicon. XRD results were analyzed using Pearson's crystallography database [132].

3. Results and Discussion

In this chapter, typical results from studies on reactions in binary aluminum-transition metal (Ti, Fe, Nb and Ta) powder compacts are presented first, followed by those for the ternary Al-Ni-Ti samples. A general discussion of the results is also included.

3.1 Transition metal-aluminum binary systems

DSC data for systems involving titanium and iron, which are relatively low melting transition metals, show that the combustion reaction can occur in the solid-state before aluminum starts melting. Further, aluminides were observed to form in these systems prior to the combustion reaction, indicating the importance of solid-state interdiffusion between the reactant elements. In Nb-Al and Ta-Al powder compacts, the combustion reaction occurred at temperatures well above the melting point of aluminum and the solid-state pre-combustion stage was not detected. In all the systems studied, the combustion reaction was observed to continue until the aluminum content was completely consumed in the sample through the reaction with the transition metal particles. This resulted in the formation of aluminum-rich compounds as products of the combustion reaction, regardless of the initial composition of the powder mixtures. The heated samples showed large expansions in volume after undergoing the combustion reaction which reached completion only in aluminum-rich samples, where a porous and single-phase product was yielded. Samples with relatively lower aluminum contents showed incomplete reactions, leaving behind a considerable amount of unreacted transition metal in each system. Upon further heating to higher temperatures, multiphase products were observed to

form through diffusional reactions between the aluminum-rich product and the residual transition metal. In these samples, relatively homogenized products were obtained after prolonged heating at elevated temperatures. The compound corresponding to the initial composition of the sample was the predominant phase in the homogenized product. In general, the onset temperature of the combustion reaction showed a tendency to increase with increasing heating rate. Increasing the particle size of the reactant powders also resulted in a higher onset temperature for the combustion reaction in most of the samples. The reaction behavior in Ti-50at.%Al, Fe-40at.%Al, Nb-33.3at.%Al and Ta-50at.%Al powder compacts is described in the following sections.

3.1.1 Ti-Al system

Fig. 6 presents the DSC plot obtained for the Ti-50at.%Al powder compacts heated to 1000°C at 15°C min^{-1}. Samples were prepared using titanium and aluminum powders with maximum particle sizes of 45 and 15 μm, respectively. In this plot, a relatively small exothermic peak (A) is observed prior to the aluminum melting peak (B), which suggests a mild pre-combustion stage during heating. The aluminum melting peak is immediately followed by a relatively large exotherm (C) which corresponds to the combustion reaction occurring between titanium particles and molten aluminum. The small endothermic peak (D) observed at ~882°C corresponds to the allotropic α→β transformation in titanium.

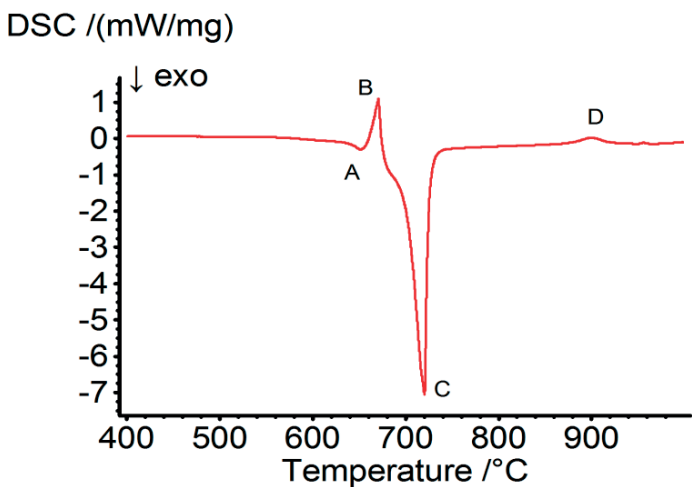

Fig. 6. DSC plot for the Ti-50at.%Al sample heated to 1000°C at 15°C min^{-1}.

In order to follow the phase evolution during reaction, a few samples were heated to carefully selected temperatures, and the corresponding micrographs are presented in Fig. 7. For the sample heated to 645°C (peak A) and then cooled to room temperature, the micrograph mainly shows the presence of unreacted elemental particles. However, a minor grey phase is also seen around the titanium particles. Using EDS analysis, this phase was identified as $TiAl_3$ which has formed through solid-state reaction during the pre-combustion stage. The formation of $TiAl_3$ phase is more pronounced after heating to 680°C where the combustion peak (C) initiates. In this micrograph, almost each titanium particle is surrounded by a thin layer of $TiAl_3$. At 730°C, where the combustion peak ends, $TiAl_3$ phase is seen to grow into the titanium cores while the elemental aluminum is fully consumed. At this stage, some large pores were observed at the regions initially covered by aluminum, associated with a large volume expansion in the sample.

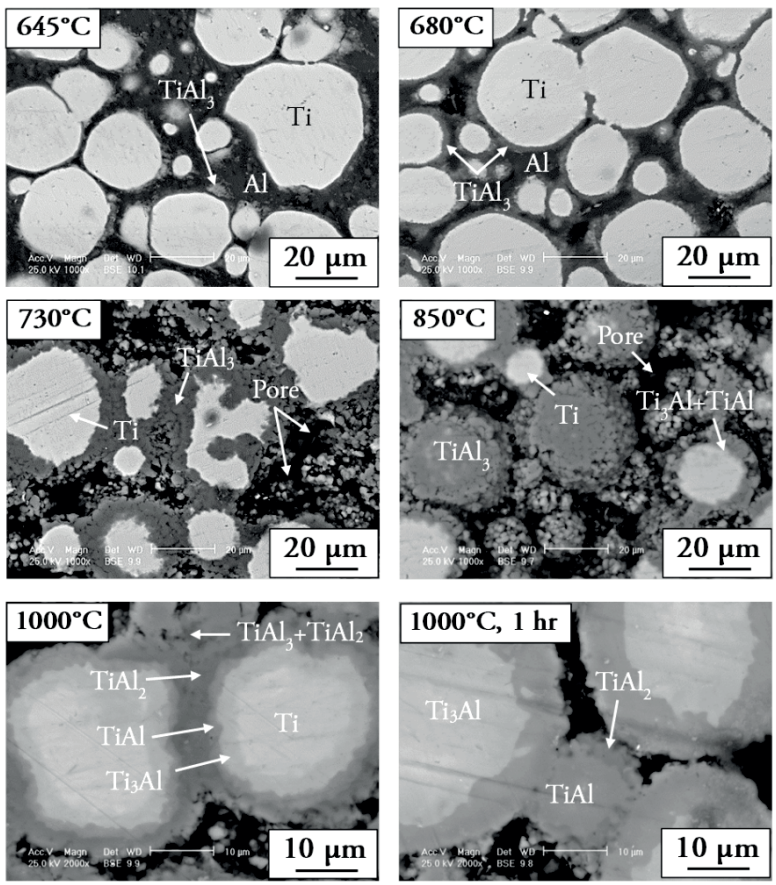

Fig. 7. SEM images of Ti-50at.%Al samples heated to selected temperatures at 15°C min^{-1}.

The micrograph of the sample heated to 850°C (prior to peak D), showed some regions in between the titanium cores and $TiAl_3$ layers, where EDS analysis indicated a different composition (~44 at.% Al). According to the Ti-Al phase diagram, this composition corresponds to the two-phase region Ti_3Al+TiAl. The presence of these phases as minor products was confirmed by X-ray diffraction data (see Fig. 8). Unreacted titanium cores were also observed in the sample, explaining the occurrence of the allotropic peak (D) in the DSC plot (Fig. 6). Further, $TiAl_3$ phase is seen as globular clusters with very small particles, which appear to be formed on the spherical titanium particles. Since each powder particle generally consists of numerous small grains, this may suggest that aluminum has diffused along the grain boundaries in titanium and reacted with titanium grains. However, it is seen that while some titanium particles are thoroughly transformed to $TiAl_3$, the cores of some other particles remained unreacted. The formation of new phases including Ti_3Al, TiAl and $TiAl_2$ is more pronounced in the micrograph of the sample heated to 1000°C, while $TiAl_3$ is getting consumed. As seen in the presented micrographs, titanium cores seem to have shrunk on further heating. Consequently, a series of aluminides have been formed around the titanium cores with a gradual change in composition, which is in accordance with the Ti-Al phase diagram. These observations suggest the occurrence of reactions involving solid-state diffusion in the samples, which can proceed further when heating is continued. After heating a sample for an hour at 1000°C, $TiAl_3$ regions and unreacted titanium cores disappear, and the TiAl phase predominates. This is consistent with XRD data (Fig. 8) showing TiAl as the major phase at this temperature.

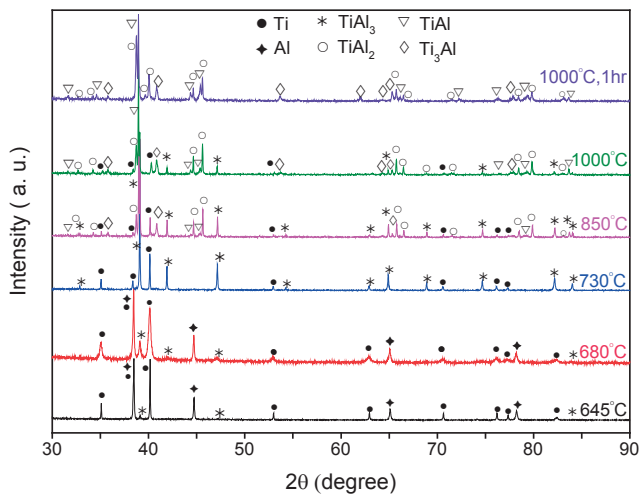

Fig. 8. Diffractograms of Ti-50at.%Al samples heated to different temperature at 15°C min^{-1}.

It may be noted that aluminum-rich (Ti-75at.%Al) samples showed relatively broader combustion peaks at higher temperatures as compared to those observed for equiatomic and titanium-rich (Ti-25at.%Al) samples. In titanium-rich samples, the combustion peak was shifted to temperatures below the melting point of aluminum, while no melting peak was identified in the DSC plots. More details can be found in appended paper I.

3.1.2 Fe-Al system

Fe-40at.%Al samples were prepared using elemental powder mixtures, with various particle size combinations. The reaction behavior in compacted discs was found to be influenced particularly by the particle size of iron. Fig. 9 shows the DSC plot for a compacted sample containing relatively coarse iron (Max. particle size: 60μm) and fine aluminum powders (Max. particle size: 15μm). The sample was heated at 7.5°C min^{-1} up to 1000°C. This plot shows two consecutive exothermic peaks. The first peak (A) is relatively diffuse, whereas the second peak (B) is sharper. This implies that the mechanism governing the first peak is more time-dependent, while the reaction associated with the second peak is more instantaneous. The first peak initiates at temperatures where the reaction takes place in the solid state, whereas the second peak occurs at considerably higher temperatures which are close to the formation of an aluminum-rich liquid phase.

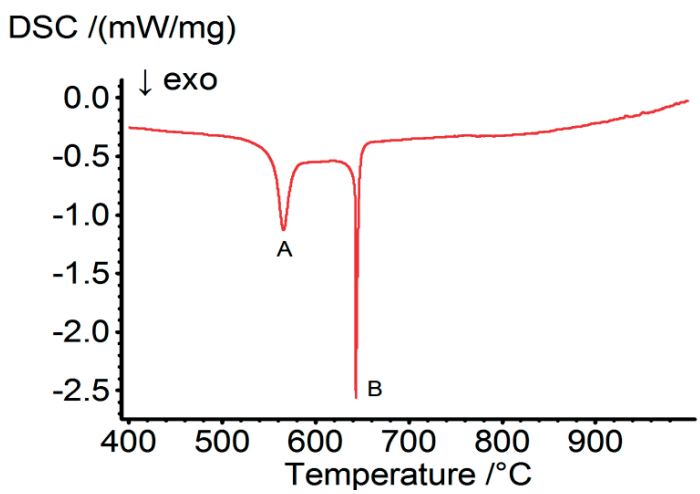

Fig. 9. DSC plot of the Fe-40at.%Al sample heated to 1000°C at 7.5°C min^{-1}.

Further, the relative heat release associated with the exothermic peaks was found to be influenced by aluminum particle size. At a given heating rate, for fine aluminum

particles, the first peak (A) was associated with a larger heat release, followed by a smaller heat effect for the second exothermic peak (B). This indicates that the first reaction, to some extent, inhibits the second reaction and is typical of a pre-combustion reaction. This is consistent with data showing the formation of some intermetallic compounds through diffusion, prior to the combustion reaction [63,75,77,78,133]. Samples containing fine aluminum particles showed a more uniform distribution of the reactant particles, enhancing the contribution from diffusion. Therefore, a larger content of the sample reacts prior to the combustion stage, forming significant amounts of pre-combustion products. This is associated with a stronger pre-combustion peak (A), but also decreases the direct contact between the elemental particles, which is essential for the combustion reaction. In order to study the evolution of phases during heating, a few compacted discs with coarse iron and fine aluminum particles were heated to selected temperatures, and the observed SEM images are shown in Fig. 10.

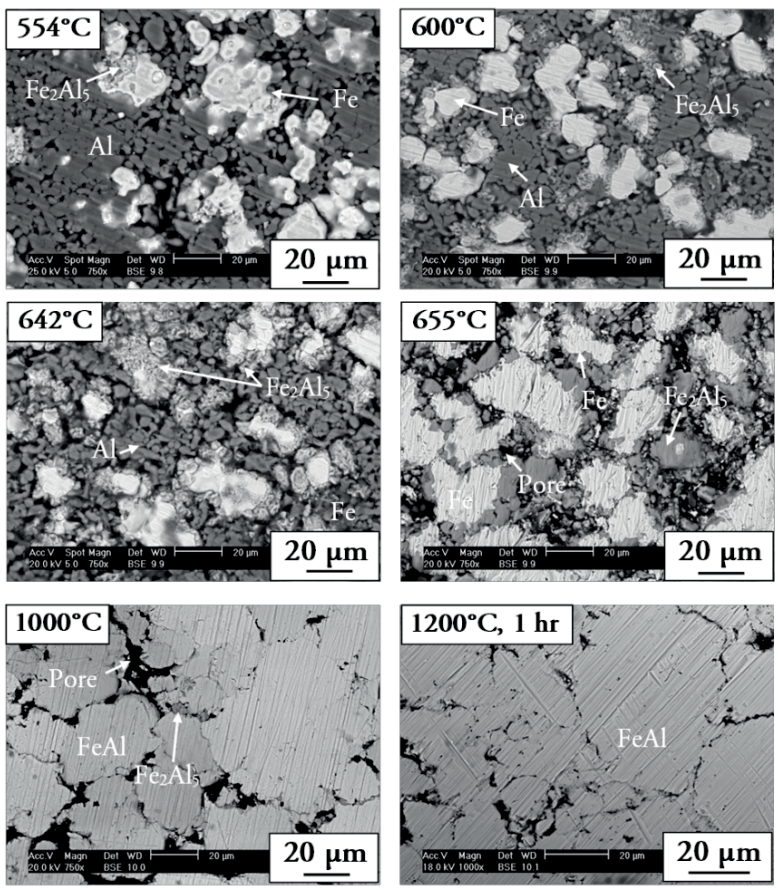

Fig. 10. SEM images of Fe-40at.% Al samples heated to selected temperatures at 15°C min^{-1}.

The micrograph of the sample heated to 554°C, which is close to the onset temperature of the pre-combustion peak (A), is mainly covered by unreacted elements. At a few points on the iron particles, an additional phase with a fuzzy appearance was identified as Fe_2Al_5 by EDS analysis. This shows that the formation of Fe_2Al_5 phase during the pre-combustion stage. The micrograph of the sample heated to 600°C clearly shows a noticeable growth of Fe_2Al_5. At this temperature where the pre-combustion peak (A) has just ended, elemental iron and aluminum areas still dominate in the micrograph. These data confirm the role played by solid-state diffusional reactions occuring during the pre-combustion stage, leading to the formation of Fe_2Al_5. After heating a sample to the onset temperature of the combustion peak B (642°C), significant amounts of unreacted iron and aluminum are seen in the micrograph, indicating slow reaction rates at solid state. Fe_2Al_5 is seen to form layers around the iron particle and covers the particle surface increasingly as it grows. This suggests that Fe_2Al_5 is mainly formed through the diffusion of aluminum into iron particles [63,68,77]. The larger intrinsic diffusivity of aluminum compared to iron [68,134] can explain the swelling behavior observed at this stage. The micrograph of the sample heated to 655°C where the combustion reaction has ended shows a significant growth of the Fe_2Al_5 as the product. Further, the micrograph shows a considerable amount of residual iron and seemingly no aluminum. The volume expansion of the sample showed a significant increase at this stage, characterizing the combustion reaction [63,68]. This swelling has been attributed to the formation of some large pores at the sites originally occupied by aluminum particles [63,68]. Heating the sample further to 1000°C resulted in the formation of a dominant FeAl product, as can be seen in the corresponding micrograph. Beyond the combustion temperature, FeAl is formed by the solid-state diffusional reaction between unreacted iron and Fe_2Al_5. This reaction does not go to completion at 1000°C, as some Fe_2Al_5 is still seen in the micrograph. It is also interesting to note that the variation of the size of FeAl grains matches the particle size variation of the coarse iron powder used to prepare the powder mixture. The micrograph of a sample heated to 1200°C for an hour showed a single-phase product of FeAl, indicating that the reaction between Fe_2Al_5 and iron has gone to completion. The formation of Fe_2Al_5 and FeAl at different stages of heating was also confirmed by XRD results.

The DSC plot of the compacted sample containing fine iron (average size: 7 μm) and aluminum powders (Max. particle size: 15 μm), showed a single, sharp combustion peak during heating. This result was in contrast to those observed for samples containing relatively coarser iron particles which showed a diffuse pre-combustion peak prior to the combustion peak (Fig. 9). The pre-combustion reaction appears to be not strong enough to be noticed in samples with fine iron particles. The micrograph of a sample heated above the combustion peak consisted of residual iron

particles as the major phase together with some FeAl and Fe_2Al_5 as the products. Further heating to 1000°C and above resulted in a stable, single-phase FeAl. The reaction behavior was also studied in loose powder mixtures where the DSC plots showed a single, sharp exothermic peak representing the combustion reaction, while no pre-combustion was observed during heating. More information is presented in appended paper II.

3.1.3 Nb-Al system

Fig. 11 presents the DSC plot of a Nb-33.3at.%Al compacted sample containing coarse niobium (max. particle size: 74 μm) and fine aluminum (Max. particle size: 15 μm) powders, heated to 1000°C at 7.5°C min^{-1}. The plot shows two peaks during heating, an endothermic peak (A) which corresponds to the melting of aluminum, followed by a diffuse exothermic peak (B). The exothermic peak initiating at temperatures above 700°C indicates the combustion reaction in the sample. It is generally agreed that the combustion reaction occurs through a dissolution-precipitation process [81,85,86]. The solubility of niobium in solid aluminum is practically zero and is very limited even in liquid aluminum. However, it shows an increase with increasing temperature. At 700°C the solubility of niobium in liquid aluminum is reported as ~0.02 wt.%, increasing to 0.1 wt.% at 850°C [84]. These data can explain the relatively higher temperatures required for the initiation of combustion reaction in the Nb-Al system. Other factors which could contribute to higher onset temperatures for the combustion reaction include difficulties in the wetting of the niobium particle surface by molten aluminum and the presence of oxides on the surface of the particles.

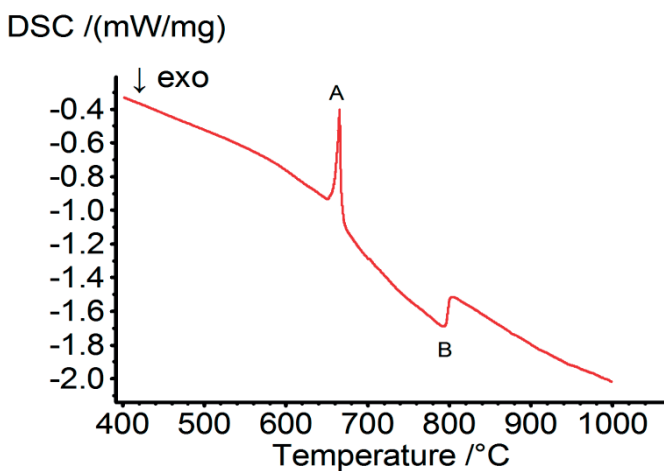

Fig. 11. DSC plot of the Nb-33.3at.%Al sample heated to1000°C at 7.5°C min^{-1}.

Microscopic observations revealed the formation of $NbAl_3$ during the combustion reaction. Fig. 12 shows the evolution of phases in Nb-33.3at.%Al compacted powders (with fine aluminum particles) heated to selected temperatures. At 670°C where the melting of aluminum is complete, the micrograph shows unreacted elemental regions. Heating the sample to 690°C, which is lower than the combustion onset temperature, resulted in some traces of $NbAl_3$ identified by EDS analysis. The formation of $NbAl_3$ phase is more pronounced after heating the sample to 710°C. This observation is in agreement with DSC data showing the initiation of the combustion peak (B), close to this temperature.

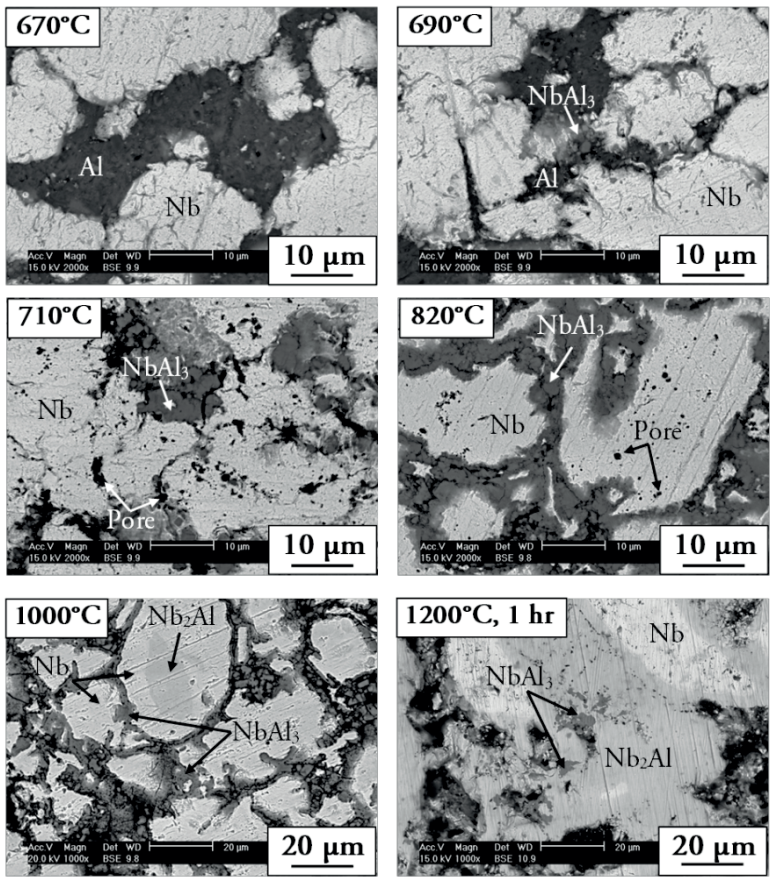

Fig. 12. SEM images of Nb-33.3at.%Al samples heated to different temperatures at 15°C min^{-1}.

Fig. 12 also shows that if heating is continued to a temperature at which the combustion peak ends (820°C), the sample surface is largely covered by $NbAl_3$. While niobium constituted the major phase, no elemental aluminum was observed in the

micrograph. This indicates that the reaction between molten aluminum and niobium particles has been inhibited, due to limited availability of molten aluminum. At this stage, the sample showed a large expansion in volume, which is typical in combustion reactions. Increasing the temperature to 1000°C resulted in the formation of Nb_2Al as a new product. This can be attributed to the diffusional reaction between the residual niobium and $NbAl_3$ regions. In general, the progress of a solid-solid reaction is considerably slower compared to a solid-liquid reaction. Therefore, longer times and higher temperatures are required to get a high degree of conversion. This effect is seen in the micrograph of a sample heated for an hour at 1200°C showing Nb_2Al as the dominant phase. However, some unreacted niobium and traces of $NbAl_3$ are still present in the product. This result confirms that the initially formed $NbAl_3$ is an intermediate phase which transforms to Nb_2Al through the solid-state reaction with niobium at higher temperatures. This conclusion was supported by XRD results presented in Fig. 13.

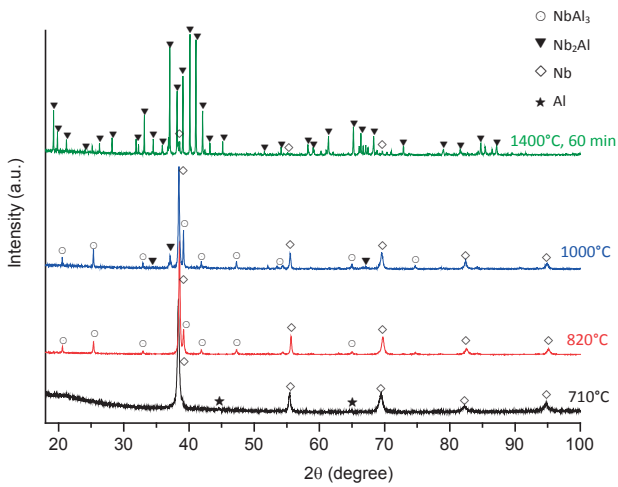

Fig. 13. Diffractograms of Nb-33.3at.%Al samples heated to different temperatures at 15°C min^{-1}.

After heating a sample to 710°C, which is close to the onset temperature of the combustion peak (B), the diffraction peaks correspond to the elemental components. However, increasing the heating temperature to 820°C, where the comustion peak ends, resulted in the formation of $NbAl_3$ phase as the combustion product. Aluminum reflections are absent at this temperature, wheraeas niobium peaks are visible in the X-ray diffractogram. The XRD pattern of the sample heated to 1000°C shows some reflections from Nb_2Al phase, while the presence of $NbAl_3$ and elemental niobium is still significant, which is consistent with the presented micrographs.

Finally, when the sample is heated for an hour at 1400°C, the product contains mainly Nb_2Al, while only a few small niobium peaks can be detected in the diffraction pattern.

DSC results from samples having different aluminum particle sizes showed that fine aluminum particles lead to lower onset temperatures for the combustion peak. This is apparently due to better surface coverage of niobium particles by fine aluminum particles. The onset temperature of the combustion peak was also seen to decrease with increasing niobium content in the sample. Loose powder samples showed higher onset temperatures for the combustion peak. In all the niobium-aluminum samples, regardless of the initial composition, the combustion reaction was initiated between the aluminum melt and niobium particles resulting in the formation of $NbAl_3$ compound. In the case of Nb-75at.%Al samples, this reaction reached completion, forming a single-phase product of $NbAl_3$. Nb-25at.%Al samples exhibited a similar behavior to Nb-33.3at.%Al samples, showing a considerable amount of unreacted niobium after the combustion reaction. In these samples, a stable product corresponding to the initial composition was obtained after prolonged heat treatment, as described in paper III.

3.1.4 Ta-Al system

Fig. 14 presents the DSC plot of a Ta-50at.%Al compacted sample heated to temperatures above 1200°C at 15°C min^{-1}. The sample was prepared using tantalum and aluminum powders with maximum particle sizes of 75 and 60 μm, respectively.

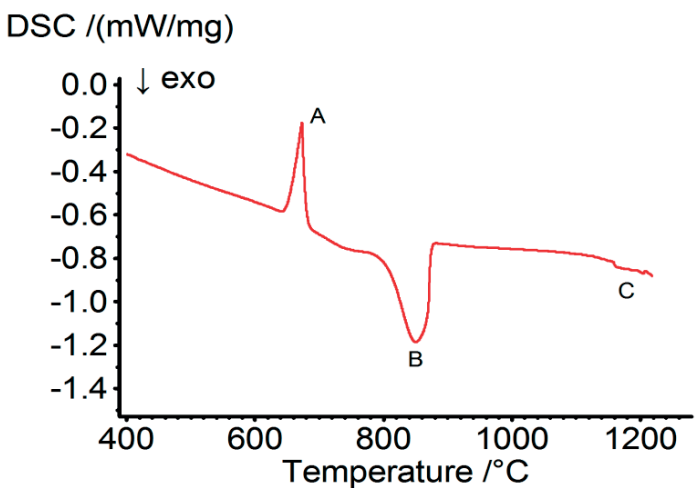

Fig. 14. DSC plot of the Ta-50at.%Al sample heated to 1200°C at 15°C min^{-1}.

In this plot, the aluminum melting peak (A) is followed by an exothermic peak (B) corresponding to the combustion reaction in the sample. On heating the sample to higher temperatures, a weak and mildly exothermic peak (C) is observed, which may be due to a phase change associated with a small heat effect. In order to understand the phase evolution during heating, a few compacted samples were heated at 15°C min^{-1} to selected temperatures of interest, and the corresponding micrographs are presented in Fig. 15.

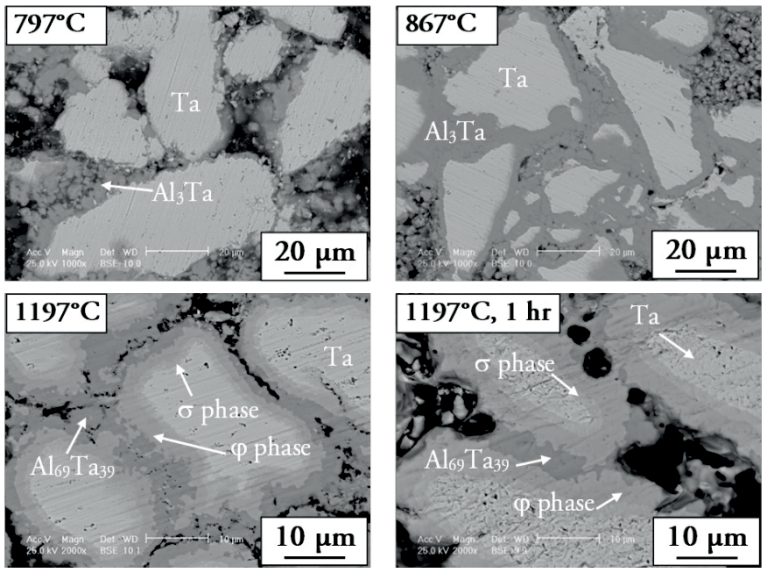

Fig. 15. SEM images of Ta-50 at.%Al samples heated to different temperatures at 15°C min^{-1}.

Microscopic examination and EDS analyses of the sample heated to 797°C (near the onset temperature of the reaction reaction peak B) revealed the formation of Al_3Ta as the product of reaction between tantalum particles and molten aluminum. Heating a sample to 867°C, where the combustion reaction had ended, showed consolidation of the Al_3Ta phase, covering the unreacted tantalum particles. At this stage, the formation of Al_3Ta could not proceed further significantly after elemental aluminum had been fully consumed. While no microstructural change was observed at lower temperatures, heating a sample to 1197°C resulted in the formation of new phases. This temperature falls within the range of the exothermic peak C and the observation confirms that the peak is associated with phase changes. As seen in the corresponding micrograph, the Al_3Ta phase formed at lower temperatures is replaced by another aluminum-rich phase with an average composition of 38 at.% Ta corresponding to $Al_{69}Ta_{39}$. This is consistent with the Al-Ta phase diagram [94] showing the formation of $Al_{69}Ta_{39}$ phase at temperatures above 1098°C. Further, a series of thin layers with

different contrasts are visible in the peripheral regions of unreacted tantalum cores. EDS analyses revealed average compositions of 64 and 52 at.% Ta for the inner and outer layers, which according to the phase diagram [94] correspond to σ and φ phases, respectively. The multilayer pattern indicates the diffusion of aluminum from the aluminum-rich regions (initially Al_3Ta, and then $Al_{69}Ta_{39}$) towards the unreacted tantalum cores. This has led to formation of the tantalum-rich and equiatomic phases, namely σ and φ around the unreacted tantalum cores. The solid-state diffusional reaction can occur if the temperature is high enough for crossing the activation barrier. The φ-phase was found to grow considerably after prolonged heating at 1197°C for 1 hour and the presence of σ and particularly $Al_{69}Ta_{39}$ phases had weakened. This indicates that φ is the more stable phase at this stage, which is closer to the initial composition of the sample.

The formation of various phases in the heated samples was also examined using X-ray diffraction analysis. Fig. 16 presents the results of phase analysis for samples heated to selected temperatures. The diffraction patterns for samples heated to 797° and 867°C showed reflections corresponding to Al_3Ta and elemental tantalum phases. Heating a sample further to 997°C for an hour did not lead to changes in the diffractogram. On the other hand, a new diffraction pattern was observed after a prolonged heating at a temperature above the exothermic peak C. The major reflections observed in the diffraction pattern of a sample heated to 1197°C for an hour correspond to the equiatomic φ phase, while σ and $Al_{69}Ta_{39}$ were also identified as minor phases.

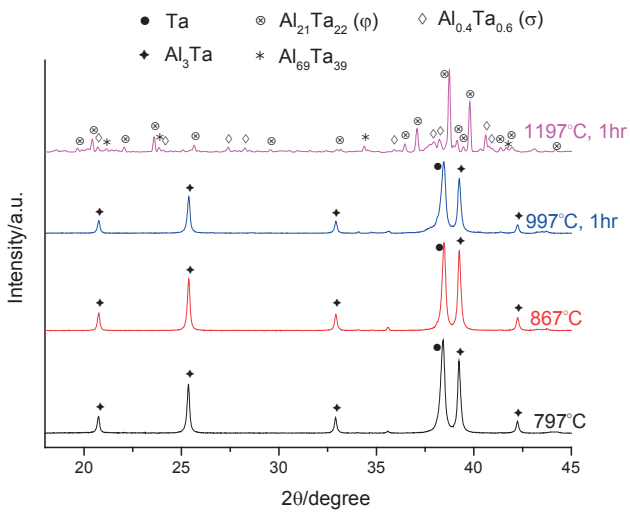

Fig. 16. Diffractograms of Ta-50at.%Al samples heated to different temperatures at 15°C min^{-1}.

The combustion reaction in Ta-75at.%Al samples resulted in a single-phase product which was stable at higher temperatures. However, an incomplete combustion reaction was observed in the Ta-33.3at.%Al samples, resulting in a multilayer product in which the phase corresponding to the stoichiometric composition dominated after a prolonged heat treatment at elevated temperatures. Further observations made during the heating of tantalum-aluminum powder compacts are presented in paper IV.

3.1.5 Effect of process variables on reaction behavior

The reaction behavior during the synthesis of intermetallic compounds from elemental powder mixtures is influenced by process variables such as compaction, particle sizes of the reactants, initial composition of the powder mixture and heating rate. These aspects are discussed in the following sections.

Powder compaction

Experimental data showed that the pre-combustion stage appeared in the DSC plot only for the compacted samples and not for the samples in the loose powder condition. This is due to good inter-particle contact (aluminum-transition metal) in the compacted samples, which is essential for solid-state diffusional reactions prior to combustion. For a given particle size combination and at a constant heating rate, compacted samples were associated with lower onset temperatures for the combustion reaction, indicating an enhanced reaction due to better contact between the reacting particles.

Powder particle size

Decreasing the particle size of the transition metal powder was associated with a more uniform distribution of the elemental powder particles, resulting in a decrease in the onset temperature for the combustion reaction in the samples. An improved distribution of the reactant particles was also obtained using fine aluminum particles in the samples. As an example, despite a tendency for clustering, Nb-33.3at.%Al samples consisting of fine aluminum particles exhibited a more uniform distribution and a better surface coverage for the elemental particles, as shown in Fig. 17. Fine aluminum particles led to lower onset temperatures for the combustion reaction in most of the samples.

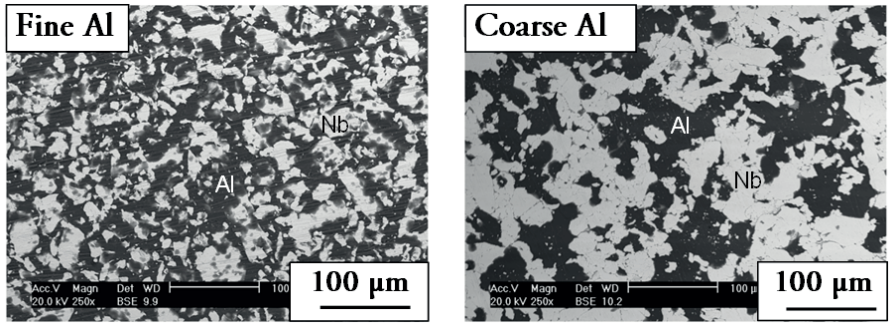

Fig. 17. SEM images of unreacted Nb-33.3at.%Al samples with different aluminum particle sizes.

Initial composition

The combustion reaction in the samples was observed to reach completion in samples rich in aluminum, namely M+3Al samples where M=Ti, Nb, Ta. A porous, but homogeneous product (MAl_3) was obtained in these samples. The combustion peaks observed in Al-rich samples were relatively diffuse, covering wider temperature range and longer times. Decreasing the aluminum content in the samples gave rise to narrower combustion peaks in the DSC plots, but the combustion reaction was incomplete and considerable amounts of transition metal particles remained unreacted. Relatively higher amounts of the transition metal in the samples resulted in lower onset temperatures for the combustion reaction. This can be attributed to an enhanced dissolution-precipitation process through which the combustion products are generated in the heated sample [81,85,86].

Heating rate

In general, increasing the heating rate was observed to shift the combustion reaction to higher temperatures, which is commonly observed behavior for thermally activated reactions [135]. Higher heating rates are associated with larger heat transfer effects and thermal lag, and the reaction occurs at higher temperatures. Fig. 18 presents such an observation for the Ta-75at. %Al samples at different heating rates.

Data on the shift in onset temperatures at different heating rates introduces the possibility of estimating the apparent activation energy of such reactions through model-free, isoconversion methods by determining the temperatures at which a certain fraction of conversion is obtained at different heating rates. Since a single-phase product was obtained in Al-rich samples, the DSC data obtained for these groups of samples were chosen to calculate the apparent activation energy for MAl_3 formation through the combustion reaction.

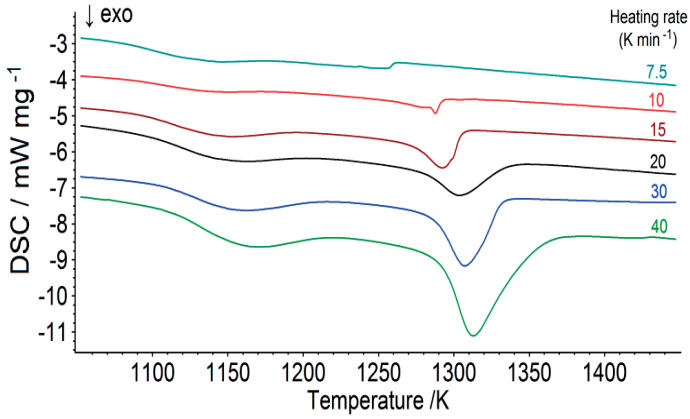

Fig. 18. DSC peaks observed during the combustion reaction in Ta-75at.%Al samples at different heating rates.

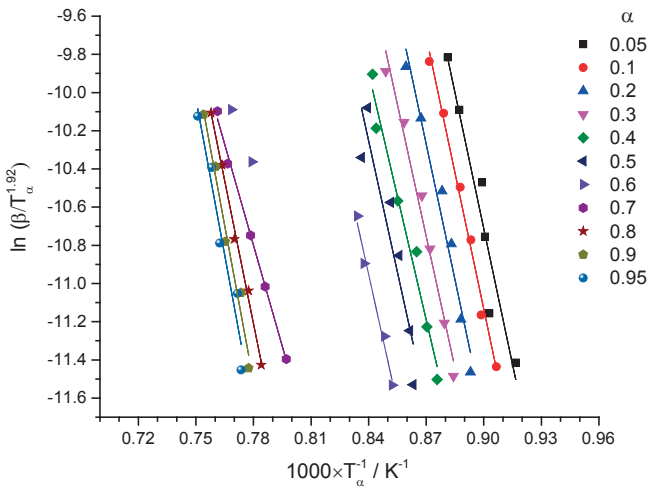

Fig. 19. Starink isoconversion plots for the determination of apparent activation energy of the combustion reaction in Ta-75at.%Al samples.

Fig. 19 presents the results obtained for Ta-75at.%Al samples using the Starink approach [136,137], which is one of the more accurate isoconversion methods. In this figure, $\ln(\beta/T_\alpha^{1.92})$ has been plotted against the reciprocal of T_α for a series of conversion fractions, where β is the linear heating rate (K min^{-1}) and T_α is the temperature (K) corresponding to a given degree of conversion (α). Regarding the Arrhenius-type equations considered in such approaches, the slope of the fitted lines shows a proportional relationship with the apparent activation energy of reaction.

Estimated values for the apparent activation energy of MAl_3 formation in different systems show larger temperature dependence for the combustion reaction in systems involving refractory transition metals like niobium and tantalum as compared to the relatively low melting transition metal like titanium. Reaction enthalpies for combustion reaction leading to the formation of MAl_3 compounds in different systems were also estimated from the combustion peaks in the respective DSC plots and the results are presented in the appended papers I, III and IV.

3.2 Al-Ni-Ti ternary system

The formation of various aluminides and intermetallic compounds during the reactive sintering of compacted Al-Ni-Ti powder mixtures was studied. The effect of sample composition on reaction behavior was investigated by varying the aluminum addition (0 to 40 at.%) to equiatomic nickel-titanium powder mixtures. The DSC plots of the Al-Ni-Ti samples showed two main exothermic peaks corresponding to reactions taking place below and above the melting point of aluminum. The first exothermic peak was found to represent the combustion reaction between nickel and aluminum, while the second peak was connected mainly to the combustion reaction between nickel and titanium. Titanium-rich and nickel-rich ternary phases, in addition to some binary phases have been observed after the second exothermic reaction in all the ternary powder compacts. The results obtained during the reactive sintering of the equiatomic Ni-Ti samples are presented below, followed by those for 25AlNiTi samples containing 25 at.% Al (Ni:Ti=1).

3.2.1 Ni-Ti samples

Fig. 20 shows the DSC plot of Ni-50at.%Ti samples heated to 1200°C at 20°C min^{-1}, and then cooled to room temperature. On closer scrutiny, the plot reveals a small endothermic peak during heating, in the temperature interval 760°-850°C. According to the Ni-Ti phase diagram, a eutectoid transformation occurs at 765°C, through which α-Ti and Ti_2Ni phases transform to β-Ti. The observed endothermic peak is therefore suggestive of the eutectoid transformation in the sample, which is in accordance with the data available in literature [122]. This plot also shows a characteristic exothermic peak upon heating to temperatures above 945°C, indicating a combustion reaction in the sample. This temperature is very close to the eutectic transformation temperature (942°C) in the Ni-Ti phase diagram, where a liquid phase forms from a mixture of β-Ti and Ti_2Ni phases. It has been suggested that the formation of the eutectic melt leads to better wetting of the particle surfaces and leads

to the initiation of a combustion reaction in the sample, and a sharp exothermic peak in the DSC plot [15,40,138].

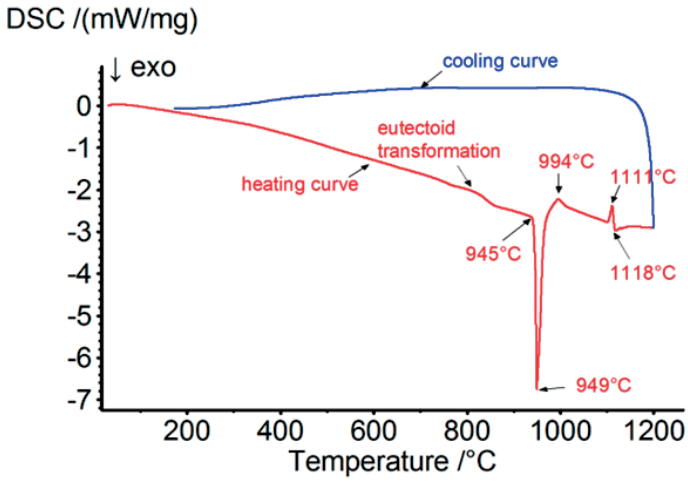

Fig. 20. DSC plot of the Ni-50at.%Ti sample heated to 1200°C at 20°C min^{-1}.

Fig. 20 shows that the combustion peak is immediately followed by an endothermic peak at 994°C, which can be attributed to the peritectic transformation ($Ti_2Ni \rightarrow NiTi+L$) occurring at 984°C, as shown in the Ni-Ti phase diagram. Further heating of the sample to 1200°C was associated with an endothermic peak at 1111°C, followed immediately by a small exothermic peak. The endothermic peak can be attributed to the eutectic transformation ($NiTi+Ni_3Ti \rightarrow L$) occurring at 1118°C [122]. The liquid formed at this stage reacts with the existing phases, giving rise to an exothermic reaction, as observed in the DSC plot. The absence of any solidification peak upon cooling the sample from 1200°C confirms that the liquid phase has been fully consumed through interaction with other phases.

Two Ni-Ti samples were heated to 1050°C (above the major exothermic peak) and 1200°C, followed by the microscopic analysis (Fig. 21). The micrograph of the sample heated to 1050°C is dominated by some light and dark grey regions which were identified as NiTi and Ti_2Ni phases, respectively. The bright areas corresponded to Ni_3Ti phase and unreacted Ni (<10 at.%Ti), which are seen adjacent to each other. Intermetallic compounds such as Ni_3Ti, NiTi and Ti_2Ni can form through reactions driven by solid-state diffusion [120,121]. However, the formation of NiTi and Ti_2Ni phases is more pronounced after the combustion reaction triggered by eutectic melt formation at 942°C [122,138]. A coring pattern can be observed in some areas in the sample heated to 1050°C, which is attributed to peritectic solidification during cooling.

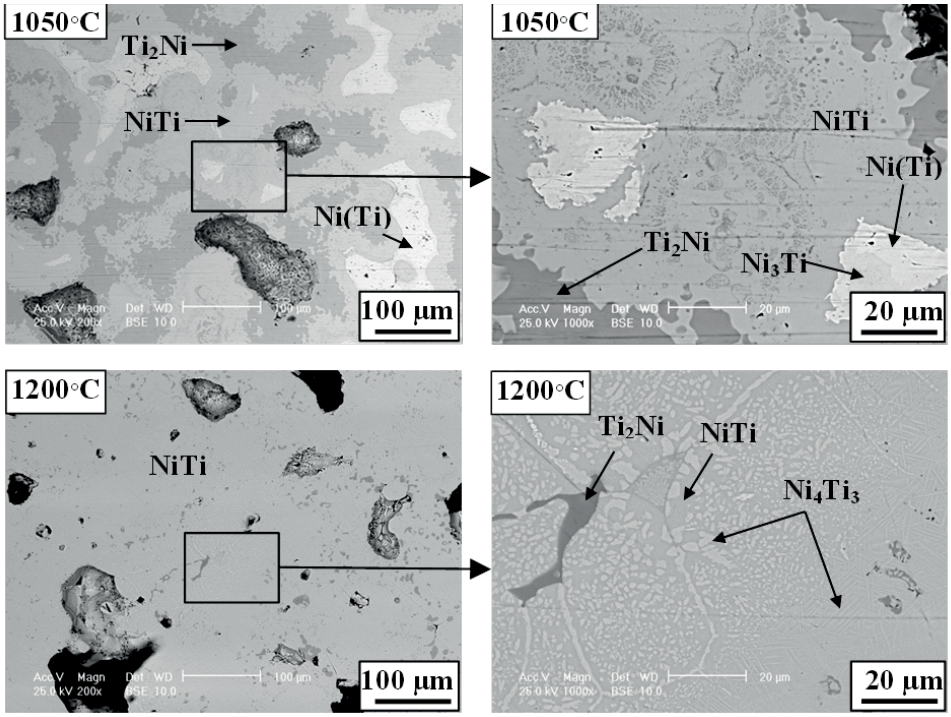

Fig. 21. SEM images of Ni-50at.%Ti samples heated to 1050° and 1200°C at 20°C min^{-1}.

The micrograph of the sample heated to 1200°C consisted of a dominant NiTi matrix, while the Ti_2Ni phase was also observed as small, dark regions. No Ni-rich phase was identified in the sample. This indicates that during the heating cycle, the residual Ti-rich (i.e. Ti_2Ni) and Ni-rich phases have reacted with each other, resulting in a NiTi product. However, small amounts of precipitates were also observed within the NiTi matrix. EDS analysis suggested a chemical composition of ~60 at.% Ni and ~40 at.% Ti for this phase, which is very close to the Ni_4Ti_3 compound. The formation of metastable Ni_4Ti_3 precipitates within the NiTi phase has also been reported in literature [139–142]. These conclusions are supported by XRD data.

3.2.2 25AlNiTi samples

Two major exothermic peaks are seen during the heating cycle in Fig. 22 which presents the DSC plot for the 25AlNiTi sample heated to 1200°C at 20°C min^{-1}. The first exothermic peak occurs below the melting temperature of aluminum and apparently consists of two overlapping peaks (double-peak). A similar double-peak feature has been reported previously during the reactive sintering of aluminum-nickel powder mixtures [110,143,144]. The second exothermic peak is comparable to that

observed in the Ni-50at.%Ti samples, which is mainly related to the combustion reaction between nickel and titanium. There is also a small endothermic event (broad peak) slightly below 942°C, which corresponds to the eutectoid transformation α-Ti+$Ti_2Ni \rightarrow \beta$-Ti. At higher temperatures, small endothermic and exothermic peaks were also observed, following each other in the range 1134° to 1144°C. In order to understand the evolution of phases at different stages of reaction, a few samples were heated to selected temperatures below and above the peaks observed in the DSC plot.

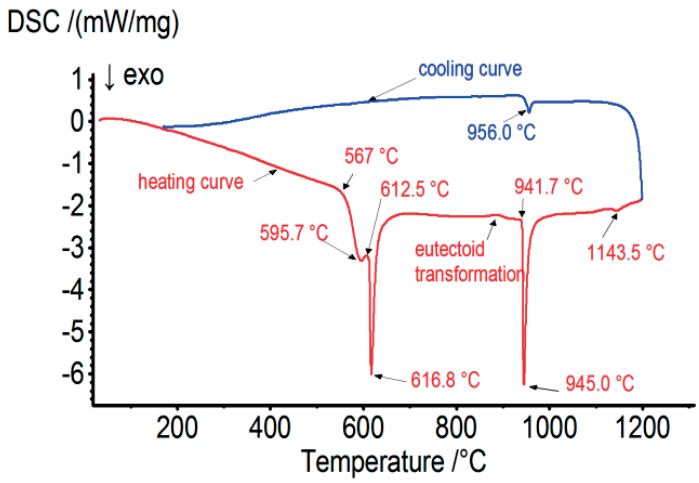

Fig. 22. DSC plot of the 25AlNiTi sample heated to 1200°C at 20°C min^{-1}.

Phase analyses of a sample heated to 600°C showed the presence of some aluminum-rich compounds, namely Al_3Ni and Al_3Ni_2, which were apparently formed during the exothermic reaction at ~595°C. The heat release at this stage can raise the temperature locally and lead to the formation of a eutectic melt and induce higher rates of reaction in the sample. The sample heated to a temperature above the sharp exothermic peak at 700°C showed the existence of Al_3Ni_2 and NiAl phases while Al_3Ni was not identified. This can be attributed to the reaction between the aluminum-rich eutectic melt and nickel particles, resulting in the formation of a thick layer of Al_3Ni_2 and a thin NiAl layer around nickel particles, as confirmed by microscopic studies. It has been suggested that the final products after the exothermic reaction depend on the aluminum content in the sample. A higher aluminum content favors the formation of NiAl phase and a lower aluminum content yields the Ni_3Al phase [110]. After heating to 700°C, a thin layer of Al_3Ti was also seen around the titanium particles, suggesting the initial formation of Al_3Ti due to the interdiffusion between the elemental particles [145,146]. The results indicate that aluminum has a greater tendency to react with nickel than titanium and forms a large number of compounds with nickel. This is supported by thermodynamic data which, for

example, predicts the formation of Al_3Ni to be more favorable relative to Al_3Ti [147]. Al_3Ti phase was observed to be transformed into Ti_3Al and AlTi phases at higher temperatures (850°C), while a eutectoid type structure was seen within the titanium particles, formed through the eutectoid transformation α-Ti+$Ti_2Ni \rightarrow \beta$-Ti.

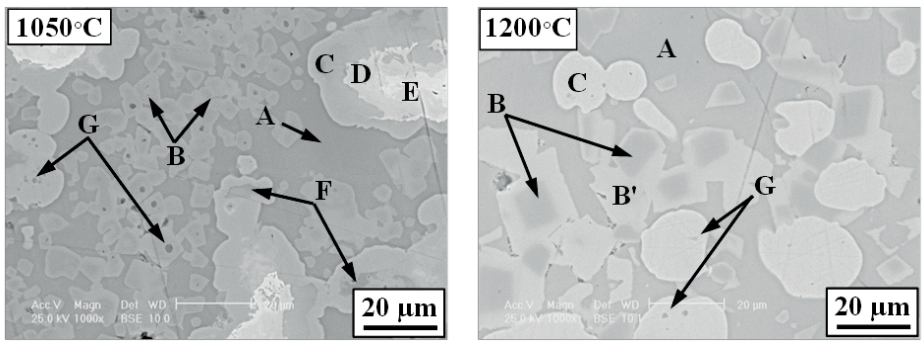

Fig. 23. SEM images of 25AlNiTi samples heated to 1050° and 1200°C at 20°C min^{-1}.

Fig. 23 shows SEM images of the samples heated to 1050° and 1200°C, which are above the second sharp exothermic peak. At 1050°C, the micrograph is characterized by a continuous phase (A), a large number of particles (B) and some multi-layered regions (C to F). Detailed EDS analysis was carried out by taking multiple data points to evaluate phase compositions. A small homogeneity range was observed for the different phases in the microstructure. The areas indicated by 'A' contain 27±1 at.% Al, 28±1 at.% Ni and 45±1 at.% Ti. Particles 'B' have a composition of 17±1 at.% Al, 31±1 at.% Ni and 52±1 at.% Ti. The inner core of the multi-layered regions with a very bright contrast (E) consists of unreacted nickel which is surrounded by NiAl phase (D) and the broad outer layer show another nickel-rich ternary compound (C) with the composition 25 at.% Al, 50 at.% Ni and 25 at.% Ti. 'F' (dark grey areas within the multi-layered region) has a composition corresponding to $Ni_{75}(Al,Ti)_{25}$. The formation of ternary compounds in this sample involves reaction between various binary compounds formed prior to the exothermic reaction at 942°C and the eutectic melt in the nickel-titanium system. The titanium-rich melt, with ~28 at.% Ni, reacts with the surrounding titanium and nickel aluminides, resulting in the formation of titanium-rich ternary compounds indicated by 'A' and 'B'. The formation of nickel-rich ternary compound (C) could involve two types of reactions: (i) Nickel-enrichment of NiAl formed prior to the exotherm at 942°C, (ii) interactions between the products of exothermic reaction at 942°C and the existing NiAl phase. On prolonged heating, small amounts of NiAl as well as nickel-rich regions could dissolve completely and contribute to the formation of a nickel-rich ternary compound like

$AlNi_2Ti$ (τ_4), which is a typical Heusler-type, $L2_1$ structure [148] observed in many conventionally cast Al-Ni-Ti samples. The XRD pattern of this sample showed diffraction peaks from AlNi, $Al_{25}Ni_{50}Ti_{25}$, $Al_{29}Ni_{27}Ti_{44}$ and $Al_{12.5}Ni_{33.33}Ti_{54.17}$, as shown in Fig. 24. The legend in the figure includes the JCPDS reference powder diffraction file numbers [149].

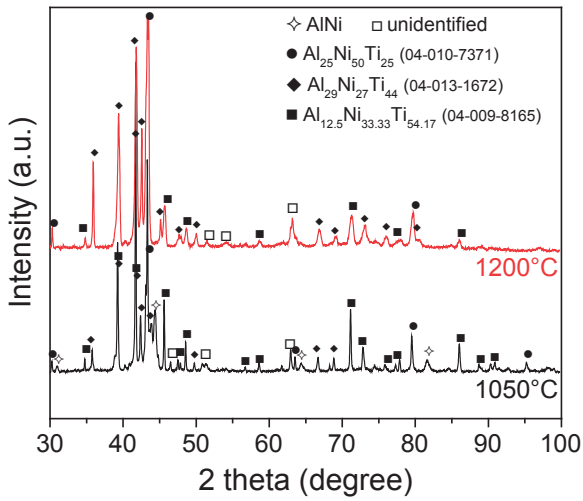

Fig. 24. Diffractograms of 25AlNiTi samples heated to 1050° and 1200°C 20°C min^{-1}.

As seen in Fig. 22, heating the sample further to 1200°C revealed reaction peaks at ~1140°C, which can be related to the peritectic transformation occurring at 1133°C ($Al_3Ni_2 \rightarrow L+AlNi$) in the nickel-aluminum phase diagram. The SEM image of the sample heated to 1200°C (Fig. 23) consists of the continuous phase 'A', large squarish particles 'B', along with rounded particles 'C'. The area 'A' is similar to that observed in the sample heated to 1050°C. Similarly, the small particles 'B' observed in the sample at 1050°C have grown larger (from ~5 μm to ~15 μm) during the heating to 1200°C. Two types of contrasts can be observed in these particles, the outer layer is brighter as compared to dark inner core which is related to the changes in chemical composition within the particles. In the sample heated to 1200°C, phase compositions are slightly different to those in the 1050°C sample. Region 'A' contains 26±2 at.% Al, 29±1 at.% Ni and 45±2 at.% Ti, while particles 'B' contain 19±1 at.% Al, 31±1 at.% Ni and 50±1 at.% Ti. The bright outer layer on these particles is indicated by 'B'', showing enrichment of titanium and a decrease in aluminum content. The composition of B' is 14±1 at.% Al, 33±1 at.% Ni and 53±1 at.% Ti. The chemical composition of the spherical particles in the sample heated to 1200°C corresponds to the $AlNi_2Ti$ (τ_4) phase which is similar in composition to area 'C' in the sample at 1050°C. The XRD pattern for the sample heated to 1200°C (Fig. 24)

shows the existence of diffraction peaks from three different ternary compositions, and the absence of any NiAl diffraction peak indicates that it has been consumed fully in the reactions occurring during heating from 1050° to 1200°C. The DSC plots of the sample heated to 1200°C (Fig. 22) and also 1050°C showed a small characteristic solidification peak upon cooling at 956°C. These observations suggest that the liquid formed due to eutectic melting at 942°C is not completely consumed even at 1200°C and a small amount of the melt is retained during cooling. This liquid solidifies and forms small round particles as indicated by area 'G' in the micrographs (Fig. 23).

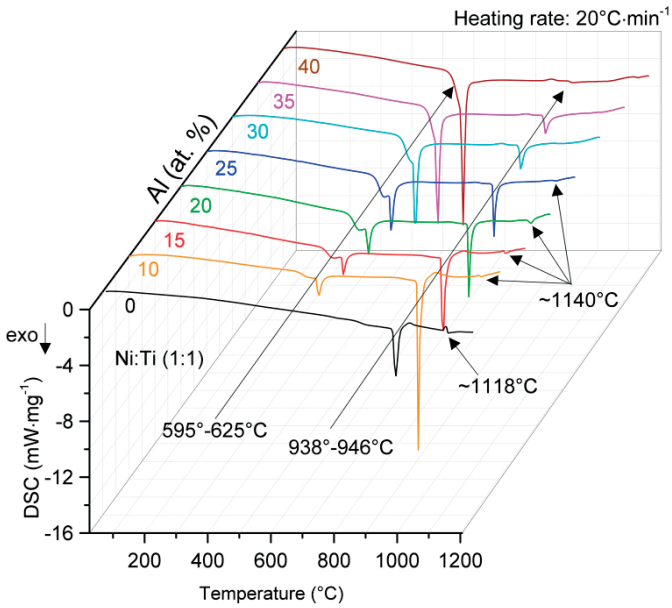

Fig. 25. DSC plots of Al-Ni-Ti samples heated to 1200°C.

Fig. 25 presents DSC plots of Al-Ni-Ti samples with various aluminum contents (0-40 at.%) and equiatomic proportions of nickel and titanium, heated to 1200°C at 20°C min^{-1}. Two major exothermic peaks are clearly seen aluminum-containing samples and they correspond to temperature intervals 595°-625°C and 938°-946°C, respectively. The first exothermic peak is seen to exhibit a larger exothermicity with increasing aluminum content while the second exothermic peak shows the opposite effect. This indicates that the reactions associated with these two peaks are complementary in nature, and the first reaction can inhibit the second reaction significantly. This behavior is understandable, as the first exothermic peak corresponds to the combustion reaction between aluminum and nickel, while the second peak corresponds to the reaction between nickel and titanium. As the aluminum content increases in the sample, more nickel reacts with aluminum during

the first reaction, and this leads to a relatively weaker interaction between nickel and titanium, as observed in the DSC plots.

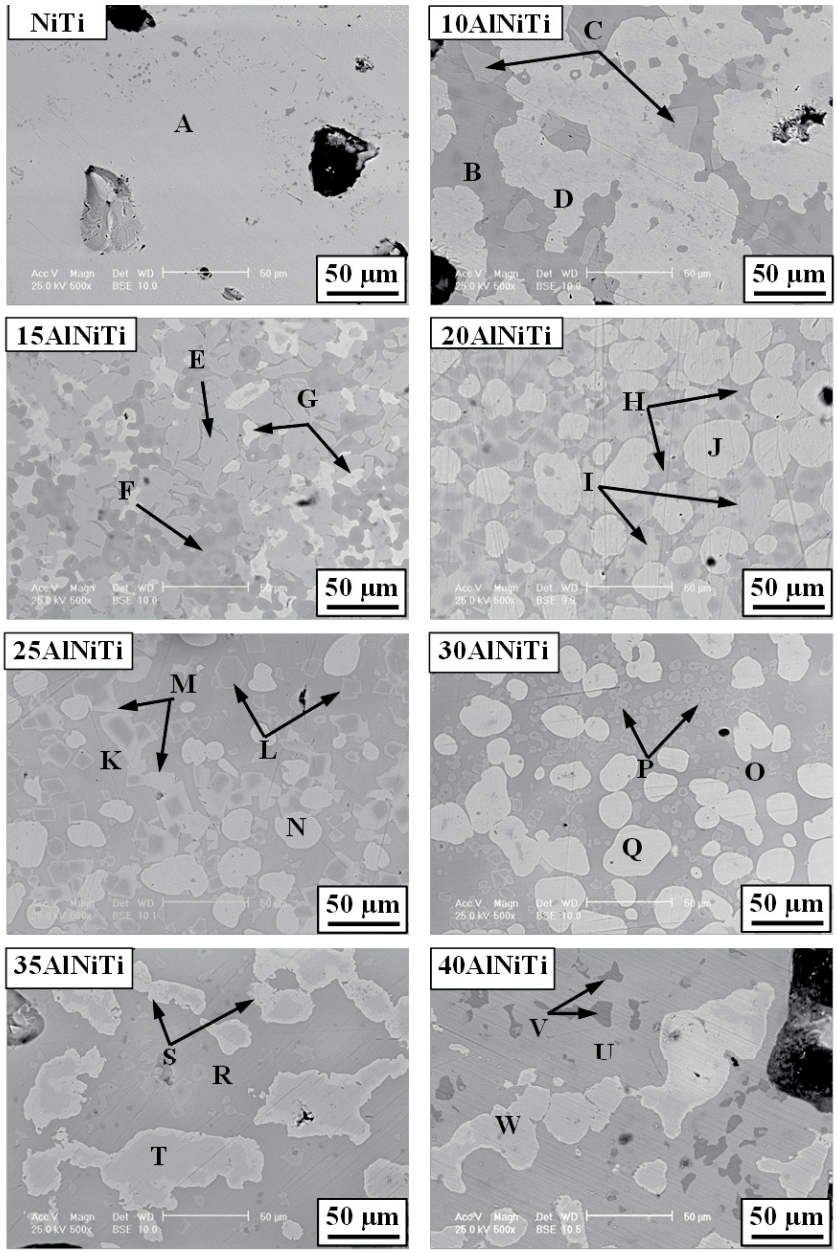

Fig. 26. SEM images of Al-Ni-Ti samples (Ni:Ti =1) heated to 1200°C at 20°C min^{-1}.

Table 3. Chemical compositions of various regions marked in Fig. 26

Sample	Different regions in micrographs	Composition (at.%)			Phase/group
		Al	Ni	Ti	
Ni-Ti (1:1)	A	-	51±1	49±1	NiTi
10AlNiTi	B	11±2	33±1	55±1	**I**
	C	21±1	29±1	50±1	**II** - $Al_2Ni_3Ti_5$
	D	9±1	50±2	41±2	NiTi(Al)
15AlNiTi	E	24±2	48±1	28±1	$AlNi_2Ti(\tau_4)$
	F	10±1	32±1	58±1	**I**
	G	10±1	46±1	44±1	NiTi(Al)
20AlNiTi	H	21±2	29±1	50±1	**II** - $Al_2Ni_3Ti_5$
	I	14±1	33±1	53±1	**I**
	J	25±1	50±1	25±1	$AlNi_2Ti(\tau_4)$
25AlNiTi	K	26±2	29±1	45±2	**II** - $Al_2Ni_3Ti_5$
	L	19±1	31±1	50±1	**II** - $Al_2Ni_3Ti_5$
	M	14±1	33±1	53±1	**I**
	N	25±1	50±1	25±1	$AlNi_2Ti(\tau_4)$
30AlNiTi	O	35±1	28±1	37±1	**III**
	P	22±1	30±1	48±1	**II** - $Al_2Ni_3Ti_5$
	Q	26±2	49±1	25±1	$AlNi_2Ti(\tau_4)$
35AlNiTi	R	38±1	26±1	36±1	**III**
	S	25±1	50±1	25±1	$AlNi_2Ti(\tau_4)$
	T	49±1	49±1	2±1	AlNi(Ti)
40AlNiTi	U	39±1	24±1	37±1	**III**
	V	29±2	2±1	69±2	$Ti_3Al(Ni)$
	W	51±1	47±1	2±1	AlNi(Ti)

The SEM images of the Al-Ni-Ti samples (Ni:Ti=1) with various aluminum contents (0-40 at.%) heated to 1200°C are presented in Fig. 26. Distinct regions with varying contrast in the micrographs are denoted by letters A-W and the corresponding chemical compositions obtained by EDS analysis are given in Table 3. In the Ni-Ti sample, region 'A' predominates and corresponds to the phase NiTi. For the 10AlNiTi sample, Fig. 26 shows grey regions 'B' and 'C' corresponding to the Ti-rich ternary compounds (Table 3), while the bright region 'D' has a composition of 9±1 at.% Al, 50±2 at.% Ni and 41±2 at.% Ti. This is close to the NiTi phase, with some dissolved aluminum and can be denoted as NiTi(Al). A similar phase has been reported in literature for small additions of aluminum (<10 at.%) to NiTi [108,150]. As the aluminum content in the sample increases to 15 at.%, three distinctive regions (E, F and G) are seen in the micrograph. Nickel is the major component in region

'E', while 'F' is rich in titanium. Region 'G' has the composition 10±1 at.% Al, 46±1 at.% Ni and 44±1 at.% Ti, which is comparable to region 'D' in the 10AlNiTi sample. The SEM micrographs of 20-30AlNiTi samples mainly show dark grey regions and rounded bright particles. The titanium-rich grey regions consist of many particles (I, L, M and P) with various sizes which seem to be precipitated from the matrix (H, K and O). The size of the particles is observed to decrease with increasing aluminum content. The bright particles are nickel-rich and the composition corresponds to $AlNi_2Ti$ (τ_4) phase. The 35 and 40AlNiTi samples, after heating to 1200°C, show a continuous titanium and aluminum rich ternary matrix with large bright areas rich in nickel.

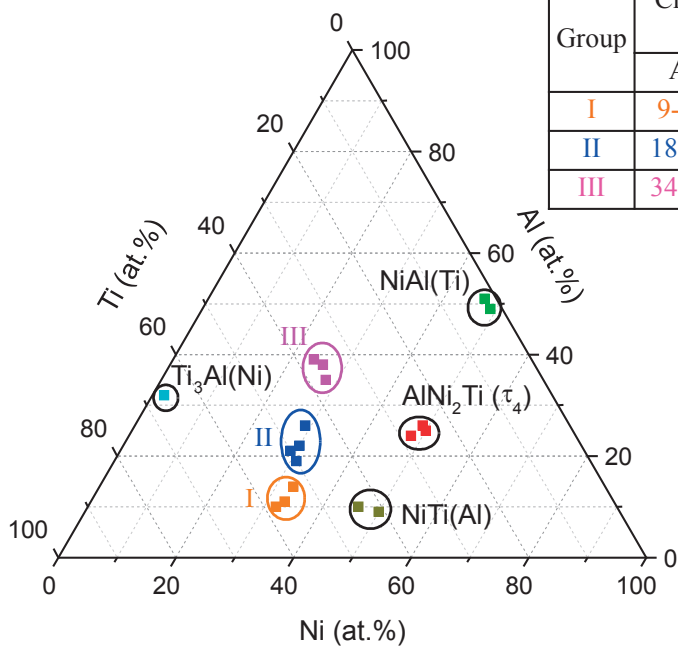

Group	Chemical composition (at. %)		
	Al	Ni	Ti
I	9-15	31-34	52-59
II	18-28	28-32	43-51
III	34-40	23-29	35-38

Fig. 27. Various phase compositions identified in the Al-Ni-Ti samples heated to 1200°C.

The compositions of the phases observed in the Al-Ni-Ti samples heated to 1200°C, which are presented in Table 3, are projected on a ternary diagram, as shown in Fig. 27. The phase compositions can be classified into several groups showing limited scatter. Each group can thus be considered as a homogeneous phase. Among these, four groups correspond to the phases $Ti_3Al(Ni)$, NiAl(Ti), NiTi(Al) and $AlNi_2Ti$ (τ_4), while the other three groups (I, II and III) do not correspond to other known ternary phases including $Al_{13}Ni_2Ti_5$ (τ_1), Al_2TiNi (τ_2), Al_3NiTi_2 (τ_3) and $Al_{65}Ni_{20}Ti_{15}$ (τ_5). This is understandable as $\tau_1$to τ_3 and τ_5 are rich in aluminum and the samples in the

present investigation contained a maximum of 40 at.% Al. Groups I and II cover titanium-rich compositions, while group III is rich in aluminum as well as titanium. The composition of group II can be represented as $Al_2Ni_3Ti_5$. This phase has been reported by Nash and Liang [115] in the isothermal section of Al-Ni-Ti at 900°C. However, the authors did not confirm this finding. Compositions in group III corresponding to $Al_{36}Ni_{28}Ti_{36}$ are also not reported in literature. Further work is required to study the structures and stabilities of the phases observed in groups I-III. Appended paper V presents details from the present study on the Al-Ni-Ti system.

4. Conclusions

In this work, an attempt has been made to characterize the reactive synthesis of transition metal aluminides and related intermetallic compounds from elemental powder mixtures in the Ti-Al, Fe-Al, Nb-Al, Ta-Al binary systems, as well as the Al-Ni-Ti ternary system. Important conclusions from the study are presented below.

- A pre-combustion stage can occur in the compacted samples when the contact between reactant particles is good enough to allow the diffusional reactions to occur in the solid state. Finer aluminum particles and slower heating rates enhance the pre-combustion reaction in the samples. Strong pre-combustion peaks in the DSC plots are generally associated with relatively weak combustion peaks.

- In the samples containing relatively low melting metals like iron and titanium, the combustion reaction can occur at temperatures below the melting point of aluminum, whereas refractory metal systems containing niobium and tantalum are associated with considerably higher onset temperatures.

- Aluminum-rich compounds were identified as initial products of the combustion reaction in all systems, regardless of the initial composition of the powder mixture. These compounds mostly showed the general formula MAl_3 where M corresponds to the respective transition metal in the system. However, Fe_2Al_5 was observed to form as the initial product of reaction between iron and aluminum.

- In general, reactive sintering of aluminum-rich samples resulted in a combustion reaction which goes to completion and forms a porous, but homogenous product (MAl_3).

- Samples with lower aluminum contents are associated with an incomplete combustion reaction and significant amounts of unreacted transition metal in the mixture. Lesser amounts of aluminum in the samples resulted in lower onset temperatures and sharper peaks for the combustion reaction.

- Further heating of samples containing unreacted particles resulted in multiphase, heterogeneous products. However, homogenized products can be obtained after prolonged heat treatment at sufficiently high temperatures, particularly in the case of refractory metals.

- Powders with relatively coarse particles and higher heating rates generally resulted in a higher onset temperature for the combustion reaction in the samples.

- In cases where the combustion peak corresponds to the formation of a single phase (for example MAl_3), enthalpy of formation of the compound can be estimated. Further, with the knowledge of the increase in onset temperature with increasing heating rate, the apparent activation energy for the reaction can be estimated using model-free, isoconversion methods.

- Addition of aluminum to equiatomic nickel-titanium powder mixtures was associated with the initiation of a combustion reaction between nickel and aluminum, resulting in the formation of some aluminum-rich compounds. This was followed by the combustion reaction between nickel and titanium at higher temperatures above which various binary and ternary compounds were formed. Further work is required to investigate the structures and stabilities of some previously unidentified phases found in this study.

- Results obtained in this study showed the possibility of obtaining various products with different phases. Optimizing the process variables is very important in order to synthesize homogeneous, single-phase intermetallic compounds or a mixture of phases with desired properties.

Future work

As a natural extension to the present study, further work can focus on characterizing the formation of aluminides in several ternary systems, similar to the current work on the Al-Ni-Ti system. This is with a view to synthesizing several binary and ternary aluminides, with potential for high temperature use. Small punch testing is suggested for determining the high temperature creep properties of these compounds.

References

[1] G.E.R. Schulze, Metallphysik, Berichte Der Bunsengesellschaft Für Phys. Chemie. 72 (1968) 359–360. doi:10.1002/bbpc.19680720284.

[2] D.J. Hartl, D.C. Lagoudas, Aerospace applications of shape memory alloys, Proc. Inst. Mech. Eng. Part G J. Aerosp. Eng. 221 (2007) 535–552. doi:10.1243/09544100JAERO211.

[3] E.A. Loria, Quo vadis gamma titanium aluminide, Intermetallics. 9 (2001) 997–1001. doi:10.1016/S0966-9795(01)00064-4.

[4] I. Gurrappa, A. Wilson, P.K. Datta, Palladium and tantalum aluminide coatings for high-temperature oxidation resistance of titanium alloy IMI 834, J. Coatings Technol. Res. 6 (2009) 257–268. doi:10.1007/s11998-008-9113-9.

[5] C.T. Liu, J. Stringer, J.N. Mundy, L.L. Horton, P. Angelini, Ordered intermetallic alloys: an assessment, 1997. doi:10.1016/S0966-9795(97)00045-9.

[6] T. Duerig, A. Pelton, D. Stöckel, An overview of nitinol medical applications, Mater. Sci. Eng. A. 273-275 (1999) 149–160. doi:10.1016/S0921-5093(99)00294-4.

[7] M.H. Elahinia, M. Hashemi, M. Tabesh, S.B. Bhaduri, Manufacturing and processing of NiTi implants: A review, Prog. Mater. Sci. 57 (2012) 911–946. doi:10.1016/j.pmatsci.2011.11.001.

[8] B.Y. Li, L.J. Rong, Y.Y. Li, V. Gjunter, A recent development in producing porous Ni–Ti shape memory alloys, Intermetallics. 8 (2000) 881–884. doi:10.1016/S0966-9795(00)00024-8.

[9] R.L. Fleischer, R.D. Field, K.K. Denike, R.J. Zabala, Mechanical properties of alloys of IrNb and other high-temperature intermetallic compounds, Metall. Trans. A. 21 (1990) 3063–3074. doi:10.1007/BF02647304.

[10] J.H. Westbrook, R.L. Fleischer, eds., Intermetallic Compounds, Volume 1-Crystal structures of intermetallic compounds, Wiley, 2000. ISBN: 9780471608806.

[11] C.T. Liu, J.O. Stiegler, F.H. Froes, Ordered intermetallics, in: ASM Handbook-Volume 2, 10th ed., ASM International, 1990: pp. 913–942. ISBN: 0-87170-378-5.

[12] S.C. Deevi, V.K. Sikka, Nickel and iron aluminides: an overview on properties, processing, and applications, Intermetallics. 4 (1996) 357–375. doi:10.1016/0966-9795(95)00056-9.

[13] V. Gauthier, F. Bernard, E. Gaffet, C. Josse, J.P. Larpin, In-situ time resolved X-ray diffraction study of the formation of the nanocrystalline $NbAl_3$ phase by mechanically activated self-propagating high-temperature synthesis reaction, Mater. Sci. Eng. A. 272 (1999) 334–341. doi:10.1016/S0921-5093(99)00488-8.

[14] D.J. Duquette, Environmental resistance of intermetallic compounds and composite materials, Mater. Sci. Eng. A. 198 (1995) 205–211. doi:10.1016/0921-5093(95)80075-6.

[15] C. Zanotti, P. Giuliani, a. Terrosu, S. Gennari, F. Maglia, Porous Ni–Ti ignition and combustion synthesis, Intermetallics. 15 (2007) 404–412. doi:10.1016/j.intermet.2006.08.002.

[16] J.J. Moore, H.J. Feng, Combustion synthesis of advanced materials: Part I. Reaction parameters, Prog. Mater. Sci. 39 (1995) 243–273. doi:10.1016/0079-6425(94)00011-5.

[17] J.J. Moore, H.J. Feng, Combustion synthesis of advanced materials: Part II. Classification, applications and modelling, Prog. Mater. Sci. 39 (1995) 275–316. doi:10.1016/0079-6425(94)00012-3.

[18] S. Gennari, U.A. Tamburini, F. Maglia, G. Spinolo, Z. A. Munir, A new approach to the modeling of SHS reactions: Combustion synthesis of transition metal aluminides, Acta Mater. 54 (2006) 2343–235. doi:10.1016/j.actamat.2006.01.009.

[19] C. Curfs, I.G. Cano, G.B.M. Vaughan, X. Turrillas, Å. Kvick, M.A. Rodriguez, TiC–NiAl composites obtained by SHS: a time-resolved XRD study, J. Eur. Ceram. Soc. 22 (2002) 1039–1044. doi:10.1016/S0955-2219(01)00414-9.

[20] L.M. Peng, Synthesis and mechanical properties of niobium aluminide-based composites, Mater. Sci. Eng. A. 480 (2008) 232–236.doi:10.1016/j.msea.2007.07.046.

[21] L. Murugesh, K.T. Venkateswara Rao, R.O. Ritchie, Powder processing of ductile-phase-toughened Nb-Nb_3Al in situ composites, Mater. Sci. Eng. A. 189 (1994) 201–208. doi:10.1016/0921-5093(94)90416-2.

[22] C.L. Yeh, Y.S. Chen, Studies of Ta, Al, and carbon sources on combustion synthesis of alumina–tantalum carbide composites, Mater. Manuf. Process. 30 (2014) 298–302. doi:10.1080/10426914.2013.852221.

[23] K. Morsi, J. Wall, J. Rodriguez, S.O. Moussa, Reactive thermomechanical processing of intermetallic materials, J. Mater. Eng. Perform. 12 (2003) 147–156. doi:10.1361/105994903770343286.

[24] B.Y. Li, L.J. Rong, Y.Y. Li, V.E. Gjunter, Synthesis of porous Ni-Ti shape-memory alloys by self propagating high temperature synthesis, Acta Metall. 48 (2000) 3895–3904. doi:10.1016/S1359-6454(00)00184-1.

[25] G. Tosun, L. Ozler, M. Kaya, N. Orhan, A study on microstructure and porosity of NiTi alloy implants produced by SHS, J. Alloys Compd. 487 (2009) 605–611. doi:10.1016/j.jallcom.2009.08.023.

[26] B.H. Rabin, R.N. Wright, Synthesis of iron aluminides from elemental powders: Reaction mechanisms and densification behavior, Metall. Trans. A. 22 (1991) 277–286. doi:10.1007/BF02656797.

[27] A. Varma, A.S. Mukasyan, Combustion synthesis of intermetallic compounds, in: A.A. Borisov, L.T. De Luca, A.G. Merzhanov (Eds.), Self-Propagating High-Temp. Synth. Mater., Taylor & Francis, 2002: pp. 1–34.

[28] E. Chin, R. Biederman, The titanium-aluminum phase diagram, A Review of the near Ti-50at.% Al phase fields, U.S. Army materials technology laboratory, Worcester, MA, 1992.

[29] G. Sauthoff, Intermetallic materials for structural high temperature applications, in: P. Beiss, R. Ruthardt, H. Warlimont (Eds.), Powder Metall. Data. Refract. Hard Intermet. Mater., Springer-Verlag, Berlin/Heidelberg, 2002: pp. 225–257. doi:10.1007/10858641_18.

[30] M.G. Mendiratta, H.A. Lipsitt, High-temperature ordered intermetallic alloys, C. Koch, C.T. Liu, N.S. Stollof (Eds.), Materials Research Society, Pittsburgh, USA, 1985: pp. 155–162.

[31] S. Vaucher, M. Stir, K. Ishizaki, J.M. Catala-Civera, R. Nicula, Reactive synthesis of Ti–Al intermetallics during microwave heating in an E-field maximum, Thermochim. Acta. 522 (2011) 151–154. doi:10.1016/j.tca.2010.11.026.

[32] B. Hugh (Ed.), ASM Handbook-Volume 3: Alloy phase diagrams, ASM International, Materials Park, Ohio, 1992, (a) p. 2.54, (b) p. 2.44, (c) p. 2.48, ISBN:0-87170-381-5.

[33] H. Okamoto, Al-Ti (Aluminum-Titanium), J. Phase Equilibria. 14 (1993) 120–121. doi:10.1007/BF02652171.

[34] M. Yamaguchi, H. Inui, K. Ito, High-temperature structural intermetallics, Acta Mater. 48 (2000) 307–322. doi:10.1016/S1359-6454(99)00301-8.

[35] L.E. Murr, S.M. Gaytan, A. Ceylan, E. Martinez, J.L. Martinez, D.H. Hernandez, et al., Characterization of titanium aluminide alloy components fabricated by additive manufacturing using electron beam melting, Acta Mater. 58 (2010) 1887–1894. doi:10.1016/j.actamat.2009.11.032.

[36] F. Appel, M. Oehering, Alloy design and properties, in: C. Leyens, M. Peters (Eds.), Titanium and titanium alloys, Wiley-VCH Verlag GmbH, Weinheim, 2003: pp. 89–152.

[37] J.H. Westbrook, R.L. Fleischer, eds., Intermetallic compounds-principles and practice, John Wiley & Sons, Inc., Chichester, UK, 2002. doi:10.1002/0470845856.

[38] H.C. Yi, A. Petric, J.J. Moore, Effect of heating rate on the combustion synthesis of Ti-Al intermetallic compounds, J. Mater. Sci. 27 (1992) 6797–6806. doi:10.1007/BF01165971.

[39] M. Adeli, S.H. Seyedein, M.R. Aboutalebi, M. Kobashi, N. Kanetake, A study on the combustion synthesis of titanium aluminide in the self-propagating mode, J. Alloys Compd. 497 (2010) 100–104. doi:10.1016/j.jallcom.2010.03.050.

[40] N. Bertolino, M. Monagheddu, A. Tacca, P. Giuliani, C. Zanotti, U. Anselmi Tamburini, Ignition mechanism in combustion synthesis of Ti–Al and Ti–Ni systems, Intermetallics. 11 (2003) 41–49. doi:10.1016/S0966-9795(02)00128-0.

[41] Y. Mishin, C. Herzig, Diffusion in the Ti–Al system, Acta Mater. 48 (2000) 589–623. doi:10.1016/S1359-6454(99)00400-0.

[42] R. Orru, G. Cao, Z.A. Munir, Mechanistic investigation of the field-activated combustion synthesis (FACS) of titanium aluminides, Chem. Eng. Sci. 54 (1999) 3349–3355. doi:10.1016/S0009-2509(98)00459-X.

[43] S. Lee, J. Lee, Y. Lee, Effect of heating rate on the combustion synthesis of intermetallics, Mater. Sci. Eng. A. 281 (2000) 275–285. doi:10.1016/S0921-5093(99)00715-7.

[44] T. Wang, R. Liu, M. Zhu, J. Zhang, Physical simulation of the effect of sample volume on ignition temperature in the thermal explosion synthesis of Ti+3Al→$TiAl_3$, Mater. Lett. 57 (2003) 2151–2155. doi:10.1016/S0167-577X(02)01164-3.

[45] T. Wang, R. Liu, M. Zhu, J. Zhang, Activation energy of self-heating process studied by DSC, J. Therm. Anal. Calorim. 70 (2002) 507–519. doi:10.1023/A:1021684726126.

[46] J. Maas, G. Bastin, F. van Loo, R. Metselaar, The texture in diffusion-grown layers of trialuminides $MeAl_3$ (Me= Ti, V, Ta, Nb, Zr, Hf) and VNi_3, Zeitschrift Fuer Met. 74 (1983) 294–299.

[47] J.G. Luo, V.L. Acoff, Using cold roll bonding and annealing to process Ti/Al multi-layered composites from elemental foils, Mater. Sci. Eng. A. 379 (2004) 164–172. doi:10.1016/j.msea.2004.01.021.

[48] F.J. van Loo, G. Rieck, Diffusion in the titanium-aluminium system–I. Interdiffusion in the composition range between 25 and 100 at.% Ti, Acta Metall. 21 (1973) 73–84. doi:10.1016/0001-6160(73)90221-6.

[49] M. Mirjalili, M. Soltanieh, K. Matsuura, M. Ohno, On the kinetics of $TiAl_3$ intermetallic layer formation in the titanium and aluminum diffusion couple, Intermetallics. 32 (2013) 297–302. doi:10.1016/j.intermet.2012.08.017.

[50] J.K. Howard, R.F. Lever, P.J. Smith, Kinetics of compound formation in thin film couples of Al and transition metals, J. Vac. Sci. Technol. 13 (1976) 68. doi:10.1116/1.568959.

[51] E.G. Colgan, J.W. Mayer, Thin-film reactions of Al with Co, Cr, Mo, Ta, Ti, and W, J. Mater. Res. 4 (2011) 815–820. doi:10.1557/JMR.1989.0815.

[52] D.J. Goda, N.L. Richards, W.F. Caley, M.C. Chaturvedi, The effect of processing variables on the structure and chemistry of Ti-aluminide based LMCS, Mater. Sci. Eng. A. 334 (2002) 280–290. doi:10.1016/S0921-5093(01)01894-9.

[53] X.A. Zhao, F.C.T. So, M.A. Nicolet, $TiAl_3$ formation by furnace annealing of Ti/Al bilayers and the effect of impurities, J. Appl. Phys. 63 (1988) 2800. doi:10.1063/1.340981.

[54] M. Thuillard, L.T. Tran, M.A. Nicolet, Al_3Ti formation by diffusion of aluminum through titanium, Thin Solid Films. 166 (1988) 21–28. doi:10.1016/0040-6090(88)90362-8.

[55] L.Z. Zhang, D.N. Wang, B.Y. Wang, R.S. Yu, L. Wei, Annealing studies of Ti/Al multilayer film by slow positron beam, Appl. Surf. Sci. 253 (2007) 7309–7312. doi:10.1016/j.apsusc.2007.03.016.

[56] L. Xu, Y.Y. Cui, Y.L. Hao, R. Yang, Growth of intermetallic layer in multi-laminated Ti/Al diffusion couples, Mater. Sci. Eng. A. 435-436 (2006) 638–647. doi:10.1016/j.msea.2006.07.077.

[57] K. Natesan, Corrosion performance of iron aluminides in mixed-oxidant environments, Mater. Sci. Eng. A. 258 (1998) 126–134. doi:10.1016/S0921-5093(98)00925-3.

[58] M. Eggersmann, H. Mehrer, Diffusion in intermetallic phases of the Fe-Al system, Philos. Mag. A. 80 (2000) 1219–1244. doi:10.1080/01418610008212112.

[59] N.S. Stoloff, Iron aluminides: present status and future prospects, Mater. Sci. Eng. A. 258 (1998) 1–14. doi:10.1016/S0921-5093(98)00909-5.

[60] C.T. Liu, E.P. George, P.J. Maziasz, J.H. Schneibel, Recent advances in B2 iron aluminide alloys: deformation, fracture and alloy design, Mater. Sci. Eng. A. 258 (1998) 84–98. doi:10.1016/S0921-5093(98)00921-6.

[61] S.C. Deevi, V.K. Sikka, C.T. Liu, Processing, properties, and applications of nickel and iron aluminides, Prog. Mater. Sci. 42 (1997) 177–192. doi:10.1016/S0079-6425(97)00014-5.

[62] S.C. Deevi, Powder processing of FeAl sheets by roll compaction, Intermetallics. 8 (2000) 679–685. doi:10.1016/S0966-9795(99)00129-6.

[63] S. Gedevanishvili, S.C. Deevi, Processing of iron aluminides by pressureless sintering through Fe+Al elemental route, Mater. Sci. Eng. A. 325 (2002) 163–176. doi:10.1016/S0921-5093(01)01442-3.

[64] A. Bahadur, B.R. Kumar, O.N. Mohanty, Ductility improvement in iron aluminides, J. Mater. Sci. 30 (1995) 3690–3696. doi:10.1007/BF00351886.

[65] D.A. Eelman, J.R. Dahn, G.R. MacKay, R.A. Dunlap, An investigation of mechanically alloyed Fe–Al, J. Alloys Compd. 266 (1998) 234–240. doi:10.1016/S0925-8388(97)00508-2.

[66] M.H. Enayati, M. Salehi, Formation mechanism of Fe_3Al and FeAl intermetallic compounds during mechanical alloying, J. Mater. Sci. 40 (2005) 3933–3938. doi:10.1007/s10853-005-0718-4.

[67] D. Oleszak, P.H. Shingu, Mechanical alloying in the Fe-Al system, Mater. Sci. Eng. A. 181-182 (1994) 1217–1221. doi:10.1016/0921-5093(94)90834-6.

[68] H. Gao, Y. He, P. Shen, J. Zou, N. Xu, Y. Jiang, et al., Porous FeAl intermetallics fabricated by elemental powder reactive synthesis, Intermetallics. 17 (2009) 1041–1046. doi:10.1016/j.intermet.2009.05.007.

[69] B.H. Rabin, R.N. Wright, Microstructure and tensile properties of Fe_3Al produced by combustion synthesis/hot isostatic pressing, Metall. Trans. A. 23 (1992) 35–40 doi:10.1007/BF02660848.

[70] X. Wang, J. V. Wood, Y. Sui, H. Lu, Formation of intermetallic compound in iron-aluminum alloys, J. Shanghai Univ. (English) Ed. 2 (1998) 305–310. doi:10.1007/s11741-998-0045-5.

[71] H.R. Shahverdi, M.R. Ghomashchi, S. Shabestari, J. Hejazi, Microstructural analysis of interfacial reaction between molten aluminium and solid iron, J. Mater. Process. Technol. 124 (2002) 345–352. doi:10.1016/S0924-0136(02)00225-X.

[72] D. Naoi, M. Kajihara, Growth behavior of Fe_2Al_5 during reactive diffusion between Fe and Al at solid-state temperatures, Mater. Sci. Eng. A. 459 (2007) 375–382. doi:10.1016/j.msea.2007.01.099.

[73] R.M. German, Transient thermal effects in the synthesis of intermetallic alloys, in: R.D. Shull, A. Joshi (Eds.), Therm. Anal. Metall., The Minerals, Metals and Materials Society, 1992: pp. 205–231.

[74] K. Bouche, F. Barbier, A. Coulet, Intermetallic compound layer growth between solid iron and molten aluminium, Mater. Sci. Eng. A. 249 (1998) 167–175. doi:10.1016/S0921-5093(98)00573-5.

[75] M. Kajihara, Quantitative Evaluation of interdiffusion in Fe_2Al_5 during reactive diffusion in the binary Fe–Al system, Mater. Trans. 47 (2006) 1480–1484. doi:10.2320/matertrans.47.1480.

[76] H.Z. Kang, C.T. Hu, Swelling behavior in reactive sintering of Fe–Al mixtures, Mater. Chem. Phys. 88 (2004) 264–272. doi:10.1016/j.matchemphys.2004.03.001.

[77] J.S. Sheasby, Powder metallurgy of iron-aluminum, Int. J. Powder Metall. Powder Technol. 15 (1979) 301–305.

[78] D.L. Joslin, D.S. Easton, C.T. Liu, S. A. David, Reaction synthesis of Fe-Al alloys, Mater. Sci. Eng. A. 192-193 (1995) 544–548. doi:10.1016/0921-5093(94)03272-6.

[79] B.H. Rabin, R.N. Wright, J.R. Knibloe, Reaction processing of iron aluminides, Mater. Sci. Eng. A. 153 (1992) 706–711. doi:10.1016/0921-5093(92)90275-6.

[80] J.L. Jorda, R. Flükiger, J. Muller, A New metallurgical investigation of the niobium-aluminium system, J. Less Common Met. 75 (1980) 227–239. doi:10.1016/0022-5088(80)90120-4.

[81] C. Milanese, F. Maglia, A. Tacca, U. Anselmi-Tamburini, C. Zanotti, P. Giuliani, Ignition and reaction mechanism of Co–Al and Nb–Al intermetallic compounds prepared by combustion synthesis, J. Alloys Compd. 421 (2006) 156–162. doi:10.1016/j.jallcom.2005.08.091.

[82] Z. Liu, Y. Chen, L. Du, P. Li, Y. Cui, X. Pan, et al., Preparation of Nb_3Al superconductor by powder metallurgy and effect of mechanical alloying on the phase formation, J. Mod. Transp. 22 (2014) 55–58.doi:10.1007/s40534-014-0036-0.

[83] N. Koizumi, T. Takeuchi, K. Okuno, Development of advanced Nb_3Al superconductors for a fusion demo plant, Nucl. Fusion. 45 (2005) 431–438. doi:10.1088/0029-5515/45/6/004.

[84] V.N. Yerembnko, Y.V. Natanzon, V.I. Dybkov, Interaction of the refractory metals with liquid aluminium, J. Less Common Met. 50 (1976) 29–48. doi:10.1016/0022-5088(76)90251-4.

[85] V. Gauthier, F. Bernard, E. Gaffet, D. Vrel, M. Gailhanou, J.P. Larpin, Investigations of the formation mechanism of nanostructured $NbAl_3$ via MASHS reaction, Intermetallics. 10 (2002) 377–389. doi:10.1016/S0966-9795(02)00010-9.

[86] R.M.L. Neto, P.I. Ferreira, Progress of the $NbAl_3$ combustion synthesis reaction, J. Mater. Synth. Process. 7 (1999) 245–252.doi:10.1023/A%3A1021853627411.

[87] C.R. Kachelmyer, A.S. Rogachev, A. Varma, Mechanistic and processing studies in combustion synthesis of niobium aluminides, J. Mater. Res. 10 (1995) 2260–2270. doi:10.1557/JMR.1995.2260.

[88] F. Buracovas, V.S. Gonçalves, C.J. Rocha, R.M.L. Neto, Combustion synthesis of mechanically-activated Nb-Al mixtures, Mater. Sci. Forum. 498-499 (2005) 152–157. doi:10.4028/www.scientific.net/MSF.498-499.152.

[89] K.R. Coffey, K. Barmak, D. A. Rudman, S. Foner, Thin film reaction kinetics of niobium/aluminum multilayers, J. Appl. Phys. 72 (1992) 1341. doi:10.1063/1.351744.

[90] T. Oğurtani, Kinetics of diffusion in the Nb-Al system, Metall. Trans. 3 (1972) 425–429. doi:10.1007/BF02642046.

[91] P.R. Subramanian, D.B. Miracle, S. Mazdiyasni, Phase relationships in the Al-Ta system, Metall. Trans. A. 21 (1990) 539–545, doi:10.1007/BF02671926.

[92] P. Kofstad, S. Espevik, Oxidation of tantalum coated with aluminum and aluminum-chromium alloys, J. Less Common Met. 12 (1967) 117–138. doi:10.1016/0022-5088(67)90095-1.

[93] J.C. Schuster, Phases and phase relations in the system Ta-Al, Zeitschrift Fuer Met. Res. Adv. Tech. 76 (1985) 724–727. ISSN: 0044-3093.

[94] H. Okamoto, Al-Ta (Aluminum-Tantalum), J. Phase Equilibria Diffus. 31 (2010) 1–2. doi:10.1007/s11669-010-9786-5.

[95] A. Boulineau, J.M. Joubert, R. Černý, Structural characterization of the Ta-rich part of the Ta–Al system, J. Solid State Chem. 179 (2006) 3385–3393. doi:10.1016/j.jssc.2006.07.001.

[96] Y. Du, R. Schmid-Fetzer, Thermodynamic modeling of the Al-Ta system, J. Phase Equilibria. 17 (1996) 311–324. doi:10.1007/BF02665557.

[97] V.T. Witusiewicz, A.A. Bondar, U. Hecht, J. Zollinger, V.M. Petyukh, O.S. Fomichov, et al., Experimental study and thermodynamic re-assessment of the binary Al-Ta system, Intermetallics. 18 (2010) 92–106.doi:10.1016/j.intermet.2009.06.015.

[98] S. Mahne, F. Krumeich, B. Harbrecht, Phase relations in the Al-Ta system: on the translational symmetries of Al_3Ta_2 and AlTa, J. Alloys Compd. 201 (1993) 167–174. doi:10.1016/0925-8388(93)90879-R.

[99] S. Mahne, B. Harbrecht, F. Krumeich, Phase relations in the Al-Ta system: on the translational symmetries of a triclinic structure and a new hexagonal giant cell structure, J. Alloys Compd. 218 (1995) 177–182.doi:10.1016/0925-8388(94)01411-6.

[100] S. Mahne, B. Harbrecht, $Al_{69}Ta_{39}$ – a new variant of a face-centred cubic giant cell structure, J. Alloys Compd. 203 (1994) 271–279.doi:10.1016/0925-8388(94)90746-3.

[101] C.K. Chung, Y.L. Chang, T.S. Chen, P.J. Su, Annealing effects on microstructure and properties of Ta–Al thin film resistors, Surf. Coatings Technol. 201 (2006) 4195–4200. doi:10.1016/j.surfcoat.2006.08.059.

[102] C.L. Yeh, H.J. Wang, Formation of Ta–Al intermetallics by combustion synthesis involving Al-based thermite reactions, J. Alloys Compd. 491 (2010) 153–158. doi:10.1016/j.jallcom.2009.10.203.

[103] V. Raghavan, Al-Ni-Ti (Aluminum-Nickel-Titanium), J. Phase Equilibria Diffus. 31 (2010) 55–56. doi:10.1007/s11669-009-9626-7.

[104] J.C. Schuster, Z. Pan, S. Liu, F. Weitzer, Y. Du, On the constitution of the ternary system Al-Ni-Ti, Intermetallics. 15 (2007) 1257–1267.doi:10.1016/j.intermet.2007.03.003.

[105] A. Debski, W. Gąsior, A. Sypień, A. Góral, Enthalpy of formation of intermetallic phases from Al-Ni and Al-Ni-Ti systems, Intermetallics. 42 (2013) 92–98. doi:10.1016/j.intermet.2013.05.016.

[106] S.O. Gashti, A. Shokuhfar, R. Ebrahimi-Kahrizsangi, B. Nasiri-Tabrizi, Synthesis of nanocrystalline intermetallic compounds in Ni-Ti-Al system by mechanothermal method, J. Alloys Compd. 491 (2010) 344–348.doi:10.1016/j.jallcom.2009.10.169.

[107] R. Hu, P. Nash, Q. Chen, Enthalpy of formation in the Al-Ni-Ti system, J. Phase Equilibria Diffus. 30 (2009) 559–563.doi:10.1007/s11669-009-9573-3.

[108] T. Kurita, H. Matsumoto, K. Sakamoto, K. Tanji, H. Abe, Effect of aluminum addition on the transformation of NiTi alloy, J. Alloys Compd. 396 (2005) 193–196. doi:10.1016/j.jallcom.2004.12.032.

[109] J.C. Schuster, Critical data evaluation of the aluminium-nickel-titanium system, Intermetallics. 14 (2006) 1304–1311.doi:10.1016/j.intermet.2005.11.027.

[110] K. Morsi, Review: Reaction synthesis processing of Ni-Al intermetallic materials, Mater. Sci. Eng. A. 299 (2001) 1–15. doi:10.1016/S0921-5093(00)01407-6.

[111] S.L. Draper, D. Krause, B. Lerch, I.E. Locci, B. Doehnert, R. Nigam, et al., Development and evaluation of TiAl sheet structures for hypersonic applications, Mater. Sci. Eng. A. 464 (2007) 330–342.doi:10.1016/j.msea.2007.02.020.

[112] K. Otsuka, X. Ren, Physical metallurgy of Ti-Ni-based shape memory alloys, Prog. Mater. Sci. 50 (2005) 511–678.doi:10.1016/j.pmatsci.2004.10.001.

[113] L. Krone, E. Schüller, M. Bram, O. Hamed, H.P. Buchkremer, D. Stöver, Mechanical behaviour of NiTi parts prepared by powder metallurgical methods, Mater. Sci. Eng. A. 378 (2004) 185–190.doi:10.1016/j.msea.2003.10.345.

[114] K.J. Lee, P. Nash, The Al-Ni-Ti system (Aluminum-Nickel-Titanium), J. Phase Equilibria. 12 (1991) 551–562. doi:10.1007/BF02645068.

[115] P. Nash, W.W. Liang, Phase equilibria in the Ni-Al-Ti system at 1173K, Metall. Trans. A. 16 (1985) 319–322. doi:10.1007/BF02814329.

[116] P. Nash, V. Vejins, W.W. Liang, The Al–Ni–Ti system, Bull. Alloy Phase Diagrams. 3 (1982) 367–374. doi:10.1007/BF02869316.

[117] K. Zeng, R. Schmid-fetzer, B. Huneau, P. Rogl, J. Bauer, The ternary system Al-Ni-Ti Part I: Isothermal section at 900°C; Experimental investigation and thermodynamic calculation, Intermetallics. 7 (1999) 1337–1345.doi:10.1016/S0966-9795(99)00055-2.

[118] V. Raghavan, Al-Ni-Ti (Aluminum-Nickel-Titanium), J. Phase Equilibria Diffus. 26 (2005) 268–272. doi:10.1361/15477030523652.

[119] A.S. Jabur, J.T. Al-Haidary, E.S. Al-Hasani, Characterization of Ni-Ti shape memory alloys prepared by powder metallurgy, J. Alloys Compd. 578 (2013) 136–142. doi:10.1016/j.jallcom.2013.05.029.

[120] P. Novák, P. Pokorný, V. Vojtěch, A. Knaislová, A. Školáková, J. Čapek, et al., Formation of Ni–Ti intermetallics during reactive sintering at 500–650°C, Mater. Chem. Phys. 155 (2015) 113–121.doi:10.1016/j.matchemphys.2015.02.007.

[121] M. Whitney, S.F. Corbin, R.B. Gorbet, Investigation of the mechanisms of reactive sintering and combustion synthesis of NiTi using differential scanning calorimetry and microstructural analysis, Acta Mater. 56 (2008) 559–570. doi:10.1016/j.actamat.2007.10.012.

[122] M. Whitney, S.F. Corbin, R.B. Gorbet, Investigation of the influence of Ni powder size on microstructural evolution and the thermal explosion combustion synthesis of NiTi, Intermetallics. 17 (2009) 894–906. doi:10.1016/j.intermet.2009.03.018.

[123] G.K. Dey, Micropyretic synthesis of NiTi in propagation mode, Acta Mater. 51 (2003) 2549–2568. doi:10.1016/S1359-6454(03)00055-7.

[124] M. Sharma, B.C. Maji, M. Krishnan, A study on the phase transformation behavior of Al substituted Ni-rich and Ti-rich Ni-Ti-Al alloys, Phys. Procedia. 10 (2010) 28–32. doi:10.1016/j.phpro.2010.11.070.

[125] A. Biswas, S.K. Roy, Comparison between the microstructural evolutions of two modes of SHS of NiAl: Key to a common reaction mechanism, Acta Mater. 52 (2004) 257–270. doi:10.1016/j.actamat.2003.08.018.

[126] T.S. Dyer, Z.A. Munir, The synthesis of nickel aluminides by multilayer self-propagating combustion, Metall. Mater. Trans. B. 26 (1995) 603–610. doi:10.1007/BF02653881.

[127] K.A. Philpot, Z.A. Munir, J.B. Holt, An investigation of the synthesis of nickel aluminides through gasless combustion, J. Mater. Sci. 22 (1987) 159–169. doi:10.1007/BF01160566.

[128] L. Plazanet, F. Nardou, Reaction process during relative sintering of NiAl, J. Mater. Sci. 3 (1998) 2129–2136. doi:10.1023/A:1004375304423.

[129] G.K. Dey, Physical metallurgy of nickel aluminides, Sadhana. 28 (2003) 247–262. doi:10.1007/BF02717135.

[130] N.S. Stoloff, Physical and mechanical metallurgy of Ni_3Al and its alloys, Int. Mater. Rev. 34 (1989) 153–184. doi:10.1179/imr.1989.34.1.153.

[131] P.R. Strutt, R.S. Polvani, J.C. Ingram, Creep behavior of the heusler type structure alloy Ni_2AlTi, Metall. Trans. A. 7 (1976) 23–31.doi:10.1007/BF02644035.

[132] P. Villars, K. Cenzual, Pearson's crystal data: Crystal structure database for inorganic compounds, Release 2012/13, ASM International, Materials Park, Ohio, USA.

[133] E. Pocheć, S. Jóźwiak, K. Karczewski, Z. Bojar, Maps of Fe–Al phases formation kinetics parameters during isothermal sintering, Thermochim. Acta. 545 (2012) 14–19. doi:10.1016/j.tca.2012.06.015.

[134] M. Salamon, H. Mehrer, Interdiffusion, Kirkendall effect, and Al self-diffusion in iron–aluminium alloys, Zeitschrift Für Met. 96 (2005) 4–16. doi:10.3139/146.018071.

[135] M.J. Starink, Activation energy determination for linear heating experiments: deviations due to neglecting the low temperature end of the temperature integral, J. Mater. Sci. 42 (2006) 483–489.doi:10.1007/s10853-006-1067-7.

[136] M.J. Starink, Analysis of aluminium based alloys by calorimetry: quantitative analysis of reactions and reaction kinetics, Int. Mater. Rev. 49 (2004) 191–226. doi:10.1179/095066004225010532.

[137] M.J. Starink, The determination of activation energy from linear heating rate experiments: a comparison of the accuracy of isoconversion methods, Thermochim. Acta. 404 (2003) 163–176. doi:10.1016/S0040-6031(03)00144-8.

[138] A. Biswas, Porous NiTi by thermal explosion mode of SHS: processing, mechanism and generation of single phase microstructure, Acta Mater. 53 (2005) 1415–1425. doi:10.1016/j.actamat.2004.11.036.

[139] Z. Yang, D. Schryvers, Composition gradients surronding Ni_4Ti_3 precipitates in a NiTi alloy studied by EELS, EFTEM and EDX, Int. J. Appl. Electromagn. Mech. 23 (2006) 17–24.

[140] C.H. Kuang, C. Chien, S.K. Wu, Multistage martensitic transformation in high temperature aged Ti48Ni52 shape memory alloy, Intermetallics. 67 (2015) 12–18. doi:10.1016/j.intermet.2015.07.012.

[141] B.Y. Tay, C.W. Goh, M.S. Yong, A.M. Soutar, Q. Li, M.K. Ho, et al., Self-propagating high-temperature synthesis of porous NiTi, SIMTech Tech. Reports. 7 (2006) 21–25.

[142] T. Tadaki, Y. Nakata, K. Shimizu, K. Otsuka, Crystal structure, composition and morphology of a precipitate in an aged Ti-51 at.%Ni shape memory alloy, Trans. JIM. 27 (1986) 731–740. ISSN:0021-4434.

[143] H.X. Dong, Y. Jiang, Y.H. He, M. Song, J. Zou, N.P. Xu, et al., Formation of porous Ni-Al intermetallics through pressureless reaction synthesis, J. Alloys Compd. 484 (2009) 907–913. doi:10.1016/j.jallcom.2009.05.079.

[144] E. Ma, C. V. Thompson, L. A. Clevenger, Nucleation and growth during reactions in multilayer Al/Ni films: The early stage of Al_3Ni formation, J. Appl. Phys. 69 (1991) 2211–2218. doi:10.1063/1.348722.

[145] G. Wang, M. Dahms, Synthesizing gamma-TiAl alloys by reactive powder processing, JOM. 45 (1993) 52–56. doi:10.1007/BF03223221.

[146] H. Sina, S. Iyengar, Reactive synthesis and characterization of titanium aluminides produced from elemental powder mixtures, J. Therm. Anal. Calorim. In Press. (2015). doi:10.1007/s10973-015-4815-6.

[147] I. Barin, Thermochemical data of pure substances, Wiley-VCH Verlag GmbH, Weinheim, Germany, Germany, 1995.doi:10.1002/9783527619825.

[148] Y. Yan, Y. Zheng, H. Yu, H. Bu, X. Cheng, N. Zhao, Effect of sintering temperature on the microstructure and mechanical properties of Ti(C, N)-based cermets, Powder Metall. Met. Ceram. 46 (2007) 449–453. doi:10.1007/s11106-007-0070-0.

[149] ICDD (2010) pdf4+ 2010 (Database), edited by S. Kabekkodu, International Centre for Diffraction Data, Newtown Square, PA, USA.

[150] M.M. Verdian, Fabrication of supersaturated NiTi(Al) alloys by mechanical alloying, Mater. Manuf. Process. 25 (2010) 1437–1439.doi:10.1080/10426914.2010.501093

Paper I

H. Sina, S. Iyengar

Reactive synthesis and characterization of titanium aluminides produced from elemental powder mixtures

Journal of Thermal Analysis and Calorimetry, 2015
DOI: 0.1007/s10973-015-4815-6

J Therm Anal Calorim
DOI 10.1007/s10973-015-4815-6

Reactive synthesis and characterization of titanium aluminides produced from elemental powder mixtures

H. Sina[1] · **S. Iyengar**[1]

Received: 5 February 2015 / Accepted: 27 May 2015

Abstract The formation of titanium aluminides in Ti–Al elemental powder mixtures containing 25, 50 and 75 at.% Al, has been studied using differential scanning calorimetry (DSC). Phase evolution in the mixture was followed by heating the compacted samples up to 1273 K at 7.5 and 15 K min^{-1}. The cooled samples were characterized using X-ray diffraction, scanning electron microscopy and energy-dispersive spectroscopy. The results showed that the primary combustion product in all the samples was $TiAl_3$, and the combustion reaction occurred below the melting point of aluminum only in Ti-rich samples. In Al-rich samples (75 at.% Al), $TiAl_3$ was obtained as a porous, single-phase product after combustion. In samples containing 25 and 50 at.% Al, the combustion reaction was incomplete and the unreacted titanium particles were covered by a layer of $TiAl_3$. In these samples, other intermetallic compounds such as $TiAl_2$, TiAl and Ti_3Al were observed to form upon heating beyond the combustion peak and are attributed to the solid-state reaction between unreacted titanium and $TiAl_3$. Heating the samples with 25 at.% Al to 1273 K for an hour led to the formation of a homogenous Ti_3Al product, while a multiphase product with a dominant TiAl phase was observed in samples containing 50 at.% Al. Calculations based on DSC data show that the formation of $TiAl_3$ through the reaction between solid titanium and molten aluminum is associated with an apparent activation energy of 195 ± 20 kJ mol^{-1} and an enthalpy of −114 ± 5 kJ mol^{-1}.

✉ S. Iyengar
Srinivasan.Iyengar@material.lth.se

[1] Materials Engineering, Lund University, P.O. Box 118, 22100 Lund, Sweden

Keywords Aluminides · Intermetallics · Reactive synthesis · Diffusion · DSC

Introduction

Intermetallic compounds like titanium aluminides have attractive properties such as relatively low density, high melting point, good strength as well as corrosion and creep resistance at elevated temperatures. The combination of these properties makes these compounds suitable for advanced applications in the aerospace and automotive industries as well as in energy generation [1, 2]. Although there are several processing methods for producing intermetallic compounds [3], combustion synthesis or reactive sintering has drawn special attention due to its technical and practical advantages such as relatively low cost, faster production and simplicity [4–13]. In a process based on combustion synthesis, the reactant powders are typically mixed and pressed into green compacts and are subsequently heated to synthesize the desired intermetallic compound. Depending on the heating procedure, combustion synthesis can be divided into two different modes: self-propagating high temperature synthesis (SHS) and thermal explosion (TE). SHS involves localized heating of the sample very quickly to the ignition temperature at which the combustion reaction can initiate in the heated region. Subsequently, the combustion front can propagate along the sample in a self-sustaining manner if sufficient amount of heat had been released during the initial combustion reaction. In the thermal explosion mode, the whole sample is heated at a constant rate until combustion is initiated. Titanium aluminides can be synthesized through both SHS and TE methods. However, due to the relatively low exothermicity of the reactions involved [5], thermal

Published online: 24 June 2015

explosion is considered more suitable, particularly for industrial applications [1]. The role played by chemical and diffusional effects in the formation of intermetallic compounds is determined by factors such as particle size and heating rate. In general, the products obtained through combustion synthesis are porous and could be advantageous in applications such as filters, catalysts and medical implants. However, there are consolidation techniques like hot-press sintering through which a denser product can be obtained.

Several intermetallic compounds such as Ti_3Al (α_2), TiAl (γ), $TiAl_2$ and $TiAl_3$ have been identified as equilibrium phases in the Ti–Al system [14, 15]. The α_2 and γ phases exhibit $D0_{19}$ hexagonal and $L1_0$ face-centered tetragonal ordered structures, respectively. These phases play a prominent role in strengthening titanium alloys for structural applications at elevated temperatures.

The formation of intermetallic compounds in the Ti–Al system has been studied by several workers. Adeli et al. [5] used inductive heating to initiate a SHS reaction for the synthesis of TiAl from elemental powder mixtures. They found that mechanical activation of the powder mixture led to higher velocities of propagation for the reaction front. According to this study, dissolution of the titanium particles in molten aluminum was found to be a major limiting step in the combustion synthesis of titanium aluminides, and finer titanium particles speeded up the ignition process. Based on further observations on the velocity of the reaction front and combustion temperatures, the authors calculated an activation energy of about 300 kJ mol^{-1} for the combustion synthesis of TiAl. In another study, Mishin and Herzig [16] investigated the effect of aluminum particle size and heating rate on reaction kinetics and densification of TiAl compound produced by reactive sintering. They observed that mechanical activation of the aluminum powder initially through ball milling and subsequent heating of the powder mixture at an optimal rate (30 K min^{-1}) could increase the density of the product. Yi et al. [17] obtained a more densified and homogenous product at relatively higher heating rates. They also noted that increasing the heating rate could change the nature of the combustion reaction from solid–liquid to solid–solid. However, this is contrary to the findings of Vaucher et al. [11].

Bertolino et al. [8] studied reactive sintering in Ti–Al powder mixtures with different initial compositions and heating rates. Based on the temperature profiles obtained, they reported the initiation of combustion at 918 $\pm$ 10 K. The reaction was observed to proceed in the explosion mode after the aluminum had melted completely. X-ray diffraction (XRD) data revealed that in addition to the presence of $TiAl_3$ in all the samples, Ti_3Al and TiAl were also identified in samples containing 25 and 50 at.% aluminum. Orru et al. [18] also reported the formation of $TiAl_3$ phase during the initial stages of combustion in Ti-25 at.% Al samples, which gradually transformed to Ti_3Al through the reaction with the intermediate TiAl phase and residual titanium particles. Wang et al. [6] heated Ti-75 at.% Al samples in a DSC and observed the formation of $TiAl_3$ compound at temperatures much higher than the melting point of aluminum. They suggested that diffusion through the $TiAl_3$ layer was rate limiting.

$TiAl_3$ has been identified as the single dominant phase which forms during the heating of Ti–Al diffusion couples [19–24]. This observation has been explained on the basis of the higher diffusivity of aluminum ions in $TiAl_3$ in comparison with other aluminides, which in any case might be formed in small amounts [23]. Formation of $TiAl_3$ on the titanium side of the diffusion couple, together with the movement of markers, proved that aluminum is the dominant diffusing specie [4, 21, 22, 25–27]. However, diffusion of titanium has also been reported by some workers [28, 29].

Knowledge about the combustion phenomenon and the effect of different parameters on ignition behavior can enable us to design and optimize processes to synthesize the desired compounds. Therefore, the present study aims to contribute further to the understanding of the important aspects of the combustion synthesis of titanium aluminides from elemental powders. Samples with varying initial compositions were heated to different temperatures at two heating rates. Synthesized products were examined using scanning electron microscopy (SEM), energy-dispersive spectroscopy (EDS) and XRD methods.

Materials and methods

Titanium powder (Max. particle size: 45 μm, 99.5 % pure) and aluminum powder (Max. particle size: 15 μm, 99 % pure) were thoroughly mixed in proportions corresponding to Ti + 3Al, Ti + Al and 3Ti + Al compositions. Disk samples (4 mm in diameter, 1 mm in thickness) were prepared by pressing the powder mixtures in a tool-steel die. Figure 1 shows the SEM images of the uncompacted elemental powders, as well as the backscattered electron image of an untreated Ti + 3Al sample. It is seen that the titanium particles are spherical, while the aluminum particles are irregular. The backscattered electron image of the untreated Ti + 3Al disk sample shows a fairly uniform distribution of bright titanium particles in a gray aluminum matrix.

The disk samples were placed in alumina crucibles and heated in a Netzsch TG-DSC (F3-Jupiter STA) unit. The DSC unit was calibrated for temperature and heat sensitivity using pure metal standards, and baseline corrections were made by running blank heating cycles. In order to protect the samples against oxidation, the DSC chamber

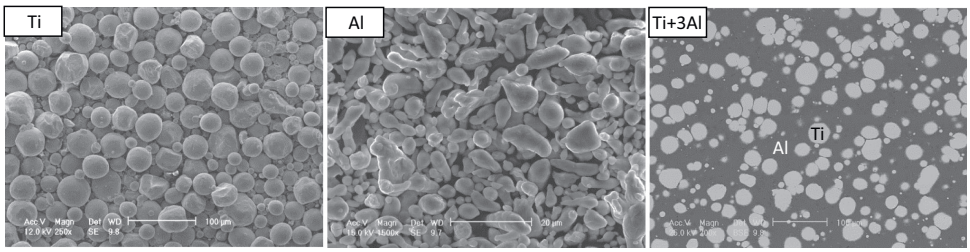

Fig. 1 SEM images of elemental powders and an unreacted disk (Ti + 3Al)

was evacuated and flushed with dried argon gas 3–4 times before starting the experiment, and a constant flow of argon was maintained during heating. DSC plots were obtained by heating the samples at a constant rate (7.5, 15 K min^{-1}) up to 1273 K. No mass change was observed in the samples during heating. In order to study the phase evolution during heating, some samples were heated to temperatures above and below the observed peaks in the DSC plots. The stabilities of the products were tested by prolonged heating at 1273 K.

After cooling to room temperature, a microstructural examination of the sample surface was made using a scanning electron microscope (Philips XL-30 ESEM). The distribution of titanium and aluminum in the microstructure was checked using energy-dispersive spectroscopy. The EDAX unit, mounted on the SEM, consisted of a liquid nitrogen-cooled Si(Li) detector, with a super ultra-thin polymer window and a resolution of 127.4 eV (with reference to Mn-K_α). X-ray mapping, line scanning and selected area/spot analysis techniques were used to check the distribution of elements. Genesis software (version 5.21) was used for quantification, using ZAF correction and standardless calibration. EDS results were checked at different acceleration voltages and spot sizes to minimize the effect of signals from adjacent areas. The phases present in the heat-treated samples were also characterized by X-ray diffraction, using a vertical Stoe Stadi X-ray machine equipped with a germanium monochromator (Johan geometry), a copper tube and a linear PSD as the detector in a transition setup.

Results and discussion

Ti + 3Al samples

Figure 2 shows DSC plots obtained while heating the samples to 1273 K at different heating rates (7.5 and 15 K min^{-1}). In these graphs, an endothermic peak 'a'

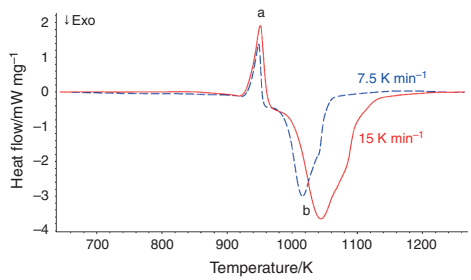

Fig. 2 DSC plots for Ti + 3Al samples

corresponding to aluminum melting was observed initially, followed by an exothermic peak 'b' which represents the combustion reaction in the sample. The peak is shifted to higher temperatures at a higher heating rate, consistent with the behavior generally observed for thermally activated reactions. However, diffusional effects are also indicated by the relatively broader peaks observed in this case.

In order to study the evolution of intermetallic phases, a few samples were heated to temperatures below and above the peak temperatures in the DSC plot (15 K min^{-1}), followed by cooling to room temperature at 30 K min^{-1}. The cooled samples were examined by X-ray diffraction, and the results are presented in Fig. 3. These data show that after heating a sample to 918 K, the diffraction pattern contains the elemental peaks, and does not lead to formation of any intermetallic phase. However, the diffractogram of a sample heated to 973 K shows small peaks corresponding to the intermetallic compound $TiAl_3$. These data suggest that intermetallic compound formation is the result of the reaction between molten aluminum and titanium particles. This observation is in accordance with previous studies [6, 17, 18, 20, 30].

X-ray diffractogram of a sample heated to 1113 K, which is close to the ending temperature of the exothermic

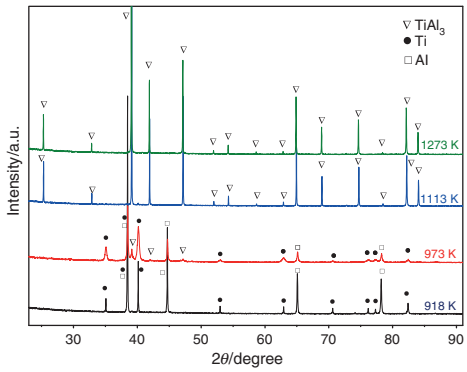

Fig. 3 Diffractograms of Ti + 3Al samples heated to different temperatures (15 K min^{-1})

peak, showed a single-phase product ($TiAl_3$), and the presence of unreacted elements was not observed. This result indicates that the reaction is complete at this stage. Heating a sample to 1273 K showed no further change and confirmed the stability of the $TiAl_3$ product. The microstructures of the samples heated to different temperatures were examined using the scanning electron microscope, and the results are presented in Fig. 4. The micrograph of the sample heated to 918 K consists of titanium particles dispersed in the aluminum matrix, while thin layers of a gray phase have been formed around the titanium particles after heating to 973 K. Formation and growth of the gray phase around the titanium particles is more pronounced after heating the sample to 1023 K. Figure 5 presents EDS analysis for the selected points showing an average composition (~75 at.% Al) corresponding to the intermetallic compound $TiAl_3$, which is in agreement with X-ray diffraction data. The distribution of titanium and aluminum in the microstructure was also determined using the X-ray mapping technique, and the results are presented in Fig. 5.

The samples heated to 1113 and 1273 K were characterized by a single-phase and porous $TiAl_3$ product, as shown in Fig. 4. At the same time, these samples exhibited a large volume expansion, which is due to the formation of a sponge-like structure shown in the micrographs. However, the volume expansion was slightly less in the sample heated to 1273 K. This can be attributed to the partial shrinkage caused by the coalescence of some particles at higher temperatures.

These results show that the formation of $TiAl_3$ is associated with a tendency for pore formation, which is proportional to the degree of reaction. It seems that as the aluminum melt reacts with titanium particles, some pores are left behind at the sites originally occupied by aluminum. Similar behavior has been attributed to the formation of pores during the synthesis of various aluminides from powder mixtures [31–36]. This is also in agreement with studies suggesting that the diffusion of aluminum atoms into titanium particles is the predominant mechanism governing the formation of titanium aluminides [21, 22, 25–27]. The globular morphology of the $TiAl_3$ phase obtained in this study is quite similar to what Xu et al. [29] observed for the $TiAl_3$ phase in diffusion couple experiments.

Ti + Al samples

Figure 6 presents DSC plots obtained for Ti + Al samples heated to 1273 K at two different rates. Comparing these graphs with those for the Ti + 3Al disks (Fig. 2), two extra peaks ('a' and 'd') can be seen in addition to the endothermic melting ("b") and exothermic reaction ('c') peaks. The relatively small exothermic peak 'a', prior to the aluminum melting stage, can signify the formation of some intermetallic compounds due to the solid-state interdiffusion of reactants observed in several investigations [21, 22, 25–27, 29, 30]. According to these studies, it is most likely that aluminum atoms diffuse through titanium particles and forms Al-rich intermetallic compounds like $TiAl_3$. This effect is more pronounced once the titanium content of the sample is large enough to provide a sufficient number of interfacial contacts between particles, enabling the detection of the solid-state reaction in the sample. This effect is not observed in the Ti + 3Al sample due to insufficient titanium content and consequently, much lower interfacial contacts between titanium and aluminum particles.

Further, the higher content of titanium in Ti + Al samples leads to relatively smaller aluminum melting ('b') peaks and less diffuse, sharper reaction peaks ('c'), as compared to those observed for Ti + 3Al samples. Another small endothermic peak was also observed in the Ti + Al samples close to 1155 K. This temperature is associated with the allotropic $\alpha \rightarrow \beta$ transformation in titanium. This observation indicates that titanium has partially reacted with aluminum during the combustion reaction, and the unreacted titanium portion has undergone the allotropic transformation once the temperature reached 1155 K. In Ti + 3Al samples, the reaction was complete at this temperature and hence the peak corresponding to the allotropic change was absent.

Figure 7 presents X-ray diffractograms from studies on Ti + Al samples heated to different temperatures at 15 K min^{-1}. The pattern obtained for the sample heated to 918 K showed weak reflections corresponding to the $TiAl_3$ compound, confirming the formation of this phase through a solid-state reaction in the sample. Relatively stronger

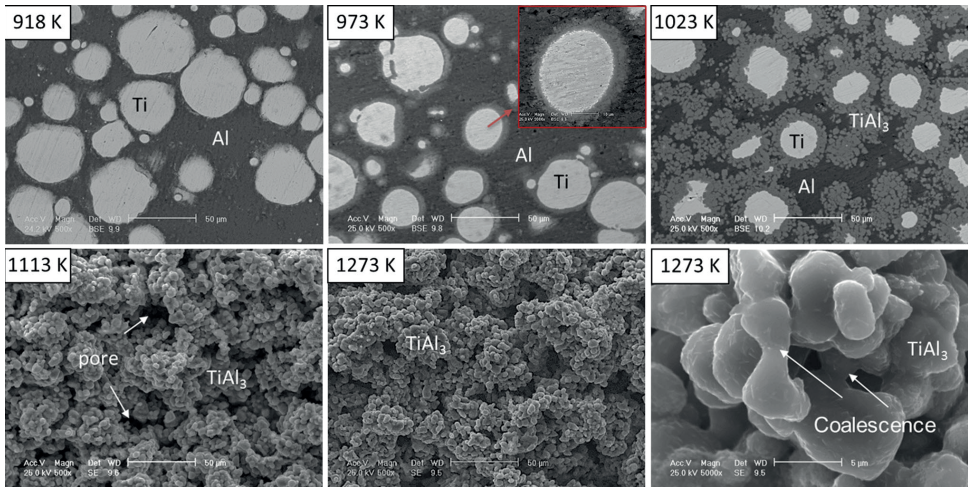

Fig. 4 SEM micrographs of Ti + 3Al samples heated to different temperatures (15 K min^{-1})

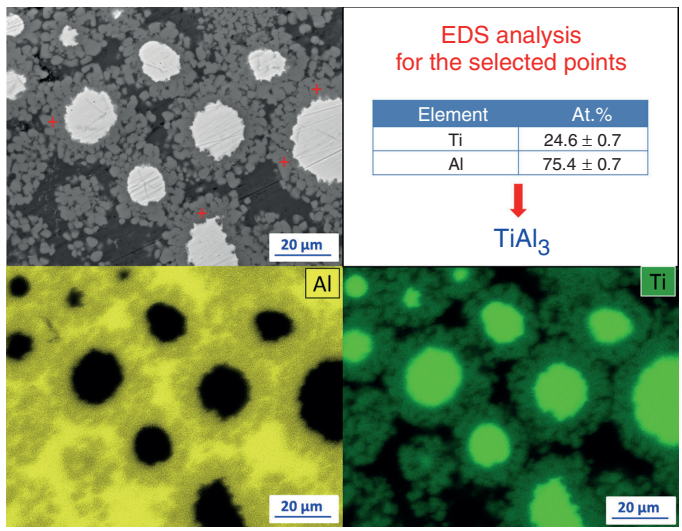

Fig. 5 EDS spot analysis and X-ray mapping for the sample heated to 1023 K

reflections for the $TiAl_3$ compound are observed in the sample heated to 953 K, which corresponds to the start of the combustion reaction (Fig. 6) at this temperature. The reflections for the $TiAl_3$ compound are stronger on heating the sample to 1003 K, where the combustion reaction is ended. While there is no evidence of elemental aluminum remaining at this stage, titanium reflections are still seen in the diffractogram, indicating the presence of unreacted titanium in the sample. It is seen that further heating the sample to 1123 and 1273 K gives rise to some new reflections corresponding to $TiAl_2$, TiAl and Ti_3Al compounds, in addition to titanium and $TiAl_3$ peaks. This can be due to the diffusional interactions between the initially formed $TiAl_3$ and unreacted titanium particles, leading to

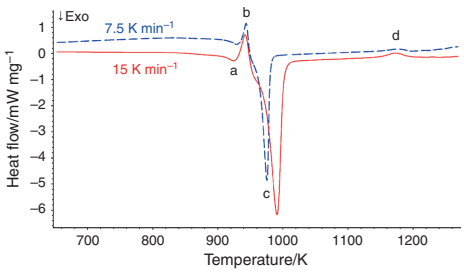

Fig. 6 DSC plots for Ti + Al samples

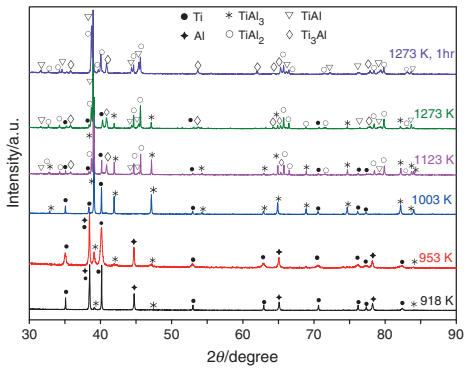

Fig. 7 Diffractograms of Ti + Al samples heated to different temperatures (15 K min^{-1})

the formation of new compounds in the sample. In general, such reactions which are based on solid-state interdiffusion of the elements, are very slow and require sufficient time to form a homogenized product in the sample. This explains the presence of unreacted titanium and $TiAl_3$ in the sample after heating to 1273 K. The presence of titanium is consistent with the DSC data showing the allotropic peak for titanium in Ti + Al samples. The intensities of the titanium and $TiAl_3$ peaks decrease on further heating and the reflections disappear completely after holding the sample at 1273 K for an hour. This observation shows that the $TiAl_3$ compound formed initially is a metastable product in Ti + Al samples. It may be noted that after prolonged heating at 1273 K, the strong reflections in the diffractogram of the sample corresponded to the TiAl phase, which was expected from the stoichiometry of the starting powder mixture.

Ti + Al samples heated to different temperatures were examined in the scanning electron microscope, and phase analysis was carried out using energy-dispersive spectroscopy. Figure 8 presents the micrographs observed. It is seen that the sample heated to 918 K mainly consists of the reacting elements. However, a gray phase was also observed in small amounts close to the interface of titanium particles with the aluminum matrix. This phase was identified as $TiAl_3$ by EDS analysis, as the presence of this compound prior to the melting of aluminum was also confirmed by X-ray diffraction. At 953 K, it is seen that almost each titanium particle is surrounded by a thin layer of $TiAl_3$, suggesting the initiation of the main combustion reaction in the sample. Once the combustion peak ended at 1003 K, $TiAl_3$ is seen to grow into the titanium cores and pure aluminum is fully consumed. This step is associated with the generation of some large pores seen in the micrograph and explains the large volume expansion observed in the samples. However, the volume change in Ti + Al specimens was smaller compared to the Ti + 3Al samples. This could be due to the lower aluminum content and lesser extent of solid–liquid reaction in Ti + Al samples.

In the sample heated to 1123 K, a different composition (~44 at.% Al) was identified by EDS in some regions at the interface of titanium cores and $TiAl_3$ layers. According to the Ti–Al phase diagram [14], this composition corresponds to the two-phase region Ti_3Al + TiAl. This is in agreement with X-ray diffraction data showing the presence of these compounds as the minor phases at 1123 K (Fig. 7). Further, the $TiAl_3$ phase is seen as some globular clusters with very small particles, which appear to be formed on the spherical titanium particles. Since each powder particle generally consists of numerous small grains, this may suggest that aluminum melt has diffused through the titanium grain boundaries within the particles and reacted with the titanium grains. However, it is seen that while some titanium particles are thoroughly transformed to $TiAl_3$, the cores of some other particles remain unreacted. The formation of new phases including Ti_3Al, TiAl and $TiAl_2$ is more pronounced after heating the sample to 1273 K, while $TiAl_3$ is getting consumed. As seen in the micrographs, titanium cores seem to have shrunk on further heating. Consequently, a series of aluminides have been formed around the cores with a gradual composition change which is in accordance with the Ti–Al phase diagram. It may be noted that after heating the sample for 1 h at 1273 K, $TiAl_3$ regions and unreacted titanium cores disappeared, while TiAl phase was found to dominate. This is consistent with XRD data showing TiAl as the major phase.

3Ti + Al samples

Figure 9 shows the DSC plots for 3Ti + Al samples heated to 1273 K at two different heating rates. No melting peak

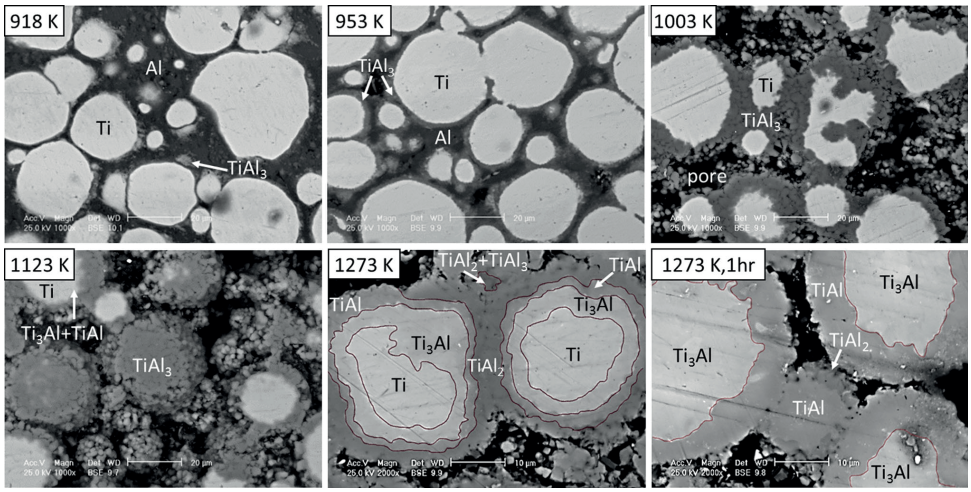

Fig. 8 SEM micrographs of Ti + Al samples heated to different temperatures (15 K min^{-1})

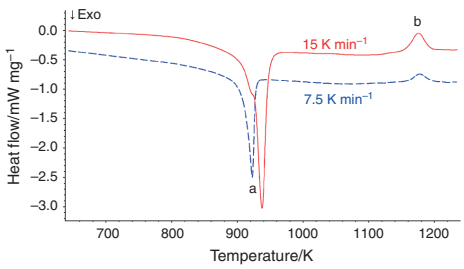

Fig. 9 DSC plots for 3Ti + Al samples

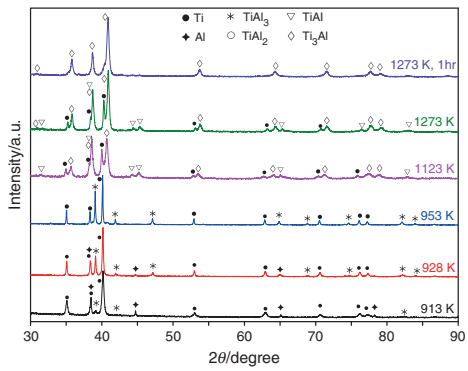

Fig. 10 Diffractograms of 3Ti + Al samples heated to different temperatures (15 K min^{-1})

can be seen in these plots, unlike those for Ti + 3Al and Ti + Al samples. However, due to the relatively low aluminum content in the 3Ti + Al samples, the endothermic peak corresponding to the melting of aluminum is expected to be relatively minor. A comparison of Fig. 9 with Figs. 2 and 6 also shows that the combustion peak is shifted to lower temperatures as the titanium content in the sample increased. This introduces the possibility of a small endothermic peak in the present case being covered by the larger exothermic peaks occurring close to the melting temperature for aluminum. It may also be noted that higher titanium contents in the sample provide larger contacts between the titanium particles and molten aluminum, promoting the initiation of combustion at lower temperatures. Further, Fig. 9 shows an endothermic peak ('b') upon heating to higher temperatures, similar to those observed for Ti + Al samples (Fig. 6). These peaks correspond to the allotropic transformation of titanium (α → β) and are relatively larger for the 3Ti + Al sample due to a larger amount of unreacted titanium present at that stage.

In order to determine the phases present during various stages of heating, a few 3Ti + Al samples were heated at 15 K min^{-1} to temperatures below and above the peak temperatures shown in the corresponding DSC plot. The samples were then examined using X-ray diffraction for phase identification, and the resulting diffractograms are presented in Fig. 10. For the sample heated to 913 K, which

is below the melting point of aluminum, the diffractogram shows a few weak reflections corresponding to $TiAl_3$ in addition to those for titanium and aluminum. A similar observation was also made for Ti + Al samples, showing the formation of $TiAl_3$ compound in the solid state. The $TiAl_3$ reflections were relatively stronger for the sample heated to 928 K (which is the starting temperature of the exothermic peak), while aluminum peaks became weaker, suggesting the combustion reaction to occur at this temperature. Relatively stronger $TiAl_3$ peaks were observed in the sample heated to 953 K, which is close to the ending temperature of the combustion peak in the DSC plot. At this stage, aluminum reflections were absent in the diffractogram. This indicates that all the aluminum in the sample has reacted with titanium to form $TiAl_3$, ending the combustion reaction. This observation is in agreement with DSC data.

Heating the samples further to 1123 and 1273 K leads to the formation of new phases including TiAl and Ti_3Al, while $TiAl_3$ reflections are absent in the corresponding diffraction patterns. This observation confirms that the $TiAl_3$ compound formed initially is a metastable phase which disappears on further heating through the reaction with unreacted titanium. Only Ti_3Al reflections are associated with the sample held at 1273 K for an hour, indicating a homogenous product.

Figure 11 shows the micrographs of the 3Ti + Al samples heated to different temperatures. In the sample heated to 913 K, the micrograph shows small, gray regions in between the aluminum and titanium particles. EDS analyses revealed an average composition of ~75 at.% Al for these areas. This result is in agreement with XRD data which show the formation of $TiAl_3$ phase at this temperature.

Heating the sample further to 928 and 953 K showed the growth of thin layers of $TiAl_3$ around the titanium particles. According to the DSC plot, combustion should have occurred at these temperatures. Aluminum-containing regions were still present in the sample heated to 928 K, and these regions were seemingly replaced by pores as aluminum was completely consumed for the sample heated to 953 K. The volume of the sample increased considerably at this stage, although much less relative to Ti + Al and Ti + 3Al samples. The sample heated to 1123 K showed relatively thick layers of Ti_3Al around the unreacted titanium particles. However, the TiAl phase was also identified by EDS analysis in some areas between Ti_3Al layers while no $TiAl_3$ could be observed. This result is consistent with diffraction data showing the coexistence of TiAl with Ti_3Al and unreacted titanium. In the sample heated to 1273 K, unreacted titanium particles were found to be transformed to Ti_3Al phase. However, some aluminum-enriched titanium cores were also identified at a few locations. These observations confirm the occurrence of reactions involving solid-state diffusion in the samples, which ultimately resulted in a homogenous Ti_3Al product after holding the sample at 1273 K for an hour.

The results of this study confirm that $TiAl_3$ is the initial product of the combustion reaction between aluminum and titanium particles, irrespective of the composition of the powder mixtures. For the samples Ti + 3Al and Ti + Al,

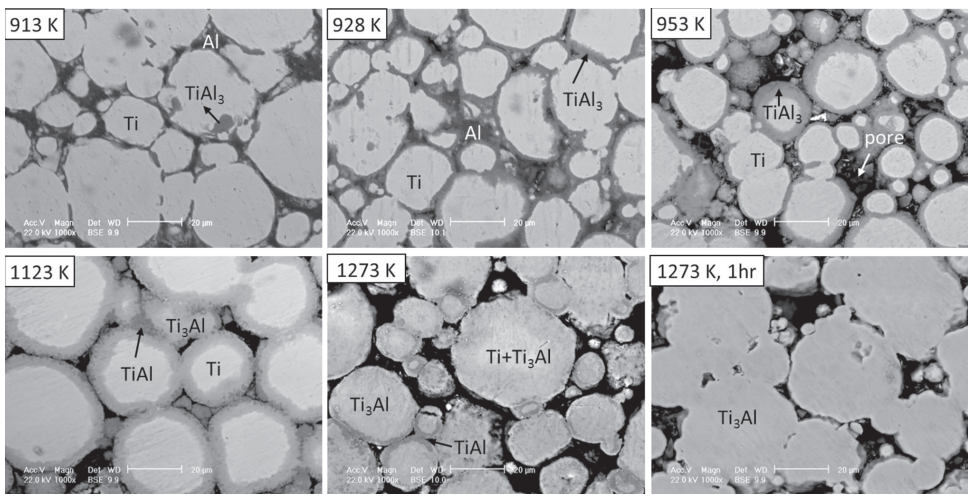

Fig. 11 SEM micrographs of 3Ti + Al samples heated to different temperatures (15 K min^{-1})

this reaction occurs only after the melting of aluminum. Further, experimental data show that the combustion peaks in the DSC plots shift to higher temperatures on increasing the heating rate. The apparent activation energy of the product formation can thus be estimated using a non-isothermal analysis of DSC data [6, 36, 37]. For this purpose, model-free isoconversion methods are considered to be accurate and reliable enough to estimate the activation energy of thermally activated reactions [37, 38]. The Kissinger–Akahira–Sunose (KAS) equation [39] can be used for analyzing DSC data and is given below.

$$\ln\frac{\beta}{T_p^2} = -\frac{E_a}{RT_p} + c \quad (1)$$

where β is the linear heating rate (K min^{-1}), T_p the reaction peak temperature (K), R is the universal gas constant (J mol^{-1} K^{-1}), c is an independent constant and E_a is the activation energy (J mol^{-1}).

Using DSC data obtained for Ti + 3Al samples which yielded a homogenous combustion product of $TiAl_3$, a reaction enthalpy of -114 ± 5 kJ mol^{-1} and an apparent activation energy of 195 ± 20 kJ mol^{-1} were calculated for $TiAl_3$ formation from the solid titanium–molten aluminum reaction. These results compare favorably with the values found in literature. Barin et al. [40] have reported the enthalpy of $TiAl_3$ formation as -142 kJ mol^{-1}. From DSC studies on Ti-75 at.% Al, Wang et al. [6] observed combustion peaks at $\sim$1073 K and reported an activation energy of 169 ± 15 kJ mol^{-1} for $TiAl_3$ formation. In another study, Khoshhal et al. [41] studied the formation and growth of titanium aluminide layers on the surfaces of titanium sheets immersed in molten aluminum at temperatures in the range 1023–1223 K and determined an activation energy of 170 kJ mol^{-1} for the formation of $TiAl_3$. These data suggest that the growth of $TiAl_3$ phase is a diffusion-limited process which is controlled by the interdiffusion of reactants through the $TiAl_3$ product layer.

Conclusions

Titanium aluminide formation in Ti–Al powder mixtures containing 25, 50 and 75 at.% Al has been studied in this work. Experimental results have shown that aluminide formation in the solid state is possible in Ti-rich samples, while the combustion reaction occurs between molten aluminum and titanium particles in aluminum-rich samples. $TiAl_3$ is the first product to form in all the samples, irrespective of the initial composition. The reaction continues until all the aluminum present in the mixture has reacted with titanium particles. In Ti + 3Al samples, the combustion reaction reached completion with the formation of $TiAl_3$ phase as the final product, which was stable on further heating. $TiAl_3$ formation was associated with the generation of pores, leading to swelling in the samples.

The combustion reaction was incomplete in Ti + Al and 3Ti + Al samples where the aluminum content was insufficient to react with all the titanium present to form $TiAl_3$. These samples consisted of a considerable amount of unreacted titanium particles covered by layers of $TiAl_3$. In these samples, solid-state reactions based on diffusion were found to govern the phase evolution on further heating. The $TiAl_3$ phase was seen to disappear at higher temperatures due to the reaction with unreacted titanium, resulting in the formation of $TiAl_2$, TiAl and Ti_3Al compounds. However, after holding the Ti + Al samples for an hour at 1273 K, a multiphase product was obtained in which TiAl was the dominant phase. Heating the 3Ti + Al samples at 1273 K for an hour resulted in a homogenous product of Ti_3Al.

DSC plots showed that, at a constant heating rate, increasing the titanium content in the sample resulted in relatively sharper combustion peaks at relatively lower temperatures. For all sample compositions, increasing the heating rate resulted in a shift of the combustion peak to relatively higher temperatures. Based on combustion peak data measured at two different heating rates and using the isoconversion approach, a value of 195 ± 20 kJ mol^{-1} has been calculated as the apparent activation energy of $TiAl_3$ formation through the combustion reaction between molten aluminum and solid titanium particles. The enthalpy of this reaction has been determined to be -114 ± 5 kJ mol^{-1}.

References

1. Varma A, Mukasyan AS. Combustion synthesis of intermetallic compounds. In: Borisov AA, De Luca LT, Merzhanov AG, editors. Self-propagating high-temperature synth. Mater. New York: Taylor & Francis; 2002. p. 1–34.
2. Chin ESC, Biederman RR. The titanium-aluminum phase diagram. A review of the near Ti-50 At.% Al phase fields. Report AD-A255 685. Watertown, MA: Army Materials Technology Laboratory; 1992. p. 1–2.
3. Froes FH, Suryanarayana C, Eliezer D. Synthesis, properties and applications of titanium aluminides. J Mater Sci. 1992;27:5113–40.
4. Wang T, Liu R, Zhu M, Zhang J. Physical simulation of the effect of sample volume on ignition temperature in the thermal explosion synthesis of Ti + 3Al → $TiAl_3$. Mater Lett. 2003;57:2151–5.
5. Adeli M, Seyedein SH, Aboutalebi MR, Kobashi M, Kanetake N. A study on the combustion synthesis of titanium aluminide in the self-propagating mode. J Alloys Compd. 2010;497:100–4.
6. Wang T, Liu R, Zhu M, Zhang J. Activation energy of self-heating process studied by DSC. J Therm Anal Calorim. 2002;70:507–19.
7. Lee S, Lee J, Lee Y. Effect of heating rate on the combustion synthesis of intermetallics. Mater Sci Eng A. 2000;281:275–85.
8. Bertolino N, Monagheddu M, Tacca A, Giuliani P, Zanotti C, Anselmi Tamburini U. Ignition mechanism in combustion synthesis of Ti–Al and Ti–Ni systems. Intermetallics. 2003;11:41–9.

9. Lee W-C, Chung S-L. Ignition phenomena and reaction mechanisms of the self-propagating high-temperature synthesis reaction in the titanium–carbon–aluminum system. J Am Ceram Soc. 1997;80:53–61.
10. Jokisaari JR, Bhaduri S, Bhaduri SB. Microwave activated combustion synthesis of titanium aluminides. Mater Sci Eng A. 2005;394:385–92.
11. Vaucher S, Stir M, Ishizaki K, Catala-Civera J-M, Nicula R. Reactive synthesis of Ti–Al intermetallics during microwave heating in an E-field maximum. Thermochim Acta. 2011;522: 151–4.
12. Moore JJ, Feng H. Combustion synthesis of advanced materials: part I. Reaction parameters. Prog Mater Sci. 1995;39:243–73.
13. Yi HC, Moore JJ. Review self-propagating high-temperature (combustion) synthesis (SHS) of powder-compacted materials. J Mater Sci. 1990;25:1159–68.
14. Murray JL. Ti–Al binary phase diagram. In: Baker H, editor. Alloy phase diagrams. Materials Park: ASM International; 1992. p. 54.
15. Okamoto H. Al–Ti (aluminum–titanium) phase diagram. J Phase Equilibria. 1993;14:120–1.
16. Mishin Y, Herzig C. Diffusion in the Ti–Al system. Acta Mater. 2000;48:589–623.
17. Yi HC, Petric A, Moore JJ. Effect of heating rate on the combustion synthesis of Ti–Al intermetallic compounds. J Mater Sci. 1992;27:6797–806.
18. Orru R, Cao G, Munir ZA. Mechanistic investigation of the field-activated combustion synthesis (FACS) of titanium aluminides. Chem Eng Sci. 1999;54:3349–55.
19. Maas J, Bastin G, van Loo F, Metselaar R. The texture in diffusion-grown layers of trialuminides MeAl 3(Me = Ti, V, Ta, Nb, Zr, Hf) and VNi_3. Zeitschrift fuer Met. 1983;74:294–9.
20. Luo J-G, Acoff VL. Using cold roll bonding and annealing to process Ti/Al multi-layered composites from elemental foils. Mater Sci Eng A. 2004;379:164–72.
21. Van Loo FJ, Rieck G. Diffusion in the titanium–aluminium system—I. Interdiffusion in the composition range between 25 and 100 at.% Ti. Acta Metall. 1973;21:73–84.
22. Mirjalili M, Soltanieh M, Matsuura K, Ohno M. On the kinetics of $TiAl_3$ intermetallic layer formation in the titanium and aluminum diffusion couple. Intermetallics. 2013;32:297–302.
23. Howard JK. Kinetics of compound formation in thin film couples of Al and transition metals. J Vac Sci Technol. 1976;13:68.
24. Colgan EG, Mayer JW. Thin-film reactions of Al with Co, Cr, Mo, Ta, Ti, and W. J Mater Res. 2011;4:815–20.
25. Goda DJ, Richards NL, Caley WF, Chaturvedi MC. The effect of processing variables on the structure and chemistry of Ti-aluminide based LMCS. Mater Sci Eng A. 2002;334:280–90.
26. Zhao XA, So FCT, Nicolet MA. $TiAl_3$ formation by furnace annealing of Ti/Al bilayers and the effect of impurities. J Appl Phys. 1988;63:2800.
27. Thuillard M, Tran LT, Nicolet M-A. Al_3Ti formation by diffusion of aluminum through titanium. In: KRUTENAT RCBT-MC 1988, editor. Thin solid films, vol 166. Amsterdam: Elsevier; 1988. p. 21–8.
28. Zhang LZ, Wang DN, Wang BY, Yu RS, Wei L. Annealing studies of Ti/Al multilayer film by slow positron beam. Appl Surf Sci. 2007;253:7309–12.
29. Xu L, Cui YY, Hao YL, Yang R. Growth of intermetallic layer in multi-laminated Ti/Al diffusion couples. Mater Sci Eng A. 2006;435–436:638–47.
30. Chaudhari GP, Acoff VL. Titanium aluminide sheets made using roll bonding and reaction annealing. Intermetallics. 2010;18: 472–8.
31. Gao H, He Y, Shen P, Zou J, Xu N, Jiang Y, et al. Porous FeAl intermetallics fabricated by elemental powder reactive synthesis. Intermetallics. 2009;17:1041–6.
32. Dong HX, Jiang Y, He YH, Song M, Zou J, Xu NP, et al. Formation of porous Ni–Al intermetallics through pressureless reaction synthesis. J Alloys Compd. 2009;484:907–13.
33. Paris S, Gaffet E, Bernard F. Control of FeAl composition produced by SPS reactive sintering from mechanically activated powder mixture. J Nanomater. 2013;2013:1–11.
34. Gedevanishvili S, Deevi SC. Processing of iron aluminides by pressureless sintering through Fe + Al elemental route. Mater Sci Eng A. 2002;325:163–76.
35. Gauthier V, Bernard F, Gaffet E, Josse C, Larpin JP. In-situ time resolved X-ray diffraction study of the formation of the nanocrystalline $NbAl_3$ phase by mechanically activated self-propagating high-temperature synthesis reaction. Mater Sci Eng A. 1999;272:334–41.
36. Sina H, Iyengar S. Studies on the formation of aluminides in heated Nb–Al powder mixtures. J Alloys Compd. 2015;628:9–19.
37. Starink MJ. Analysis of aluminium based alloys by calorimetry: quantitative analysis of reactions and reaction kinetics. Int Mater Rev. 2004;49:191–226.
38. Starink MJ. Activation energy determination for linear heating experiments: deviations due to neglecting the low temperature end of the temperature integral. J Mater Sci. 2006;42:483–9.
39. Kissinger HE. Variation of peak temperature with heating rate in differential thermal analysis. J Res Natl Bur Stand. 1934;57:217–21.
40. Barin I, Knacke O, Kubaschewski O. Thermochemical properties of inorganic substances, supplement. Berlin: Springer; 1977.
41. Khoshhal R, Soltanieh M, Mirjalili M. Formation and growth of titanium aluminide layer at the surface of titanium sheets immersed in molten aluminum. Iran J Mater Sci Eng. 2010;7:24–31.

Paper II

H. Sina, J. Corneliusson, K. Turba, S. Iyengar

A study on the formation of iron aluminide (FeAl) from elemental powders

Journal of Alloys and Compounds, Vol. 636, 2015, pp. 261-269
DOI: 10.1016/j.jallcom.2015.02.132

Journal of Alloys and Compounds 636 (2015) 261–269

Contents lists available at ScienceDirect

Journal of Alloys and Compounds

journal homepage: www.elsevier.com/locate/jalcom

A study on the formation of iron aluminide (FeAl) from elemental powders

H. Sina, J. Corneliusson, K. Turba, S. Iyengar *

Materials Engineering, Lund University, 22100 Lund, Sweden

ARTICLE INFO

Article history:
Received 28 September 2014
Received in revised form 25 January 2015
Accepted 17 February 2015
Available online 3 March 2015

Keywords:
Iron aluminide
Intermetallics
Ignition reaction
DSC
Onset temperature

ABSTRACT

The formation of iron aluminide (FeAl) during the heating of Fe–40 at.% Al powder mixture has been studied using a differential scanning calorimeter. The effect of particle size of the reactants, compaction of the powder mixtures as well as the heating rate on combustion behavior has been investigated. On heating compacted discs containing relatively coarser iron powder, DSC data show two consecutive exothermic peaks corresponding to precombustion and combustion reactions. The product formed during both these reactions is Fe_2Al_5 and there is a volume expansion in the sample. The precombustion reaction could be improved by a slower heating rate as well as a better surface coverage of iron particles using relatively finer aluminum powder. The combustion reaction was observed to be weaker after a strong precombustion stage. Heating the samples to 1000 °C resulted in the formation of a single and stable FeAl phase through the diffusional reaction between Fe_2Al_5 and residual iron.

DSC results for compacted discs containing relatively finer iron powder and for the non-compacted samples showed a single combustion exotherm during heating, with Fe_2Al_5 as the product and traces of FeAl. X-ray diffraction and EDS data confirmed the formation of FeAl as the final product after heating these samples to 1000 °C.

1. Introduction

Intermetallic compounds such as aluminides of transition metals like nickel, iron, titanium, niobium and cobalt have been widely studied due to their attractive physical and mechanical properties of critical importance in a variety of applications [1–5]. Among these compounds, iron aluminides are specially interesting due to their low density, low production cost, good mechanical properties and corrosion resistance at high temperatures [4,6,7]. Iron aluminides are about 30% lighter than commercial high temperature structural materials like stainless steel and nickel based superalloys [8]. Studies have shown that iron aluminides have good high temperature corrosion resistance in oxidizing and sulfidizing environments [9,10] found in typical industrial applications like power generation systems. This is attributed to the formation of dense and adherent alumina scales on the surface of the material. Natesan [11] confirmed these observations and concluded that the oxidation rates of iron aluminides in single-oxidant environments (like air or gases with low oxygen potentials) are significantly lower than those for chromia-forming commercial alloys. These properties allow intermetallic compounds in the Fe–Al system to be employed at high temperatures as structural materials, gas filters and heating elements [4,7].

Fig. 1 shows the binary phase diagram for the Fe–Al system which contains several intermetallic compounds. Two of these compounds, FeAl and Fe_3Al, are considered very attractive due to good strength and corrosion resistance at high temperatures [6–8,11].

FeAl, with a B2-ordered cubic CsCl structure, exists over a wide range of aluminum contents (35–50 at.%). The ordered DO_3 cubic structure of Fe_3Al is observed around 25 at.% Al and it is stable in the interval 23–36 at.% Al at low temperatures. The region of stability for Fe_3Al DO_3 structure tapers off at higher temperatures. Both B2 and DO_3 structures are perfectly ordered only when their compositions correspond to the stoichiometric compounds [8]. The high magnetic permeability shown by Fe_3Al makes it useful as a soft magnetic material. Relative to Fe_3Al, FeAl has a lower melting point, but a better oxidation resistance. FeAl also has a lower density and higher strength-to-weight ratio compared to steels and superalloys [2,5]. In addition, it exhibits relatively high electrical resistivity which makes it suitable for use as a heating element [2,3,13].

Iron aluminides can be produced by powder metallurgical methods involving powder consolidation [5,13–15] and sintering, which offer advantages such as net-shape processing and

* Corresponding author.

http://dx.doi.org/10.1016/j.jallcom.2015.02.132
0925-8388/

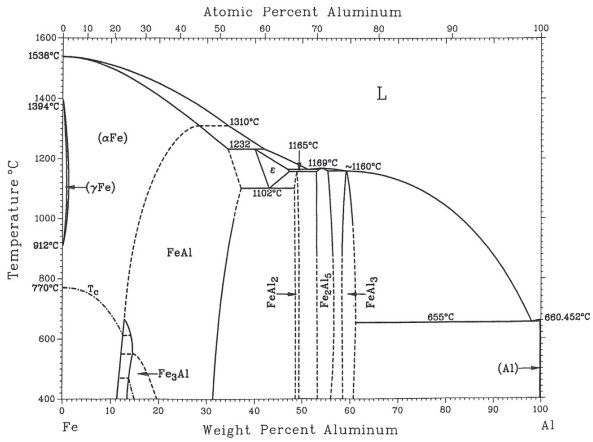

Fig. 1. Fe–Al binary phase diagram [12].

cost-effectiveness. It would be advantageous to start with metal powder mixtures as the consolidation process would be easier and cheaper than using powders of preformed intermetallics. In this context, formation of intermetallics in situ in a heated mixture of metal powders is of considerable interest. Such a process is called Combustion Synthesis, Reactive Synthesis or Self Propagating High Temperature Synthesis (SHS), in which a reaction between the reactant particles is initiated during heating. The reaction is exothermic and the generated heat can be utilized to make the process self-sustaining. Several authors like Munir et al. [16] and Mossino [17] have studied this method which can be used to fabricate near-net shape products. However, porosity levels in SHS products are high and can be minimized by sintering under pressure. Rabin et al. [18] have shown that near full density Fe_3Al and FeAl compounds can be obtained during the combustion reaction in a hot press by applying external pressure. Godlewska et al. [19] prepared FeAl (40 at.% Al) intermetallic powders using SHS in a loosely packed mixture of elemental powders. Compacted and sintered powder compacts were densified using hot forming methods. They observed that the strength and ductility of the product at room temperature were sensitive to grain size and adversely affected by the oxide phase distributed along the grain boundaries.

Gedevanishvili and Deevi [3] conducted dilatometric and DSC experiments up to 1350 °C to study the formation of iron aluminide and the sintering behavior in Fe–40 at.% Al powder mixtures. At a heating rate of 5 °C min^{-1}, they observed two exothermic peaks at 560 and 655 °C. These peaks were attributed to the formation of Fe_2Al_5 and FeAl respectively. The volume expansion observed in heated discs was linked to the formation of Fe_2Al_5. The reaction mechanism, expansion rate and product density were found to be strongly dependent on the heating rate.

Gao et al. [20] also studied the synthesis of FeAl using a Fe–40 at.% Al powder mixture. While heating the sample, they observed two successive exotherms in the interval 500–650 °C. These peaks correspond mainly to the formation of Fe_2Al_5 which transforms subsequently to FeAl by reacting with residual iron at higher temperatures. The authors have described the formation of pores during different stages of heating and noted the swelling of the sintered product to be quite significant.

Kang and Hu [21] studied the reactive sintering of Fe–Al compacted discs and found that the large swelling observed is mostly due to the formation of Fe_2Al_5. They suggested that the large thermal expansion is due to the rapid release of exothermic heat from several reactions occurring simultaneously within the sample, followed by a shrinkage due to heat dissipation. Large differences in the solid solubilities, melting points and diffusion rates [3,19,21] for the components lead to the development of pores which cause swelling in the sample.

Pochec et al. [22] have suggested a two-step mechanism for the formation of iron aluminides in Fe–50 at.% Al powder mixtures. They report the formation of two aluminum-rich phases $FeAl_3$ and Fe_2Al_5 due to a slow diffusion process at temperatures below 615 °C. The SHS reaction initiates above this temperature resulting in the formation of ordered FeAl phase together with the fragile $FeAl_2$ compound. FeAl is obtained as the final product after an additional homogenizing process.

In a Fe–Al diffusion couple study, Wang and Wood [23] found that $FeAl_3$ was dominant on the iron side of the Fe–Al interface at 600 °C, highlighting the diffusion of aluminum into iron grains. Intermetallic compound formation was also observed to be significant at the iron grain boundaries, confirming the higher mobility of aluminum atoms along the iron grain boundaries. They also observed the formation of Fe_2Al_5 above the melting point of aluminum through the diffusion of iron into aluminum melt. Although thermodynamic data indicate the formation of $FeAl_3$ before Fe_2Al_5, in general, Fe_2Al_5 forms as the major phase at the interface between aluminum and iron particles due to kinetic factors [24–26]. It may also be noted that the growth parameter is much larger for Fe_2Al_5 relative to FeAl [25,27,28].

The present study aims to continue the efforts to understand the key aspects of reactive synthesis of iron aluminides from elemental powder mixtures. Powder mixtures of Fe–40 at.% Al, both in the compacted and loose conditions, have been studied during a heating cycle in a differential scanning calorimeter. The effect of processing variables including particle size of reactants and heating rates have also been studied. The synthesized products have been characterized using scanning electron microscopy, energy dispersive spectroscopy and X-ray diffraction methods.

2. Material and methods

The metal powders used in the present work are presented in Table 1. For each metal component, two powders with relatively fine and coarse particles were chosen to study the effect of particle size combinations.

Fig. 2 presents the corresponding SEM images of the elemental powders. It is seen that both fine and coarse aluminum powders mainly contain ligamental particles, whereas spherical and irregular particles are dominant in fine and course iron powders. Further, aluminum powders exhibit a relatively broader particle size distribution as compared to the iron powders.

The elemental powders were mixed thoroughly to get a powder mixture having the composition Fe–40 at.% Al, which is in the FeAl region of the Fe–Al phase diagram. Compacted discs (4 mm in diameter, <1 mm in thickness) were prepared by cold-pressing the powder mixture at an applied stress of 380 MPa. The samples were used as loose powders as well as compacted discs. A Netzsch Simultaneous TG–DSC unit (F3-Jupiter STA 449) with alumina crucibles was used to heat the samples. The DSC unit was calibrated for temperature and heat sensitivity using pure metal standards. Baseline correction was done using data from heating cycles with empty crucibles. Before starting the experiment, the sample chamber was evacuated and flushed with dried argon gas 2–3 times in order to protect the samples against oxidation and a constant flow of argon was maintained during heating. The samples were heated at a constant rate (7.5, 15 °C min^{-1}) up to 1000 °C. The heating rates were so chosen as to minimize the risk of missing peaks associated with small thermal effects [29]. The upper temperature limit of 1000 °C corresponded well with the maximum reaction temperatures reported in the literature [21,30–32].

The evolution of phases during the process was checked by interrupting the heating of some samples. A few reacted samples were also reheated to check the stability of the product. Sample dimensions were measured, before and after heating, using a micrometer (±0.01 mm). Metallographic examination of the products was carried out using an environmental scanning electron microscope (Philips XL-30 ESEM) equipped with an EDAX unit for EDS measurements. X-ray analysis of the product was carried out using a vertical Stoe machine equipped with a Germanium monochromator (Johan geometry), a copper tube and a linear PSD as the detector in the reflection mode.

3. Results and discussion

Since the material behavior is particularly affected by the particle size of iron powder in the compacted discs, results obtained for compacted discs are presented first for two different particle sizes of iron, followed by those for loose powder mixtures.

3.1. Compacted samples with relatively coarser iron particles (max. size: 60 μm)

Fig. 3 shows the backscattered electron images of the surfaces of untreated compacted discs containing relatively coarser iron particles mixed with relatively fine or coarse aluminum powder. In both images, iron particles appear bright. It is seen that both iron and aluminum particles show a tendency to agglomerate. However, this effect is less pronounced when the sample contains finer particles of aluminum (Fig. 3a). The distribution of smaller aluminum particles is more uniform and helps to keep the iron particles separate. This results in a better surface coverage on the iron particle. Further, smudging of aluminum on the surface of iron particles can also be seen in Fig. 3, particularly for the sample with fine aluminum particles.

DSC plots for compacted discs containing coarse iron powder mixed with aluminum powder of different particle sizes are presented in Fig. 4. These samples were heated at two different heating rates (7.5, 15 °C min^{-1}) up to 1000 °C. Both the plots show two consecutive exothermic peaks. The first exothermic peak is more diffuse, whereas the second peak is sharper. This means that the mechanism governing the first peak is more time-dependent, while the reaction which causes the second peak is more instantaneous. At a given heating rate, for fine aluminum particles, a larger heat release for the first peak is followed by lesser exothermicity for the second peak. This indicates that the first reaction, to some extent, inhibits the second reaction and is typical of a precombustion reaction. This is consistent with the data showing the formation of some intermetallic compounds through diffusion prior to the combustion reaction [3,28,30,33,34]. In their review of SHS processes, Munir and Anselmi-Tamburini [16] have also pointed out that relatively slow heating rates lead to precombustion reactions, which can affect the main combustion reaction, for example, in Ni–Al powder mixtures.

The samples with a better surface coverage (fine aluminum particles) show a greater diffusional effect. Therefore, a large portion of the material reacts prior to the combustion stage forming significant amounts of precombustion products in the sample. This results in stronger precombustion peaks, but also decreases the direct contact between the elemental particles, which is essential for the combustion reaction. Fine aluminum particles with coarse iron powder are also associated with a stronger precombustion reaction at a higher heating rate. While a similar behavior is seen even for coarse aluminum particles, the precombustion peaks are much more diffuse.

Table 2 presents onset temperatures corresponding to the precombustion and combustion peaks in Fig. 4. The precombustion peak initiates at temperatures lower than 570 °C where the reaction takes place in the solid state. The combustion reaction occurs at a higher temperature (636–646 °C) without any melt formation according to the Fe–Al phase diagram (Fig. 1). However, this observation is different from those results highlighting the role of melt formation in triggering the combustion reaction [3,18,20,21]. In the present case, it is clearly seen from Fig. 4 and Table 2 that the combustion reaction occurs well below the lowest temperature (655 °C) at which a melt forms in the aluminum rich end of the Fe–Al system. While wetting of iron particle surface is undeniably promoted by melt formation, surface coverage due to enhanced diffusional flow of aluminum is possible at temperatures close to formation of a molten phase.

Lower onset temperatures for combustion in discs with fine aluminum particles can be explained on the basis of better iron–aluminum contact which makes the ignition of the powder compact possible at relatively lower temperatures. However, the onset temperature for precombustion does not follow this trend and indicates a diffusional barrier or a discontinuous supply from the layers of small particles of aluminum surrounding the coarse iron particles.

For a given particle size combination, increasing the heating rate leads to higher onset temperatures for the precombustion reaction. As solid-state diffusion is involved in precombustion, a higher heating rate decreases the time for diffusion of the atoms and consequently the reaction takes place at a higher temperature. This result is in an agreement with the observations made by Lee et al. [35] who reported higher onset temperatures for the precombustion reaction at increased heating rates. However, increasing the heating rate showed the opposite effect on the onset temperature for combustion. A possible explanation is that a larger amount of heat is given to the sample within a shorter period of time as the heating rate increases and causes enough heat accumulation within the sample for initiating combustion at lower temperatures. Precombustion is also hindered by a higher heating rate and this promotes the tendency of the sample to undergo the combustion reaction earlier. For samples containing relatively

Table 1
Metal powders used in the present work.

Powder[a]	Particle size (μm)	Particle shape	Purity (%)
Fine aluminum	<15	Ligamental	99
Coarse aluminum	<60	Ligamental	99.9
Fine iron	7[b]	Spherical	>99.0
Coarse iron	<60	Irregular	>99.0

[a] Supplied by Goodfellow Metals, UK.
[b] Average.

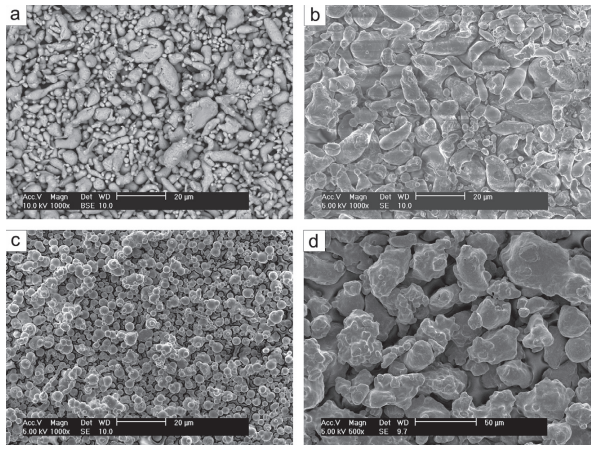

Fig. 2. SEM images of (a) fine aluminum, (b) coarse aluminum, (c) fine iron and (d) coarse iron powders.

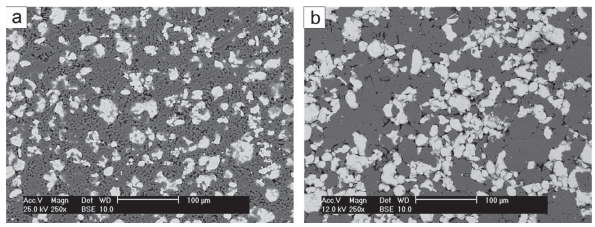

Fig. 3. SEM images of the unreacted compacted discs containing coarse iron particles mixed with relatively (a) fine and (b) coarse aluminum particles.

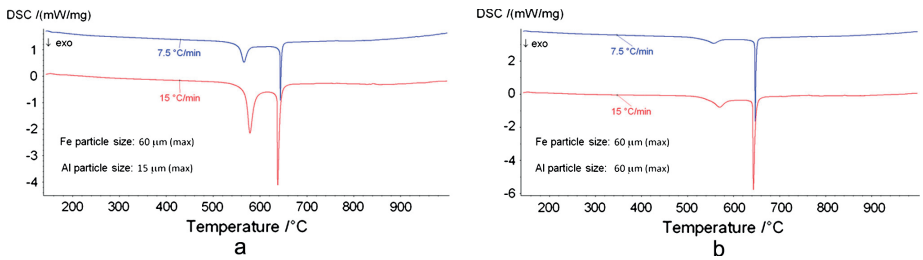

Fig. 4. Effect of heating rate and aluminum particle size on the onset of reaction in Fe–Al discs with relatively coarse iron particles.

coarser iron particles, the heat evolution rates associated with the precombustion and combustion peaks were calculated to be about 0.5 to 0.75 J/g s.

In order to study the evolution of phases during heating, a few compacted discs with fine aluminum particles were heated to different temperatures. Fig. 5 shows the SEM images of the discs after heating to the specified temperatures. Fig. 5a shows the image of a sample heated to 554 °C, which is close to the onset temperature for precombustion, and immediately cooled to room temperature (30 K/min). It is seen that aluminum (dark) and iron (bright) regions are dominant. At a few points on the iron particle surface in contact with aluminum, an additional phase with a fuzzy appearance was identified as Fe_2Al_5 compound by EDS analysis. This shows that the formation of Fe_2Al_5 phase takes place through the precombustion stage and is consistent with DSC data. At this stage, the sample showed a volume expansion of 1.8% which is

Table 2
Onset temperatures for precombustion and combustion reactions in Fe–Al discs containing coarse iron powder.[a]

Peak	Heating rate (°C min^{-1})	Onset temperature (°C) Al particle size	
		Fine[b]	Coarse[c]
Precombustion	7.5	554.4	533.8
	15	568.2	542.2
Combustion	7.5	642.5	646.0
	15	636.5	641.5

[a] 60 μm (max).
[b] 15 μm (max).
[c] 60 μm (max).

attributed to pore formation through solid-state diffusion [3,18,21].

The micrograph of a sample heated to 600 °C and cooled quickly to room temperature is shown in Fig. 5b. At this temperature, precombustion reaction in the sample has ended and the growth of Fe_2Al_5 regions is visible. However, iron and aluminum areas still dominate and the presence of this compound is not very significant. A relatively larger volume expansion (6.5%) was observed in the sample heated to 600 °C. These data confirm the role played by solid-state diffusion during the precombustion stage, leading to the formation of Fe_2Al_5.

Fig. 5c shows the micrograph for a sample heated to 642 °C, which is very close to the onset temperature of the combustion peak. However, significant amounts of unreacted iron and aluminum are still seen in the microstructure, indicating the slow reaction rates due to solid-state diffusion. The volume expansion of the sample increased to 15.2%, which is due to progress in the formation of Fe_2Al_5 during heating. It may be noted that based on lattice parameter calculations, the formation of dense Fe_2Al_5 from elemental powders could lead to a shrinkage of about 20% [21]. In this study, only a porous product was observed.

From Fig. 5, it is seen that the Fe_2Al_5 layer forms on the iron particle surface and covers the particle more and more with increase in growth. This suggests that Fe_2Al_5 is mainly formed by the diffusion of aluminum into iron particles [3,20,30], which is supported by the larger intrinsic diffusion coefficient of aluminum relative to iron at these temperatures [20,36]. The faster diffusion of aluminum atoms would also explain the swelling behavior during the formation of Fe_2Al_5.

On heating the sample further, the main combustion reaction is initiated and results in a sharp exothermic peak in the DSC plot. Fig. 5d presents the micrograph of a sample heated to a temperature (655 °C) where the combustion reaction has ended, and then cooled immediately to room temperature. A significant growth of the combustion product Fe_2Al_5 (grey regions) is seen in the micrograph. However, according to Gedevanishvili et al. [3], the combustion peak is attributed to FeAl formation, which is not confirmed by the present study. Further, the micrograph shows a considerable amount of residual iron and seemingly no aluminum. Volume expansion of the sample heated to 655 °C increased further to 29.3%. This swelling has been attributed to the formation of some large pores at the sites originally occupied by aluminum particles [3,20].

Godlewska et al. [37] have suggested that the presence of volatile species can lead to volume expansions, for example, during the preparation of $CoSb_3$ and Mg_2Si derivatives. However, in the present work, both iron and aluminum have very low vapor pressures [37,38] and the presence of volatile species is not likely to be significant. This was confirmed by heating a pure aluminum disc to 800 °C and no mass change was observed.

X-ray diffraction data for the samples heated to various temperatures are presented in Fig. 6. For the sample heated to 554 °C (close to the onset temperature for the precombustion reaction), diffraction peaks correspond mainly to the pure elements iron and aluminum. However, there are a few small peaks indicating the existence of Fe_2Al_5. The presence of Fe_2Al_5 phase is more pronounced in the sample heated to 600 °C, just after the precombustion reaction has ended. This confirms that the product of precombustion is Fe_2Al_5, while most of the iron and aluminum remain unaffected.

A similar trend is observed on heating the sample to 642 °C which is close to the onset temperature for the combustion reaction. However, Fe_2Al_5 reflections exhibit relatively higher

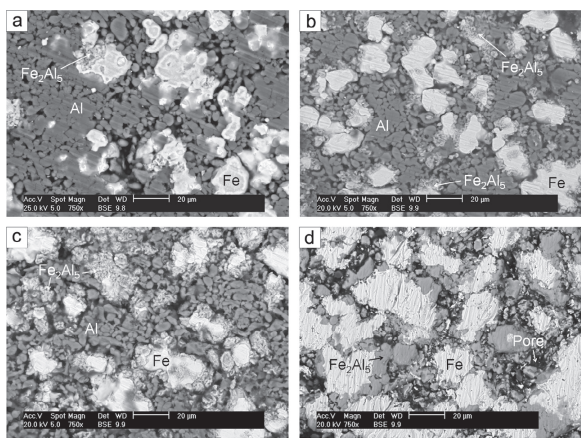

Fig. 5. SEM images of compacted discs (with coarse iron and fine aluminum particles) heated at 7.5 °C min^{-1} to (a) 554 °C + cooled, (b) 600 °C + cooled, (c) 642 °C + cooled, and (d) 655 °C + cooled.

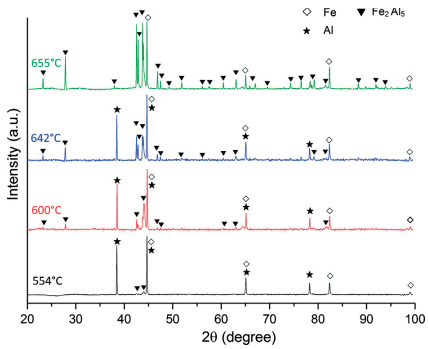

Fig. 6. X-ray diffractogram of compacted samples after heating at 7.5 °C min^{-1} to different temperatures (with coarse iron and fine aluminum particles).

intensities, which is due to the formation of more Fe_2Al_5 at this temperature. In the sample heated to 655 °C where the combustion reaction has ended, the diffraction peaks corresponding to Fe_2Al_5 are significantly stronger. Further, while the diffraction pattern does not show any peak for aluminum, the presence of unreacted iron is confirmed.

As the sample contains Fe_2Al_5 together with residual iron after the combustion reaction, further heating leads to the diffusional reaction between Fe_2Al_5 and iron resulting in the formation of FeAl compound which is more stable at higher temperatures [20]. This conclusion is supported by Fig. 7 which presents micrographs of samples heated to high temperatures after the combustion reaction has ended.

Fig. 7a shows the micrograph of a sample heated to 1000 °C and then cooled to room temperature. It is seen that the micrograph is dominated by a single phase identified as the FeAl compound by EDS analysis. Beyond the combustion temperature, FeAl is formed by the diffusional reaction between unreacted iron and Fe_2Al_5. This reaction does not go to completion at 1000 °C as some Fe_2Al_5 is still seen in the micrograph. It is also interesting to note that the variation of the size of FeAl grains matches the particle size variation of the coarse iron powder used to prepare the powder mixture. At this stage, due to increased porosity, the swelling of the sample reaches 37.4%. This may be compared with a 43.8% volume expansion under the same conditions shown by a sample with coarse aluminum particles which lead to the formation of larger pores [11].

Fig. 7b shows the micrograph of a sample heated to 1200 °C for an hour and cooled to room temperature. Clear signs of sintering are seen and EDS analysis showed the presence of only FeAl, indicating that the reaction between Fe_2Al_5 and iron has gone to completion. This observation is supported by XRD data presented in Fig. 8. After the heat treatment at 1200 °C, consolidation of the sample which occurs during sintering led to a decrease in volume expansion to 28.4%.

3.2. Compacted samples with relatively fine iron particles (average size: 7 μm)

Fig. 9 presents surface images of unreacted compacted discs containing relatively finer iron particles mixed with aluminum powders corresponding to two different size distributions. In these micrographs, iron particles appear bright while the aluminum particles are dark.

In general, agglomeration effects are observed to a larger extent when fine particles are present. In the present case, iron particles are much finer than the aluminum particles and show a tendency to agglomerate (Fig. 9b). However, the agglomeration tendency is reduced as the aluminum particle size is decreased (Fig. 9a). Further, the density of compacted discs containing fine iron particles was lower compared to those containing coarse iron particles. This is due to the lower compressibility associated with the fine iron particles.

DSC plots for the compacted discs containing fine iron powder for two different aluminum particle sizes and heating rates are presented in Fig. 10. These plots show a single, sharp exothermic peak during heating, which is indicative of the combustion reaction. This result is in contrast with those observed for samples containing relatively coarser iron particles (Fig. 4) which showed a precombustion stage prior to combustion. The precombustion reaction appears to be not strong enough to be noticed in samples with fine iron particles. For diffusion to play a dominant role in precombustion, the surface contact between aluminum and iron particles should be very good. However, factors like segregation and sample porosity decrease the effective contact area between iron and aluminum. Both these factors increase as iron particle size decreases and could explain the absence of the precombustion stage in discs containing fine iron particles.

Onset temperatures for the combustion reaction for samples containing fine as well as coarse aluminum particles are reported in Table 3. At a given heating rate, it is seen that combustion has been initiated at relatively lower temperatures for samples with fine aluminum particles. This is perhaps due to a more uniform distribution of reactants (Fig. 9a) improving the chance for combustion at lower temperatures.

The data presented in Table 3 also indicate that irrespective of aluminum particle size, the combustion reaction is hindered when the heating rate is increased. This leads to higher onset temperatures which can be attributed to higher levels of porosity observed in these samples. The decrease in thermal conductivity due to increased porosity leads to heat transfer limitations in the sample. At high heating rates, the short time available is

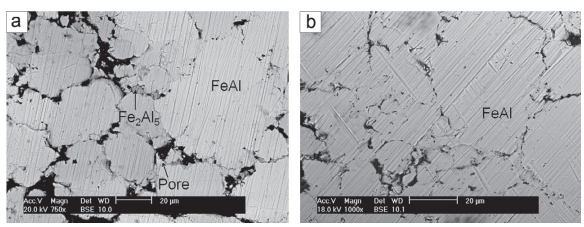

Fig. 7. SEM images of compacted samples (with coarse iron and fine aluminum particles) heated at 7.5 °C min^{-1} to (a) 1000 °C + cooled and (b) 1200 °C + 1 h + cooled.

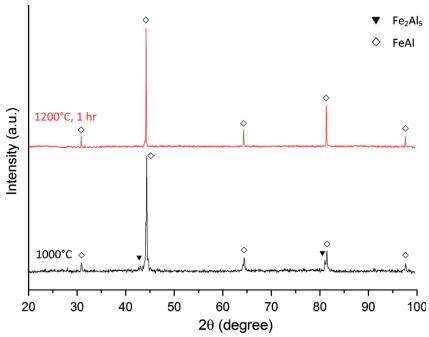

Fig. 8. Diffractogram of compacted samples (with coarse iron and fine aluminum particles) heated at 7.5 °C min^{-1} to 1000 °C and above.

insufficient for the sample to reach the combustion temperature which shifts to higher values. For samples containing relatively finer iron particles, the heat evolution rates associated with combustion peaks were calculated to be ~2 J/g s at a heating rate of 7.5 °C/min and ~3 J/g s at 15 °C/min. It may be noted that in samples containing fine iron particles, the precombustion stage is absent and results in higher heat evolution rates during combustion.

The heating of compacted discs with fine sized iron and aluminum particles was interrupted at different temperatures in order to understand how the phases evolved during heating. Micrographs of the heat treated discs are presented in Fig. 11. Fig. 11a shows the micrograph of a sample heated to 570 °C, which is lower than the onset temperature of the combustion peak, and

Table 3
Onset temperatures of the combustion peak for compacted discs containing fine iron powder.[a]

Al particle size	Heating rate (°C min^{-1})	Onset temperature (°C)
Fine[b]	7.5	573.5
	15	602.3
Coarse[c]	7.5	598.9
	15	605.7

[a] 7 μm (ave.).
[b] 15 μm (max).
[c] 60 μm (max).

then immediately cooled to room temperature. At this temperature, the sample surface is mainly covered by elemental particles. However, traces of Fe_2Al_5 compound were also detected using EDS analysis. This observation is interesting as it indicates the formation of Fe_2Al_5 compound prior to combustion, although a precombustion peak is not clearly seen in the DSC plots.

Fig. 11b presents the micrograph for a sample heated to 600 °C at which the combustion reaction has been completed. Residual iron particles constitute the major phase, together with some light and dark grey areas identified as FeAl and Fe_2Al_5 respectively. However, no residual elemental aluminum was detected. Aluminum seems to have been totally consumed during the formation of Fe_2Al_5. The small amounts of FeAl observed were probably the result of a reaction between Fe_2Al_5 and residual iron during the combustion reaction [3,20]. The heat treated sample also showed a volume expansion of 20.3%, indicating pore formation during combustion.

On heating the sample to 1000 °C, much beyond the combustion temperature, the diffusional reaction between iron and Fe_2Al_5 goes to completion resulting in a single phase product FeAl (Fig. 11c). The volume expansion for this sample is 24.7%, an increase of 4% during the diffusional reaction after combustion.

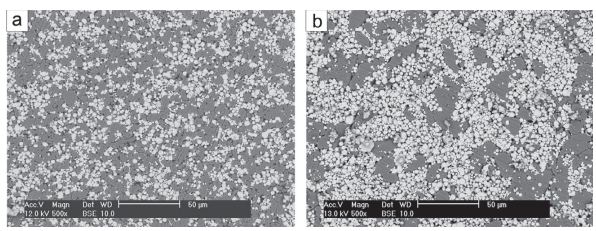

Fig. 9. SEM images of the unreacted compacted discs containing relatively fine iron particles mixed with relatively (a) fine and (b) coarse aluminum particles.

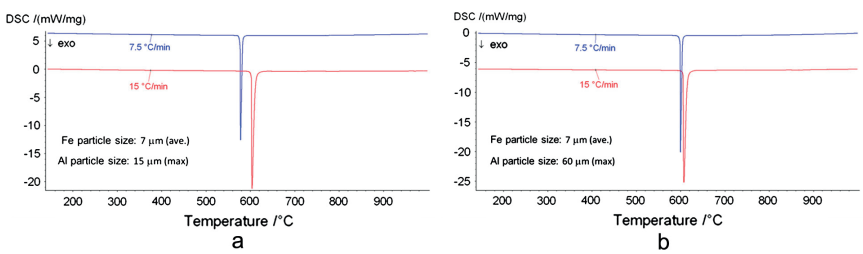

Fig. 10. Effect of heating rate and aluminum particle size on the onset of reaction in Fe–Al discs with relatively fine iron particles.

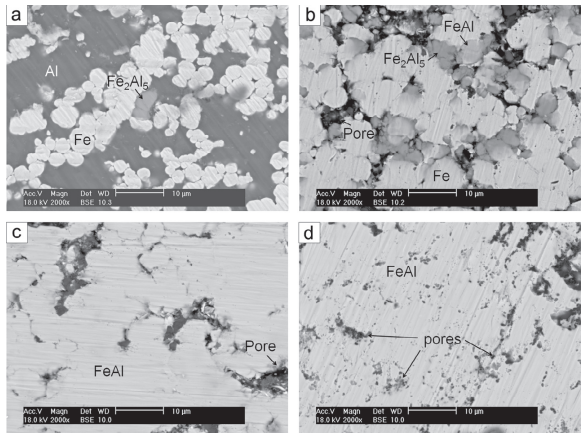

Fig. 11. Micrographs of compacted samples (with fine sized Fe and Al) heated at 7.5 °C min^{-1} to (a) 570 °C + cooled, (b) 600 °C + cooled, (c) 1000 °C + cooled, and (d) 1200 °C + 1 h + cooled.

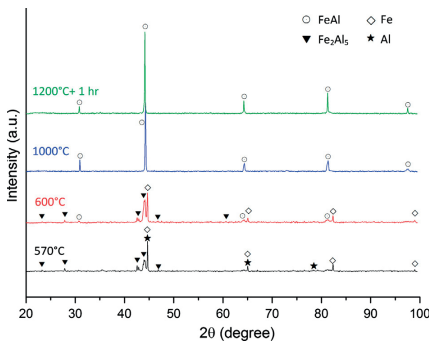

Fig. 12. Diffractogram of compacted samples (with fine iron and aluminum particles) after heating at 7.5 °C min^{-1} to different temperatures.

Fig. 11d shows the micrograph of a sample heated to 1200 °C for 1 h, before being cooled down to room temperature. FeAl is the only phase present and the sample shows a volume shrinkage after this heat treatment, indicating densification due to sintering.

X-ray diffraction data for the heat treated samples are presented in Fig. 12. For the sample heated to 570 °C, the diffraction peaks correspond mainly to the elemental components and some weak Fe_2Al_5 reflections which get stronger on heating to 600 °C, above the onset temperature for combustion. At this temperature, in addition to the residual iron peaks, weak reflections corresponding to the FeAl phase are also seen in the diffractogram. This result is in agreement with the microstructural studies reported in Fig. 11. The diffraction data in Fig. 12 also confirm FeAl as the stable phase in samples heated to 1000 °C and above.

3.3. Loose powder samples

Non-compacted, loose powder mixtures of Fe–40 at.% Al were also examined using the DSC. Regardless of the particle size combination and heating rate, the DSC plots showed a single, sharp exothermic peak, typically associated with combustion at high temperatures (see Table 4).

Table 4
Onset temperatures for combustion in loose powder mixtures.

Particle size combination	Onset temperature (°C) Heating rate	
	7.5 °C min^{-1}	15 °C min^{-1}
Fine Fe[a]–fine Al[b]	626.4	630.2
Fine Fe–coarse Al[c]	638.8	634.9
Coarse Fe[d]–fine Al	642.9	640.5
Coarse Fe–coarse Al	645.1	643.5

[a] 7 μm (ave.).
[b] 15 μm (max).
[c] 60 μm (max).
[d] 60 μm (max).

No sign of precombustion was evident during the heating of uncompacted samples, which is due to insufficient contact between the reactant particles. Further, it is seen that the onset temperature increases as we increase the particle size of the reactants. This is due to a lowering of interfacial coverage with increasing particle size. For most of the samples, increasing the heating rate has decreased the onset temperature of the reaction. Iron particle size and surface coverage are important factors in this connection. A similar effect was also observed for the compacted discs containing coarse iron particles. XRD analysis confirmed the formation of FeAl as the final product, without any residuals, after heating the loose powder mixture to 1000 °C.

4. Conclusions

In the present study, reactive synthesis of iron aluminide (FeAl) from Fe–40 at.% Al powder mixture has been investigated. DSC results confirmed the strong influence of particle size of the reactants on the combustion behavior of the mixtures. Compacted samples containing coarse iron particles revealed a precombustion reaction before the main combustion reaction. The precombustion peak in these samples exhibited larger exothermicity in the presence of relatively fine aluminum powder. This is due to better

surface contact between the reactants resulting from a more uniform distribution of iron and aluminum particles seen in the micrographs. A strong precombustion exotherm was followed by a relatively weaker combustion reaction. The precombustion stage is characterized by a diffusional reaction for which a higher onset temperature was observed at a higher heating rate. This precombustion reaction between iron and aluminum resulted in the formation of Fe_2Al_5 compound as a product, with considerable amounts of iron and aluminum remaining unreacted in the sample. After precombustion, further heating of the samples showed sharper exothermic peaks corresponding to the combustion reaction. At this stage, a significant growth of Fe_2Al_5 phase and residual iron were observed. The formation of Fe_2Al_5 was found to be associated with a volume expansion. Heating the sample to 1000 °C led to the formation of the stable FeAl compound through a diffusional reaction between Fe_2Al_5 and iron. A longer heat treatment at higher temperature (1200 °C, 1 h) resulted in a slight densification of the product due to sintering.

On heating compacted discs consisting of relatively finer iron powder, only a single and sharp exothermic peak corresponding to combustion was observed. A larger level of segregation as well as the porosity observed in these samples imply reduced interfacial contact and perhaps explain the absence of precombustion reaction. Onset temperatures for combustion in samples containing fine iron particles were found to be lower than those associated with coarser iron particles. After the combustion reaction, these samples contained residual iron particles together with Fe_2Al_5 and traces of FeAl. This result confirms the formation of Fe_2Al_5 compound as the major product of the combustion reaction. However, it also indicates that FeAl begins to form during the combustion reaction. This reaction reaches completion on heating to 1000 °C, resulting in the formation of a single phase FeAl product, which was found to be stable at higher temperatures.

DSC data for non-compacted samples revealed no evidence of precombustion due to insufficient contact between the reactant particles. Phase analysis data showed the formation of FeAl as the final product in the loose powder mixtures as well when heated to 1000 °C.

References

[1] G. Sauthoff, State of intermetallics development, Mater. Corros. Und Korros. 47 (1996) 589–594, http://dx.doi.org/10.1002/maco.19960471103.

[2] S.C. Deevi, V.K. Sikka, Nickel and iron aluminides: an overview on properties, processing, and applications, Intermetallics 4 (1996) 357–375, http://dx.doi.org/10.1016/0966-9795(95)00056-9.

[3] S. Gedevanishvili, S.C. Deevi, Processing of iron aluminides by pressureless sintering through Fe + Al elemental route, Mater. Sci. Eng., A 325 (2002) 163–176, http://dx.doi.org/10.1016/S0921-5093(01)01442-3.

[4] N.S. Stoloff, Iron aluminides: present status and future prospects, Mater. Sci. Eng., A 258 (1998) 1–14, http://dx.doi.org/10.1016/S0921-5093(98)00909-5.

[5] S.C. Deevi, V.K. Sikka, C.T. Liu, Processing, properties, and applications of nickel and iron aluminides, Prog. Mater Sci. 42 (1997) 177–192, http://dx.doi.org/10.1016/S0079-6425(97)00014-5.

[6] S.C. Deevi, R.W. Swindeman, Yielding, hardening and creep behavior of iron aluminides, Mater. Sci. Eng., A 258 (1998) 203–210, http://dx.doi.org/10.1016/S0921-5093(98)00935-6.

[7] C.T. Liu, E.P. George, P.J. Maziasz, J.H. Schneibel, Recent advances in B2 iron aluminide alloys: deformation, fracture and alloy design, Mater. Sci. Eng., A 258 (1998) 84–98, http://dx.doi.org/10.1016/S0921-5093(98)00921-6.

[8] M. Eggersmann, H. Mehrer, Diffusion in intermetallic phases of the Fe–Al system, Philos. Mag. A 80 (2000) 1219–1244, http://dx.doi.org/10.1080/01418610008212112.

[9] P.F. Tortorelli, J.H. DeVan, Behavior of iron aluminides in oxidizing and oxidizing/sulfidizing environments, Mater. Sci. Eng., A 153 (1992) 573–577, http://dx.doi.org/10.1016/B978-1-85166-822-9.50090-X.

[10] P.F. Tortorelli, K. Natesan, Critical factors affecting the high-temperature corrosion performance of iron aluminides, Mater. Sci. Eng., A 258 (1998) 115–125, http://dx.doi.org/10.1016/S0921-5093(98)00924-1.

[11] K. Natesan, Corrosion performance of iron aluminides in mixed-oxidant environments, Mater. Sci. Eng., A 258 (1998) 126–134, http://dx.doi.org/10.1016/S0921-5093(98)00925-3.

[12] J.L. Murray, Fe–Al binary phase diagram, in: H. Baker (Ed.), Alloy Phase Diagrams, ASM International, Materials Park, OH, USA, 1992, p. 54.

[13] S.C. Deevi, Powder processing of FeAl sheets by roll compaction, Intermetallics 8 (2000) 679–685, http://dx.doi.org/10.1016/S0966-9795(99)00129-6.

[14] A. Bahadur, B.R. Kumar, O.N. Mohanty, Ductility improvement in iron aluminides, J. Mater. Sci. 30 (1995) 3690–3696, http://dx.doi.org/10.1007/BF00351886.

[15] M.R. Hajaligol, S.C. Deevi, V.K. Sikka, C.R. Scorey, A thermomechanical process to make iron aluminide (FeAl) sheet, Mater. Sci. Eng., A 258 (1998) 249–257, http://dx.doi.org/10.1016/S0921-5093(98)00941-1.

[16] Z.A. Munir, U. Anselmi-Tamburini, Self-propagating exothermic reactions: the synthesis of high-temperature materials by combustion, Mater. Sci. Rep. 3 (1989) 277–365, http://dx.doi.org/10.1016/0920-2307(89)90001-7.

[17] P. Mossino, Some aspects in self-propagating high-temperature synthesis, Ceram. Int. 30 (2004) 311–332, http://dx.doi.org/10.1016/S0272-8842(03)00119-6.

[18] B.H. Rabin, R.N. Wright, Synthesis of iron aluminides from elemental powders: reaction mechanisms and densification behavior, Metall. Trans. A 22 (1991) 277–286, http://dx.doi.org/10.1007/BF02656797.

[19] E. Godlewska, S. Szczepanik, R. Mania, J. Krawiarz, S. Koziński, FeAl materials from intermetallic powders, Intermetallics 11 (2003) 307–312, http://dx.doi.org/10.1016/S0966-9795(02)00247-9.

[20] H. Gao, Y. He, P. Shen, J. Zou, N. Xu, Y. Jiang, et al., Porous FeAl intermetallics fabricated by elemental powder reactive synthesis, Intermetallics 17 (2009) 1041–1046, http://dx.doi.org/10.1016/j.intermet.2009.05.007.

[21] H.-Z. Kang, C.-T. Hu, Swelling behavior in reactive sintering of Fe–Al mixtures, Mater. Chem. Phys. 88 (2004) 264–272, http://dx.doi.org/10.1016/j.matchemphys.2004.03.001.

[22] E. Pocheć, S. Jóźwiak, K. Karczewski, Z. Bojar, Fe–Al phase formation around SHS reactions under isothermal conditions, J. Alloys Comp. 509 (2011) 1124–1128, http://dx.doi.org/10.1016/j.jallcom.2010.08.074.

[23] X. Wang, J.V. Wood, Y. Sui, H. Lu, Formation of intermetallic compound in iron–aluminum alloys, J. Shanghai Univ. English Ed. 2 (1998) 305–310, http://dx.doi.org/10.1007/s11741-998-0045-5.

[24] H.R. Shahverdi, M.R. Ghomashchi, S. Shabestari, J. Hejazi, Microstructural analysis of interfacial reaction between molten aluminium and solid iron, J. Mater. Process. Technol. 124 (2002) 345–352, http://dx.doi.org/10.1016/S0924-0136(02)00225-X.

[25] D. Naoi, M. Kajihara, Growth behavior of Fe_2Al_5 during reactive diffusion between Fe and Al at solid-state temperatures, Mater. Sci. Eng., A 459 (2007) 375–382, http://dx.doi.org/10.1016/j.msea.2007.01.099.

[26] R.M. German, Transient thermal effects in the synthesis of intermetallic alloys, in: R.D. Shull, A. Joshi (Eds.), Therm. Anal. Metall., The Minerals, Metals and Materials Society, 1992, pp. 205–231.

[27] K. Bouche, F. Barbier, A. Coulet, Intermetallic compound layer growth between solid iron and molten aluminium, Mater. Sci. Eng., A 249 (1998) 167–175, http://dx.doi.org/10.1016/S0921-5093(98)00573-5.

[28] M. Kajihara, Quantitative evaluation of interdiffusion in Fe_2Al_5 during reactive diffusion in the binary Fe–Al system, Mater. Trans. 47 (2006) 1480–1484, http://dx.doi.org/10.2320/matertrans.47.1480.

[29] K.A. Philpot, Z.A. Munir, J.B. Holt, An investigation of the synthesis of nickel aluminides through gasless combustion, J. Mater. Sci. 22 (1987) 159–169, http://dx.doi.org/10.1007/BF01160566.

[30] J.S. Sheasby, Powder metallurgy of iron–aluminum, Int. J. Powder Metall. Powder Technol. 15 (1979) 301–305.

[31] L.Z. Zhuang, L. Buekenhout, J. Duszczyk, Reaction phase-forming and mechanical properties of Fe_3Al produced from elemental powders, Scr. Metall. Mater. 30 (1994) 909–914, http://dx.doi.org/10.1016/0956-716X(94)90414-6.

[32] S. Ranganath, T.L. Prakash, J. Subrahmanyam, Synthesis of iron aluminide under thermal explosion conditions, Mater. Lett. 10 (1990) 215–217, http://dx.doi.org/10.1016/0167-577X(90)90091-Y.

[33] D.L. Joslin, D.S. Easton, C.T. Liu, S.a. David, Reaction synthesis of Fe–Al alloys, Mater. Sci. Eng., A 192–193 (1995) 544–548, http://dx.doi.org/10.1016/0921-5093(94)03272-6.

[34] E. Pocheć, S. Jóźwiak, K. Karczewski, Z. Bojar, Maps of Fe–Al phases formation kinetics parameters during isothermal sintering, Thermochim. Acta 545 (2012) 14–19, http://dx.doi.org/10.1016/j.tca.2012.06.015.

[35] S. Lee, J. Lee, Y. Lee, Effect of heating rate on the combustion synthesis of intermetallics, Mater. Sci. Eng., A 281 (2000) 275–285, http://dx.doi.org/10.1016/S0921-5093(99)00715-7.

[36] M. Salamon, H. Mehrer, Interdiffusion, Kirkendall effect, and Al self-diffusion in iron–aluminium alloys, Zeitschrift Für Met. 96 (2005) 4–16, http://dx.doi.org/10.3139/146.018071.

[37] E. Godlewska, K. Mars, K. Zawadzka, Alternative route for the preparation of $CoSb_3$ and Mg_2Si derivatives, J. Solid State Chem. 193 (2012) 109–113, http://dx.doi.org/10.1016/j.jssc.2012.03.070.

[38] C.B. Alcock, V.P. Itkin, M.K. Horrigan, Vapour pressure equations for the metallic elements, Can. Metall. Q. 23 (1984) 309.

Paper III

H. Sina, S. Iyengar

Studies on the formation of aluminides in heated Nb-Al powder mixtures

Journal of Alloys and Compounds, Vol.628, 2015, pp. 9-19
DOI: 10.1016/j.jallcom.2014.12.151

Journal of Alloys and Compounds 628 (2015) 9–19

Contents lists available at ScienceDirect

Journal of Alloys and Compounds

journal homepage: www.elsevier.com/locate/jalcom

Studies on the formation of aluminides in heated Nb–Al powder mixtures

H. Sina, S. Iyengar *

Materials Engineering, Lund University, 22100 Lund, Sweden

ARTICLE INFO

Article history:
Received 17 June 2014
Received in revised form 15 December 2014
Accepted 15 December 2014
Available online 31 December 2014

Keywords:
Niobium aluminides
Intermetallics
SHS
Onset temperature

ABSTRACT

The formation of aluminides during the heating of Nb–Al powder mixtures with different initial compositions (25, 33.3 and 75 at.% Al) has been studied using a differential scanning calorimeter. The effect of parameters like particle size, compaction and heating rate on the onset temperature of reaction has been determined. The results show that an increase in heating rate leads to an increase in onset temperature for compacted as well as loose powder samples in the particle size range considered. For Al-rich mixtures, compaction increases the onset temperature irrespective of particle size. For all samples, finer aluminum particles and slower heating rates resulted in a decrease in onset temperature while higher aluminum contents in the mixture led to a higher reaction temperature. In Nb-rich samples, compaction led to a decrease in the onset temperatures. $NbAl_3$ was the first compound to form in all the mixtures, irrespective of the initial composition. After heating to 1000 °C, EDS and XRD analyses confirmed the formation of only $NbAl_3$ in Al-rich samples and a mixture of $NbAl_3$ and Nb_2Al along with unreacted niobium particles in Nb-rich samples. A subsequent heat treatment was necessary to obtain a single aluminide corresponding to the initial composition. These observations can be explained on the basis of niobium dissolution in molten aluminum and subsequent precipitation of $NbAl_3$ in Al-rich samples and solid state diffusion through Nb_3Al and Nb_2Al phases in Nb-rich samples. For $NbAl_3$ formation through the reaction between aluminum melt and niobium particles, an enthalpy of -153 ± 15 kJ mol^{-1} and an activation energy of 255 ± 26 kJ mol^{-1} have been calculated from DSC data.

1. Introduction

Niobium is a refractory metal with a relatively low density (8.57 Mg m^{-3}) and good high temperature properties. However, its oxidation resistance is poor and can be improved by the addition of aluminum to form niobium aluminides [1,2]. These are intermetallic compounds with excellent properties at elevated temperatures and are suitable materials for turbine components in power plants, spacecrafts and other advanced applications [3–5]. Three intermetallic compounds, namely $NbAl_3$, Nb_2Al and Nb_3Al, are shown in the Nb–Al binary phase diagram, Fig. 1 [6].

$NbAl_3$ has a face centred tetragonal DO_{22} ordered structure with a narrow range of stability around the stoichiometric composition. It exhibits good oxidation resistance, low density (4.54 Mg m^{-3}), and melts congruently at 1680 °C. Nb_2Al and Nb_3Al are stable over a larger composition interval and decompose peritectically at 1940° and 2060 °C respectively [3,7]. Niobium-rich compounds in general, and Nb_3Al in particular, are refractory and superconducting materials which can be used for high-field and large-scale magnetic applications such as in nuclear fusion reactors or high-energy particle accelerators [8,9]. However, niobium aluminides are brittle and have low ductility at ambient temperatures. Improvements in ductility and fracture toughness are possible through alloying, grain refining, rapid solidification and the fabrication of composites [10–12].

Although synthesis of intermetallic compounds is possible through conventional methods such as melting and casting, the difficulties involved in handling high melting and reactive materials make it uneconomical. Alternatively, these compounds can be derived from the elemental powders through a simpler method known as reactive sintering, thermal explosion, combustion sintering or self-propagating high-temperature synthesis (SHS). In this method, a mixture of elemental powders is heated up to a temperature at which a reaction can be initiated in the sample.

This reaction can be self-sustaining if it exhibits adequate exothermicity and can proceed without any further external heating. SHS is an attractive method due to its simplicity and relatively lower demands on the cost, energy and time. Moreover, near-net shape products can also be fabricated using this method. In general, SHS products are characterized by significant levels of porosity,

* Corresponding author.

http://dx.doi.org/10.1016/j.jallcom.2014.12.151
0925-8388/

formed partly during the initial compaction of the powder mixture and mainly during the synthesis of the intermetallic compound.

Although porous structures are advantageous in specific applications such as filters, catalysts and biomedical implants, it is not a desired feature in many other applications. There are many ways of reducing porosity in the product, for example, using force-assisted heating during sintering. Further, a proper selection of processing parameters such as reactants particle size, green density and heating rate can considerably enhance the product density.

In general, the formation of a melt during the reactive sintering of a powder mixture improves the contact between the reactants due to wetting of the particle surface by the liquid phase, triggering the combustion reaction. However, this can be different in some systems like Nb–Al in which the reaction occurs considerably above the melt formation temperatures [3,13,14]. The reasons attributed to this delayed reaction include surface oxidation and poor wettability of niobium particles which hinder the initiation of reaction [13,14]. The wettability of niobium particles by the aluminum melt has also been reported to be a function of temperature [13]. Low solubility of niobium in liquid aluminum has also been suggested as the reason for relatively high ignition temperatures in Nb–Al mixtures [3].

In such a system, the interaction between solid particles and the liquid phase plays an important role and the particles should be well distributed in the melt for optimal effect. For example, the interconnection between the liquid-forming particles in the starting mixture affects material behavior, and the particle sizes of the reactants need to be chosen carefully in order to get sufficient interconnected melt during heating [15,16].

In general, it is believed that in the Nb–Al system, reaction proceeds through the initial dissolution of niobium in molten aluminum, which is followed by the subsequent precipitation of $NbAl_3$ phase on the surface of niobium particles [3,4,14]. Moreover, it has been observed that $NbAl_3$ compound is always the first phase to form through solid–solid as well as solid niobium-liquid aluminum reactions [14,17–20]. It has been suggested that the diffusion of aluminum atoms is the dominant mechanism in the aluminum–niobium reaction. The diffusion of niobium atoms is associated with a much higher activation energy and limits the formation of niobium rich compounds [21].

Neto and Ferreira [14] observed a multi-phase product ($NbAl_3 + Nb_2Al$) through reactive sintering of precompacted bars of Nb + 3Al powder mixture. They concluded that the presence of two phases in the product was due to the non-uniform distribution of molten aluminum in the sample. In addition, better conversion rates have been observed at higher heating rates [13]. Activating the powder particles has also been found to promote the combustion reaction. Ignition temperatures lower than the melting point of aluminum have been observed in powder mixtures which were initially ball-milled [17]. The particle size of niobium has a direct influence on the ignition temperature as well as the product crystallite size. Nanostructured $NbAl_3$ has been obtained by heating a heavily milled Nb + 3Al powder mixture [4].

Kachelmyer et al. [13] observed that gas adsorption during heating could affect the product density, and suggested the use of vacuum during synthesis in order to obtain higher densities.

The present study represents a continuation of the efforts to understand the key aspects of reactive sintering in the Nb–Al system. Powder mixtures of several compositions, both in the compacted and the loose condition, have been studied during a heating cycle in a differential scanning calorimeter. The effect of parameters such as aluminum particle size and the heating rate has been investigated. The products of the reaction have been characterized using scanning electron microscopy, energy dispersive spectroscopy and X-ray diffraction methods.

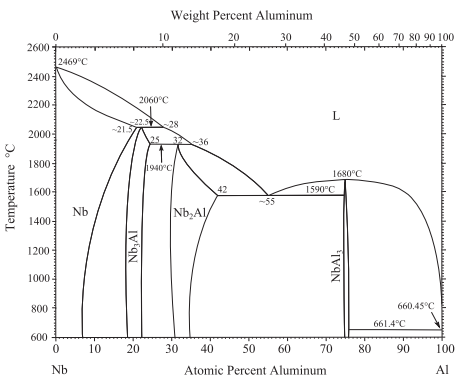

Fig. 1. Nb–Al binary phase diagram [6].

2. Material and methods

The metal powders used in the present study are shown in Table 1 and the corresponding SEM images are presented in Fig. 2. Two aluminum powders with relatively fine and coarse particles were chosen to study the effect of particle size in combination with a coarse particle size for niobium. It is seen from Fig. 2 that while the niobium powder consists of angular particles, the aluminum powders contain a mixture of ligamental and rounded particles. This indicates that aluminum and niobium powders have been produced through atomization and milling procedures, respectively. All the powders were characterized by a relatively broad particle size distribution.

The samples were prepared by mixing the elemental powders in different stoichiometric ratios (Nb + 3Al, 2Nb + Al, 3Nb + Al) corresponding to $NbAl_3$, Nb_2Al and Nb_3Al compounds, respectively. The samples were used as loose powders as well as compacted discs for which the powder mixture was cold-pressed to get a disc with 4 mm in diameter and approximately 1 mm in thickness. Green densities of the compacted samples were found to be 85–95% of the theoretical densities of the reactant mixtures.

A Netzsch Simultaneous TG–DSC unit (F3-Jupiter STA) with alumina crucibles was used to heat the samples. The DSC unit was calibrated for temperature (with an accuracy of ±0.1 °C) and heat sensitivity using standard pure metals. Baseline correction was done using data from heating cycles with empty crucibles. Before starting the experiment, the sample chamber was evacuated and flushed with dried argon gas 2–3 times in order to protect the samples against oxidation and a constant flow of argon was maintained during heating. The samples were heated at a constant rate (7.5°, 15 °C min^{-1}) up to 1000 °C. In a few cases, heating of the sample was interrupted in order to check the evolution of phases during the process. A few reacted samples were reheated to study the stability of the product. X-ray analysis of the product was carried out using a vertical Stoe machine equipped with a Germanium monochromator (Johan geometry), a copper tube and a linear PSD as the detector with transition setup. Metallographic examination of the products was carried out using an environmental scanning electron microscope (Philips XL-30 ESEM) equipped with an EDAX unit for EDS measurements. The EDS setup consisted of a liquid nitrogen cooled Si(Li) detector, with a super ultra-thin polymer window and a resolution of 127.4 eV (with reference to Mn K_α). While studying the microstructures of reacted samples in the SEM, the distribution of niobium and aluminum was first checked by X-ray mapping, followed by Line/Selected Area Scans and Spot Analyses for quantification using ZAF correction. Genesis software version 5.21 was used in these studies. Standardless calibration was used, although aluminum containing samples (like copper + aluminum) were used sporadically.

Table 1
Metal powders used in this study.

Powder[a]	Particle size (μm)	Particle shape	Purity (%)
Fine aluminum	<15	Ligamental	99
Coarse aluminum	<60	Ligamental	99.9
Coarse niobium	<74	Angular	99.85

[a] Supplied by Goodfellow Metals, UK.

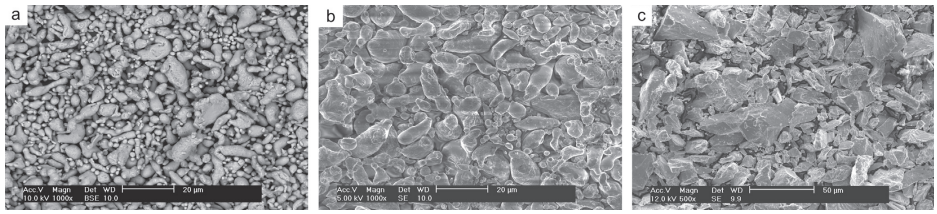

Fig. 2. SEM images of (a) fine aluminum, (b) coarse aluminum and (c) coarse niobium powders.

Signals from underlying areas were checked by reducing the acceleration voltage to minimize penetration. Similarly, the effect of changing spot size was also studied to minimize signals from adjacent areas.

3. Results and discussion

3.1. Nb + 3Al samples

Fig. 3 shows SEM images of the unpolished surfaces of untreated Nb + 3Al compacted discs with fine and coarse aluminum particles. In both samples, niobium particles are bright and exhibit a tendency to agglomerate. This effect is more pronounced in the sample containing coarse aluminum particles (Fig. 3b). The segregation of niobium particles is decreased by improving the interfacial contact between niobium and aluminum particles. This appears possible when smaller aluminum particles are used. Smudging of aluminum on the surface of niobium particles can also be seen in Fig. 3a and b, but the effect is more for the sample with fine aluminum particles.

Fig. 4 shows the DSC plots for Nb + 3Al loose powder mixtures and compacted discs with coarse and fine aluminum particles, heated to 1000 °C.

All the samples showed a similar trend during heating. An endothermic peak was observed around 660 °C which corresponds to the melting of aluminum, followed by a broad exothermic peak. This peak was observed to initiate at temperatures reported in Table 2 and indicates combustion in the sample.

At a given heating rate, samples with fine aluminum particles are associated with relatively lower onset temperatures compared to those with coarse aluminum particles. Increasing the heating rate resulted in a higher onset temperature for the reaction and lower ignition temperatures were observed for the loose powder mixtures relative to the compacted discs. Further, an exothermic peak was observed during cooling for the loose powder mixture with coarse aluminum particles (see Fig. 4a). This peak corresponds to the solidification of unreacted molten aluminum.

It is generally agreed that the combustion reaction is initiated through a dissolution-precipitation process [3,4,14]. However, the solubility of niobium in solid aluminum is practically zero and is very limited even in liquid aluminum. Yeremenko et al. [22] determined the solubility of niobium in liquid aluminum as ~0.02 wt.% at 700 °C, increasing to 0.1 wt.% at 850 °C. These data suggest that relatively higher temperatures may be required for the initiation of reaction in Nb–Al powder mixtures. Other factors which could contribute to higher onset temperatures for the reaction include difficulties in wetting the niobium particle surface by liquid aluminum and the presence of oxides on the particle surfaces. In the present study, onset temperatures in the Nb + 3Al mixtures were determined to be about 800° ± 20 °C (Table 2). In order to study the evolution of phases as a function of temperature, a few compacted samples (with fine aluminum particles) were heated to temperatures where the reaction initiates, but is not complete and the corresponding micrographs are presented in Fig. 5.

Fig. 5a shows the micrograph of a sample heated to 815 °C and cooled immediately to room temperature at 30 °C min^{-1}. The sample consists of aluminum (dark) and niobium (bright) regions together with another phase dispersed within the aluminum matrix, in particular, around the niobium particles. EDS analysis (Fig. 5) showed that the composition for this phase corresponded to about 75 at.% Al. From the Nb–Al phase diagram, it is seen that this phase is $NbAl_3$. The formation of $NbAl_3$ precipitates is in accordance with DSC results presented in Table 2. A volume expansion of about 2% was observed in this sample. It may be noted that the formation of dense $NbAl_3$ from elemental powders is associated with a shrinkage of ~5.6%.

The micrograph of a sample heated to 850 °C and cooled immediately to room temperature is shown in Fig. 5b. At this temperature, the aluminum and niobium regions are still present indicating incomplete reaction. But, the $NbAl_3$ phase has grown much more than at 800 °C. The volume expansion in the sample increased to 25%. Kachelmyer et al. [13] also report a low density product during the synthesis of $NbAl_3$. They observed that high

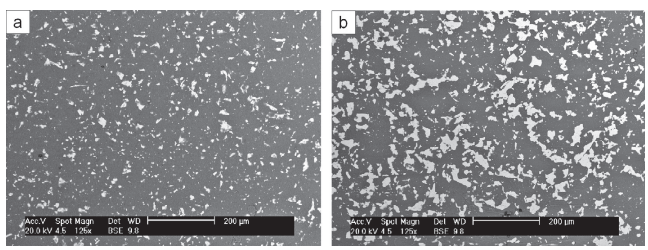

Fig. 3. SEM micrographs of unreacted Nb + 3Al compacted discs with (a) fine and (b) coarse aluminum particles.

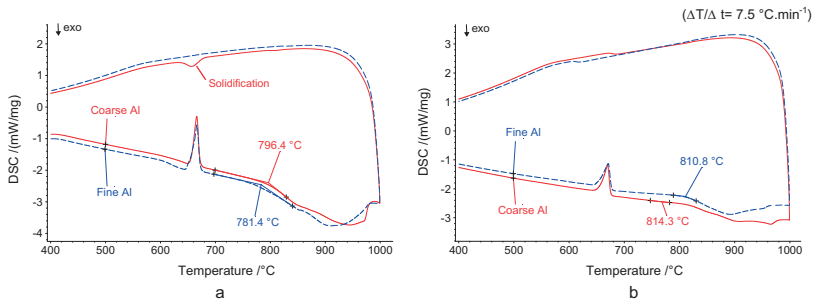

Fig. 4. DSC plots for Nb + 3Al samples (a) loose powder mix, (b) compacted discs.

Table 2
Onset temperatures of reaction for Nb + 3Al samples.

Sample condition	Heating rate (°C/min)	Onset temperature (°C) Al particle size	
		Fine	Coarse
Compacted disc	7.5	810.8	814.3
	15	815.7	820.9
Loose powder	7.5	781.4	796.4
	15	803.8	818.2

green densities led to low product densities after reaction. This effect was attributed to the expansion of adsorbed gases in the sample and synthesis in vacuum led to denser products.

Fig. 5c shows the micrograph of a sample heated to 850 °C and held at that temperature for 15 min. A significant progress in the formation of $NbAl_3$ is seen relative to Fig. 5b. At the same time, the sample showed a volume expansion of about 54%, attributed to the formation of a low density product. Fig. 5c shows the presence of some unreacted niobium in the sample which is bound to react during further heating. This was confirmed by heating the samples to higher temperatures and the corresponding micrographs are presented in Fig. 6.

Fig. 6a shows the secondary electron image of the non-polished surface of a Nb + 3Al sample heated to 1000 °C. It was observed that the sample had transformed uniformly to a single phase which was identified as $NbAl_3$ by EDS. A morphological change in the sample is also evident. After heating the sample to 1000 °C, a sponge-like structure consisting of a large number of agglomerated particles was obtained. The volume expansion in the sample dramatically increased to about 180%, due to the highly porous structure of the product. These observations indicate that the volume change in the sample is proportional to the extent of reaction, and the conversion to $NbAl_3$ being more complete at higher temperatures. In order to investigate the stability of the $NbAl_3$ phase produced at higher temperatures, the sample was reheated for

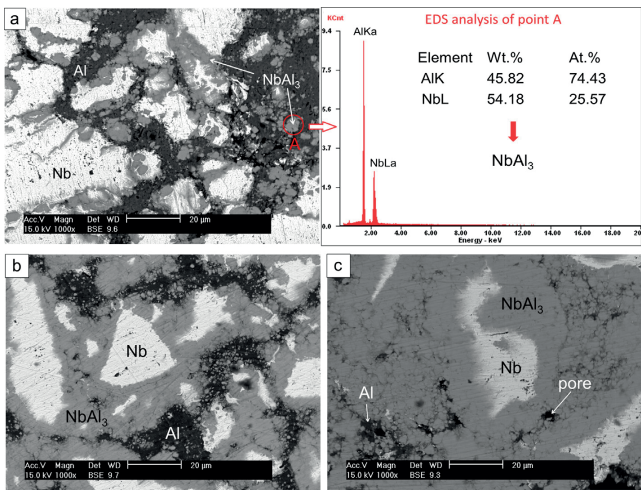

Fig. 5. SEM micrographs of Nb + 3Al samples (with fine Al particles) heated at 15 °C min^{-1} to (a) 815 °C + cooled, (b) 850 °C + cooled, (c) 850 °C + 15 min + cooled (30 °C min^{-1}).

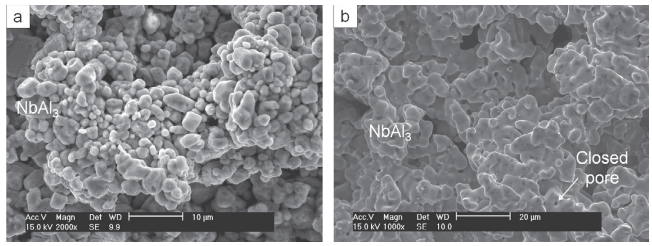

Fig. 6. SEM micrographs of Nb + 3Al samples (with fine Al particles) heated at 15 °C min^{-1} to (a) 1000 °C + cooled, (b) 1400 °C + 1 h + cooled (30 °C min^{-1}).

1 h at 1400 °C, and Fig. 6b shows the micrograph for the reheated sample.

EDS analysis and XRD data (Fig. 7) showed no phase transformation after this heat treatment. The sintering features in the sample after heating it to 1400 °C are clearly seen in Fig. 6b which shows the coalescence of particles and the formation of closed spherical pores indicating the final stage of sintering in the sample. This is followed by about 30% reduction in the sample volume which is due to the shrinkage during sintering. X-ray patterns obtained for samples heated to different temperatures (Fig. 7) also indicate the gradual progress of reaction between niobium and aluminum particles during heating which ultimately leads to the formation of single $NbAl_3$ phase in the sample, consistent with the micrographs obtained.

While this trend has been observed for niobium rich mixtures (Sections 3.2 and 3.3), compaction of an aluminum rich mixture leads to an increase in the onset temperature of reaction. This may be due to segregation tendencies enhanced by the plastic flow of aluminum during compaction.

It important to note that although the formation of $NbAl_3$ occurs above the melting point of aluminum, the ignition temperature is affected by the particle size of aluminum. As finer aluminum particles have a better interfacial contact with niobium particles (Fig. 3), a good distribution of elemental particles is obtained in the sample leading to an effective wetting of the niobium particle surface on the melting of aluminum. This leads to a reduction in the ignition temperature with fine aluminum particles.

In the loose powder mixture with coarse aluminum particles, the observation of an aluminum solidification peak during cooling (Fig. 4a) indicates the presence of some unreacted aluminum in the sample. This is due to insufficient contact between coarse aluminum and niobium particles present in the uncompacted powder mixture.

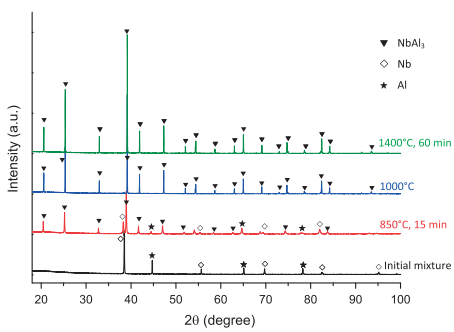

Fig. 7. Diffractograms of Nb + 3Al samples after heating to different temperatures.

As mentioned earlier, the onset temperature of reaction was observed to be lower for samples heated at 7.5 °C min^{-1} as compared to those heated at 15 °C min^{-1}. Broad reaction peaks, particularly for Al-rich mixtures, implies that the reaction takes place over a long period of time. In general, the effect of compaction is to lower the onset temperatures for reaction due to the improved contact between the reactant particles. While this trend has been observed for niobium rich mixtures, compaction of an aluminum rich mixture leads to an increase in the onset temperature of reaction. This may be due to segregation tendencies enhanced by the plastic flow of aluminum during compaction.

As $NbAl_3$ is obtained as a single phase product on heating Nb + 3Al samples, the heat of formation for this compound can be estimated using calorimetric data. The area between the combustion peak and the base line represents the exothermic heat of formation for the $NbAl_3$ compound. This value was measured as 153 ± 15 kJ mol^{-1} for the loose powder mixtures, which compares well with the value of 170 ± 30 kJ mol^{-1} reported by Coffey et al. [19] for $NbAl_3$ formation in thin film Nb–Al multilayers. However, a value of 63 ± 5 kJ mol^{-1} was obtained for compacted discs. The large deviation is perhaps due to the segregation observed after the compaction of aluminum-rich samples.

3.2. 2Nb + Al samples

Fig. 8 shows DSC plots for 2Nb + Al specimens which are similar to those for the Nb + 3Al samples. The plots basically consist of two peaks during heating, the endothermic aluminum melting peak which is followed by an exothermic combustion peak. However, the aluminum melting peaks seem to be less pronounced, and the reaction peaks are sharper and less diffuse as compared to those for the Nb + 3Al samples.

Microscopic observations confirm that the product contains considerable amount of unreacted niobium. Fig. 9 shows the micrographs for 2Nb + Al discs with fine aluminum particles, heated to temperatures corresponding to the initiation and propagation of combustion. The samples were then cooled at 30 °C min^{-1} and subjected to microscopic examination.

Fig. 9a shows the micrograph of a sample heated to 670 °C. At this temperature, the melting of aluminum is complete. However, the micrograph shows the elemental regions and EDS analysis revealed no sign of reaction. Heating the sample to 690 °C, which is lower than the combustion onset temperature, only some traces of $NbAl_3$ could be detected by EDS (Fig. 9b). However, the formation of $NbAl_3$ phase was clearly observed by increasing the temperature to 710 °C (Fig. 9c). This observation is in agreement with DSC results which show onset temperatures for the reaction close to

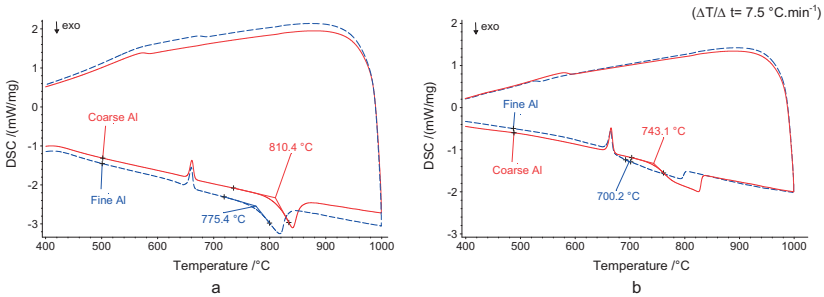

Fig. 8. DSC plots for 2Nb + Al samples (a) loose powder mix, (b) compacted discs.

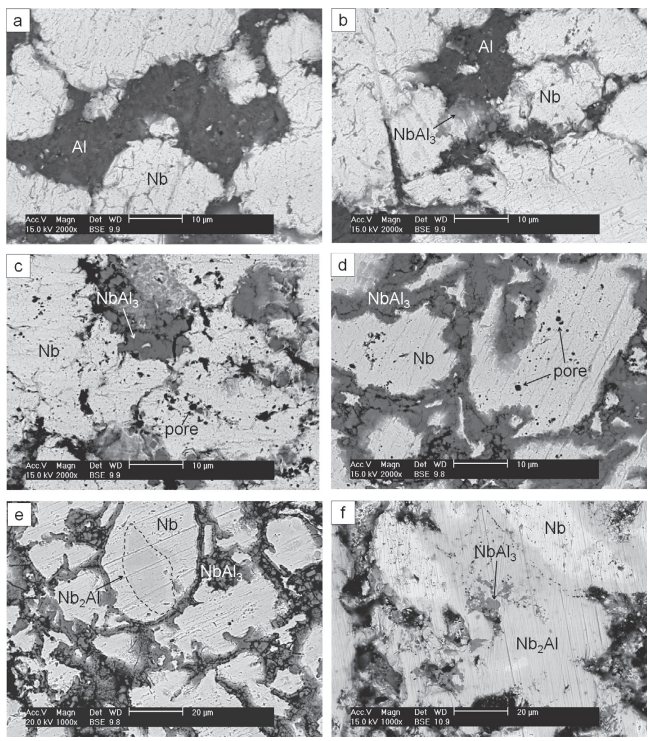

Fig. 9. SEM micrographs of 2Nb + Al samples (with fine Al particles) heated at 15 °C min^{-1} to (a) 670 °C + cooled, (b) 690 °C + cooled, (c) 710 °C + cooled, (d) 820 °C + cooled, (e) 1000 °C + cooled, (f) 1200 °C + 1 h + cooled (30 °C min^{-1}).

this value (Table 3). A considerable level of porosity can be seen within the sample, which showed ~3% increase in volume. In Section 3.1, this expansion was found to be associated with the formation of $NbAl_3$.

Fig. 9d shows that if the heating is continued to a temperature where the combustion peak ends (820 °C), a larger portion of the sample is covered by $NbAl_3$. However, niobium particles constitute the major phase in the sample. This indicates that the reaction

Table 3
Onset temperatures of reaction for 2Nb + Al samples.

Sample condition	Heating rate (°C/min)	Onset temperature (°C) Al particle size	
		Fine	Coarse
Compacted disc	7.5	700.2	743.1
	15	709.0	761.8
Loose powder	7.5	775.4	810.4
	15	800.0	833.8

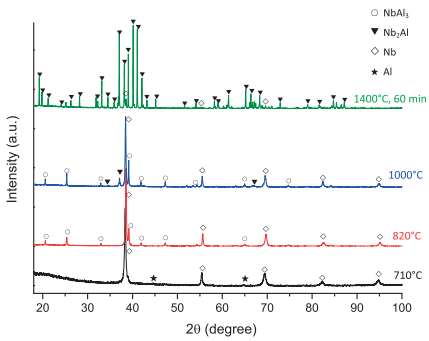

Fig. 10. Diffractogram of 2Nb + Al samples after heating to different temperatures.

between aluminum melt and niobium particles has been inhibited due to insufficient molten aluminum. At this stage, the sample showed about 14% expansion in volume. This is significantly smaller than the expansion for the Nb + 3Al disc which was cooled immediately after the combustion peak. In the present case, low expansion is due to formation of lesser amounts of the $NbAl_3$ phase through the liquid–solid reaction.

Fig. 9e shows the effect of heating the sample to 1000 °C. EDS analysis indicated that in addition to the $NbAl_3$ compound, Nb_2Al is also formed as a minor phase in some regions within the niobium particles. While the Nb_2Al layer is generally expected to be sandwiched between Nb and $NbAl_3$ regions, the present observation is unusual and may be due to the partial reaction of niobium near the interface with $NbAl_3$, assisted by easier diffusion paths and the availability of $NbAl_3$ beneath the surface. Previous studies [3,23] have also reported the presence of Nb_2Al and $NbAl_3$ compounds together with residual niobium in 2Nb + Al samples. In fact, in all the Nb–Al samples, regardless of the initial composition, the reaction initiates between the aluminum melt and niobium particles resulting in the formation of $NbAl_3$ compound which corresponds to the exothermic peak in the DSC plots. However, this reaction continues until the aluminum melt is consumed entirely. Therefore, if the sample is rich in niobium, this reaction stops earlier and further progress is possible through the reaction between $NbAl_3$ grains and niobium particles. This results in the formation of Nb_2Al phase in the sample.

In general, the progress of a solid–solid reaction is considerably slower compared to a solid–liquid reaction. Therefore, longer times and higher temperatures are required to obtain a high degree of conversion. This is shown in Fig. 9f which shows the micrograph of a 2Nb + Al sample reheated for 1 h at 1200 °C. Nb_2Al is the dominant phase after this treatment, although some unreacted niobium is present together with traces of $NbAl_3$ in the product. This result indicates that the initially formed $NbAl_3$ is an intermediate phase which transforms to Nb_2Al through solid state reaction with niobium at higher temperatures. This conclusion is confirmed by the XRD results shown in Fig. 10. If the sample is heated to 710 °C, which is close to the onset temperature of the exothermic peak in the DSC curve, the diffraction peaks mainly correspond to the elemental components. Heating the sample to the end temperature for the exothermic peak (820 °C) resulted in the formation of $NbAl_3$ phase as a product of combustion. While there is no reflection for aluminum, the presence of unreacted niobium is evident in the sample. For the sample heated to 1000 °C, the pattern shows some reflections from the Nb_2Al phase, although the presence of $NbAl_3$ and niobium is still significant. This is consistent with the micrographs presented. Finally, it is seen that if the sample is reheated for 1 h at 1400 °C, the product contains mainly Nb_2Al, while only a few small niobium peaks can be detected in the pattern. This indicates that after a heat treatment at a sufficiently high temperature, the sample transforms to Nb_2Al phase as the product of a reaction between $NbAl_3$ and niobium particles. This observation is in accordance with the Nb–Al phase diagram (Fig. 1).

Table 3 shows the onset temperatures of the combustion peaks for the 2Nb + Al samples. It is seen that using a lower heating rate and finer aluminum particles leads to a lower onset temperature. This result is consistent with that for Nb + 3Al samples. However, the effect of aluminum particles size is more significant and can be attributed to a better surface coverage of niobium particles by fine aluminum particles. This is shown in Fig. 11, where SEM images of the unpolished surfaces of untreated 2Nb + Al compacted discs with fine and coarse aluminum particles are presented. It is seen that, although there is a tendency for agglomeration in both samples, in particular for niobium particles, the surface contact between elemental particles is much better in the sample with fine aluminum particles. A more homogenous distribution of reactants is seen when fine aluminum particles get in between the coarser niobium particles and keep them separate.

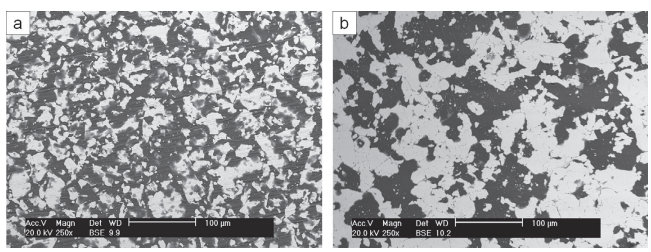

Fig. 11. SEM micrographs of unreacted 2Nb + Al compacted discs with (a) fine and (b) coarse aluminum particles.

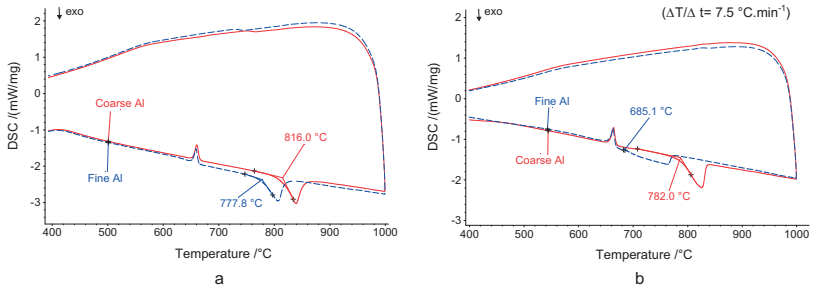

Fig. 12. DSC plots for 3Nb + Al samples (a) loose powder mix, (b) compacted discs.

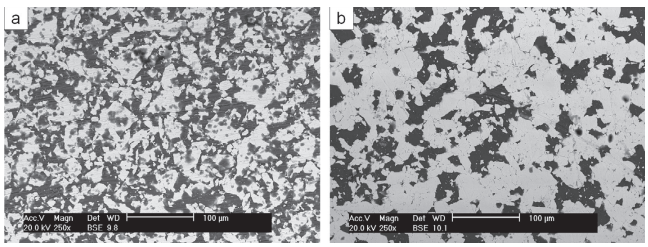

Fig. 13. SEM micrographs of unreacted 3Nb + Al compacted discs with (a) fine and (b) coarse aluminum particles.

This effect assumes more importance in samples with higher niobium content showing a larger segregation tendency and leads to a larger shift in onset temperatures for the combustion reaction in 2Nb + Al samples relative to Nb + 3Al samples.

The onset temperature was found to be lower for the 2Nb + Al discs relative to the loose powder mixtures due to better contact between the elemental particles in compacted samples. A comparison of the data in Tables 2 and 3 shows that, for 2Nb + Al compacted discs, the onset temperature for reaction decreases if the other parameters are kept constant. This result is in agreement with Kachelmyer et al. [13] who observed a lower ignition temperature for 2Nb + Al samples compared to Nb + 3Al ones. A higher concentration of niobium in the sample could trigger the combustion reaction at lower temperatures through a faster dissolution of niobium in molten aluminum which is followed by the formation of $NbAl_3$ precipitates. However, it is seen that, for loose powder mixtures with coarse aluminum particles, the onset temperature showed an increase with increasing niobium content. This indicates insufficient contact between the coarse reactant particles in the uncompacted sample. From EDS and XRD results, it is seen that, in addition to $NbAl_3$, there is a considerable amount of unreacted niobium after the combustion peak. Hence, it is difficult to estimate the heat of formation for $NbAl_3$ accurately from the area under the exothermic peak.

3.3. 3Nb + Al samples

The DSC plots for 3Nb + Al samples heated to 1000 °C are shown in Fig. 12. The graphs are similar to those observed for the other samples and consist of an endothermic melting peak for aluminum and an exothermic combustion peak. As these samples are rich in niobium and contain less aluminum, the melting peak is smaller as compared to the other two compositions. The combustion peak is sharper and narrower as molten aluminum gets consumed faster in its reaction with a larger amount of niobium particles (see Fig. 13).

Table 4
Onset temperatures of reaction for 3Nb + Al samples.

Sample condition	Heating rate (°C/min)	Onset temperature (°C) Al particle size	
		Fine	Coarse
Compacted disc	7.5	685.1	782.0
	15	701.8	804.6
Loose powder	7.5	777.8	816.0
	15	795.4	840.2

Similar to observations in the previous sections, slow heating rates and compaction lead to lower onset temperatures for reaction (Table 4). A comparison of data in Tables 2–4 shows that the onset temperatures for combustion are lower for the 3Nb + Al mixture than for Nb + 3Al and 2Nb + Al mixtures. The interaction between niobium particles in the aluminum melt increases with the niobium content in the mixture resulting in the initiation of combustion at a lower temperature. While this trend is observed for mixtures with fine aluminum particles, an increase in onset temperature is observed as the niobium content is increased in mixtures containing coarse aluminum particles. This is due to a reduction in contact between the reactant particles as the particle size for aluminum increases in samples which are rich in niobium. Agglomeration of reactants, especially niobium particles, is observed in these samples. As a result, the combustion reaction

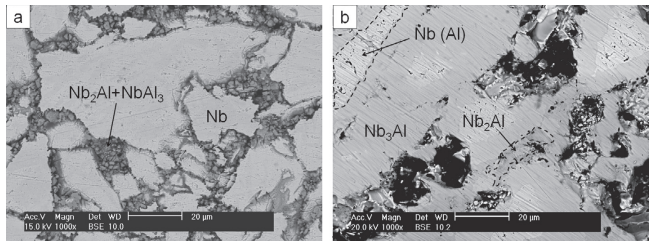

Fig. 14. SEM micrographs of 3Nb + Al samples (with fine Al particles) heated at 15 °C min^{-1} to (a) 1000 °C + cooled, (b) 1400 °C + 1 h + cooled (30 °C min^{-1}).

between aluminum melt and niobium particles initiates at relatively higher temperatures. This effect is more significant in loose powder mixtures due to poor interfacial contact between the reactant particles.

The SEM images of heated 3Nb + Al compacted discs are presented in Fig. 14. Incomplete reaction is observed after heating the sample to 1000 °C. The surface of the sample is covered mainly by unreacted niobium particles (Fig. 14a). EDS analysis of the dark regions between the niobium particles on the surface showed varying aluminum contents in the interval of 44–60 at.% which correspond to the dual phase region ($Nb_2Al + NbAl_3$) in the Nb–Al binary phase diagram (Fig. 1).

A similar observation was made in the case of the 2Nb + Al sample heated to 1000 °C. $NbAl_3$ is produced initially at low temperatures through the reaction between the aluminum melt and niobium particles and this is followed by the formation of Nb_2Al through a solid-state reaction between $NbAl_3$ and niobium particles as the temperature increases to 1000 °C. This conclusion is supported by X-ray diffraction data presented in Fig. 15.

The presence of $NbAl_3$ together with niobium was observed in the sample heated to 800 °C which corresponds to the end of the combustion peak. This again confirms that regardless of the powder mixture composition, the formation of $NbAl_3$ occurs first and the growth rate for this phase is the highest among all the niobium aluminides [23,24]. However, plenty of niobium may remain unreacted in the sample, especially in niobium rich powder mixtures. The sample heated to 800 °C also showed an expansion of ~6% in volume, which is smaller than those observed for $NbAl_3$ and Nb_2Al samples. This is due to the formation of a smaller amount of the $NbAl_3$ phase during combustion.

On further heating to 1000 °C, the presence of Nb_2Al phase is also observed in Fig. 15. This indicates that there is a limited reaction between the $NbAl_3$ and unreacted niobium particles react with each other to form the Nb_2Al compound.

In order to investigate the effect of further heating on product composition, a sample was reheated for 1 h at 1400 °C. Fig. 14b shows the observed micrograph for this sample. Nb_3Al was identified as the dominant phase in the sample through EDS analysis. However, the presence of regions corresponding to Nb(Al) solid solution (4–6% Al) and Nb_2Al were also observed, while no $NbAl_3$ was detected in this sample. This result is in agreement with XRD data showing the presence of Nb_3Al compound as the major phase in the product (Fig. 15).

Although Nb_2Al and unreacted niobium are still present in minor amounts, their reflections became significantly weaker after reheating the sample to 1400 °C. This implies that $NbAl_3$ and Nb_2Al are intermediate products and form during the initial stages of heating. Therefore, with proper heat treatment, transformation to the stable Nb_3Al phase can be achieved. Since this is a solid state transformation based on diffusion, complete conversion to Nb_3Al

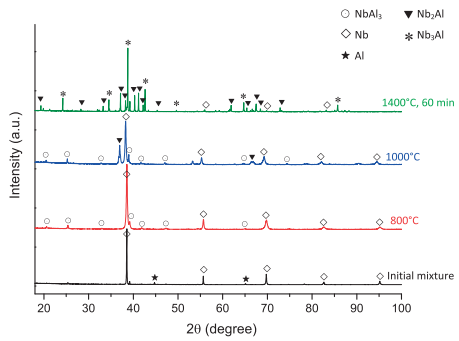

Fig. 15. Diffractogram of 3Nb + Al samples after heating to different temperatures.

takes place slowly. Use of finer reactant particles and mechanical activation of the powder mixture could lead to faster reaction rates [8].

Experimental data from this work have clearly shown that combustion in niobium-aluminum powder mixtures initiates with the formation of $NbAl_3$, irrespective of the aluminum content in the unreacted mixture. This opens up the possibility of estimating the temperature dependence of $NbAl_3$ formation from the non-isothermal data from DSC experiments. Such an approach has been used previously to determine activation energies associated with phase transformations [25,26] and other reactions [27,28].

Among the nonisothermal approaches for determining activation energies, isoconversion methods have been reported to be both accurate and reliable [29–31]. For experiments with linear heating rates, isoconversion analyses are based on the determination of temperatures (T_f) at which an equivalent degree of conversion is obtained for different heating rates. The transformation rate ($d\alpha/dt$) for a thermally activated reaction is generally expressed as the product of two functions [29–32]:

$$\frac{d\alpha}{dt} = f(\alpha) \cdot k(T) \tag{1}$$

where $f(\alpha)$ and $k(T)$ are solely dependent on temperature (T) and degree of conversion (α), respectively. Considering the temperature function, $k(T)$, to follow the Arrhenius equation for experiments with linear heating rate ($\beta = dT/dt$), Eq. (1) can be modified and integrated as:

$$\int_0^{\alpha} \frac{d\alpha}{f(\alpha)} = \frac{k_0}{\beta} \int_{T_i}^{T_f} \exp\left(-\frac{E_a}{RT}\right) dT \tag{2}$$

where T_i, k_0 and E_a are the initial temperature, pre-exponential factor and activation energy, respectively. Model-free isoconversion methods rely on approximating the temperature integral on the right hand side to determine the activation energy. It has been shown that these methods can provide consistent and reliable kinetic information for different processes [25–34]. The activation energy was calculated using the Starink expression [29,30] given below.

$$\ln\frac{\beta}{T_f^{1.92}} = -1.0008\frac{E_a}{RT_f} + Constant \quad (3)$$

where β is the linear heating rate (K min^{-1}), T_f the temperature corresponding to an equivalent degree of conversion (K), R is the universal gas constant (J mol^{-1} K^{-1}) and E_a is the activation energy (J mol^{-1}).

Combustion peaks obtained for different samples (compacted discs as well as loose powder mixtures with different compositions and particle sizes) were studied in order to determine the activation energy for the formation of $NbAl_3$ phase. The temperatures corresponding to a fixed degree of conversion ($\alpha = 0.5$) were determined from the peaks and a value of 255 ± 26 kJ mol^{-1} was calculated as the activation energy for $NbAl_3$ formation through the reaction between molten aluminum and niobium particles.

4. Conclusions

DSC studies on reactions occurring during the heating of Nb–Al powder mixtures have shown that combustion is initiated above the melting point of aluminum. Niobium particles react with molten aluminum and form $NbAl_3$ first, irrespective of the initial composition. In the case of Nb + 3Al samples, this reaction continues until the sample is completely transformed to $NbAl_3$ as a single-phase product. On the other hand, the reaction stops in niobium-rich mixtures as soon as the relatively limited amount of molten aluminum is consumed and a considerable amount of unreacted niobium is left within the sample. Heating the Nb-rich samples to 1000 °C leads to a partial transformation of the initially formed $NbAl_3$ phase, as it reacts with residual niobium particles through a solid-state reaction. This results in a mixture of $NbAl_3$ and Nb_2Al compounds as the product. It was found that reheating the sample for a longer time at higher temperatures, caused the product to transform to the stable phase corresponding to the initial composition in the mixture. Calorimetric results revealed that the onset temperature of combustion is lowered by a decrease in heating rate as well as finer aluminum particles. However, the influence of aluminum particle size is more pronounced for Nb-rich samples. For most of the samples, higher niobium contents and compaction also resulted in lower onset temperatures for the solid–liquid reaction. Based on data for all the samples, using Starink's isoconversion method, a value of 255 ± 26 kJ mol^{-1} was calculated as the activation energy for $NbAl_3$ compound formation. From the combustion peaks for Nb + 3Al loose powder mixtures, a value of −153 ± 15 kJ mol^{-1} was estimated for the enthalpy of formation of $NbAl_3$.

References

[1] H. Mitsui, H. Habazaki, K. Asami, K. Hashimoto, S. Mrowec, High temperature corrosion of sputter-deposited Al–Nb alloys, in: S. Somiya (Ed.), Adv. Mater. '93, Elsevier, 1994, pp. 243–246, http://dx.doi.org/10.1016/B978-0-444-81991-8.50066-2.

[2] M. Steinhorst, H. Grabke, Oxidation of niobium aluminide $NbAl_3$, Mater. Sci. Eng. A 120–121 (1989) 55–59, http://dx.doi.org/10.1016/0921-5093(89)90718-1.

[3] C. Milanese, F. Maglia, A. Tacca, U. Anselmi-Tamburini, C. Zanotti, P. Giuliani, Ignition and reaction mechanism of Co–Al and Nb–Al intermetallic compounds prepared by combustion synthesis, J. Alloys Comp. 421 (2006) 156–162, http://dx.doi.org/10.1016/j.jallcom.2005.08.091.

[4] V. Gauthier, F. Bernard, E. Gaffet, D. Vrel, M. Gailhanou, J.P. Larpin, Investigations of the formation mechanism of nanostructured $NbAl_3$ via MASHS reaction, Intermetallics 10 (2002) 377–389, http://dx.doi.org/10.1016/S0966-9795(02)00010-9.

[5] R.L. Fleischer, R.D. Field, K.K. Denike, R.J. Zabala, Mechanical properties of alloys of IrNb and other high-temperature intermetallic compounds, Metall. Trans. A 21 (1990) 3063–3074, http://dx.doi.org/10.1007/BF02647304.

[6] T.B. Massalski, H. Okamoto, P.R. Subramanian, L. Kacprzak (Eds.), Binary Alloy Phase Diagrams, ASM International, Materials Park, OH, USA, 1996.

[7] J.L. Jorda, R. Flükiger, J. Muller, A new metallurgical investigation of the niobium-aluminum system, J. Less Common Met. 75 (1980) 227–239, http://dx.doi.org/10.1016/0022-5088(80)90120-4.

[8] Z. Liu, Y. Chen, L. Du, P. Li, Y. Cui, X. Pan, et al., Preparation of Nb_3Al superconductor by powder metallurgy and effect of mechanical alloying on the phase formation, J. Mod. Transp. 22 (2014) 55–58, http://dx.doi.org/10.1007/s40534-014-0036-0.

[9] N. Koizumi, T. Takeuchi, K. Okuno, Development of advanced Nb_3Al superconductors for a fusion demo plant, Nucl. Fusion 45 (2005) 431–438, http://dx.doi.org/10.1088/0029-5515/45/6/004.

[10] T. Tabaru, S. Hanada, High temperature strength of Nb_3Al-base alloys, Intermetallics 6 (1998) 735–739, http://dx.doi.org/10.1016/S0966-9795(98)00052-1.

[11] L. Murugesh, K.T. Venkateswara Rao, R.O. Ritchie, Powder processing of ductile-phase-toughened Nb–Nb_3Al in situ composites, Mater. Sci. Eng. A 189 (1994) 201–208, http://dx.doi.org/10.1016/0921-5093(94)90416-2.

[12] L.M. Peng, Synthesis and mechanical properties of niobium aluminide-based composites, Mater. Sci. Eng. A 480 (2008) 232–236, http://dx.doi.org/10.1016/j.msea.2007.07.046.

[13] C.R. Kachelmyer, A.S. Rogachev, A. Varma, Mechanistic and processing studies in combustion synthesis of niobium aluminides, J. Mater. Res. 10 (1995) 2260–2270, http://dx.doi.org/10.1557/JMR.1995.2260.

[14] R.M.L. Neto, P.I. Ferreira, Progress of the $NbAl_3$ combustion synthesis reaction, J. Mater. Synth. Process. 7 (1999) 245–252, http://dx.doi.org/10.1023/A%3A1021853627411.

[15] R.M. German, P. Suri, S.J. Park, Review: liquid phase sintering, J. Mater. Sci. 44 (2009) 1–39, http://dx.doi.org/10.1007/s10853-008-3008-0.

[16] B. Rabin, R. Wright, Synthesis of iron aluminides from elemental powders: reaction mechanisms and densification behavior, Metall. Trans. A (1991).

[17] F. Buracovas, V.S. Gonçalves, C.J. Rocha, R.M.L. Neto, Combustion synthesis of mechanically-activated Nb–Al mixtures, Mater. Sci. Forum. 498–499 (2005) 152–157, http://dx.doi.org/10.4028/www.scientific.net/MSF.498-499.152.

[18] J. Maas, G. Bastin, L. VAN, The texture in diffusion-grown layers of trialuminides MeAl3 (Me = Ti, V, Ta, Nb, Zr, Hf) and VNi3, Z. Fuer Met. 74 (1983) 294–299.

[19] K.R. Coffey, K. Barmak, D.a. Rudman, S. Foner, Thin film reaction kinetics of niobium/aluminum multilayers, J. Appl. Phys. 72 (1992) 1341, http://dx.doi.org/10.1063/1.351744.

[20] V. Gauthier, F. Bernard, E. Gaffet, C. Josse, J.P. Larpin, In-situ time resolved X-ray diffraction study of the formation of the nanocrystalline $NbAl_3$ phase by mechanically activated self-propagating high-temperature synthesis reaction, Mater. Sci. Eng. A 272 (1999) 334–341, http://dx.doi.org/10.1016/S0921-5093(99)00488-8.

[21] T. Oğurtani, Kinetics of diffusion in the Nb–Al system, Metall. Trans. 3 (1972) 425–429, http://dx.doi.org/10.1007/BF02642046.

[22] V.N. Yeremenko, Y.V. Natanzon, V.I. Dybkov, Interaction of the refractory metals with liquid aluminum, J. Less Common Met. 50 (1976) 29–48, http://dx.doi.org/10.1016/0022-5088(76)90251-4.

[23] V. Maslov, I. Borovinskaya, M. Ziatdinov, Combustion of the systems niobium–aluminum and niobium–germanium, Combust. Explos. Shock Waves 15 (1979) 41–47.

[24] G. Slama, a. Vignes, Diffusion dans les aluminiures de niobium, J. Less Common Met. 29 (1972) 189–202, http://dx.doi.org/10.1016/0022-5088(72)90190-7.

[25] S.M. Ennaceur, Methodology for describing the $\alpha \rightarrow \beta$ phase transformation in plutonium, Thermochim. Acta 539 (2012) 84–91, http://dx.doi.org/10.1016/j.tca.2012.04.010.

[26] S.M. Ennaceur, Study of the $\gamma \rightarrow \delta$ phase transformation kinetics and reaction mechanism in plutonium, Thermochim. Acta 566 (2013) 181–185, http://dx.doi.org/10.1016/j.tca.2013.05.042.

[27] S. Vyazovkin, N. Sbirrazzuoli, Isoconversional kinetic analysis of thermally stimulated processes in polymers, Macromol. Rapid Commun. 27 (2006) 1515–1532, http://dx.doi.org/10.1002/marc.200600404.

[28] B. Janković, S. Mentus, M. Janković, A kinetic study of the thermal decomposition process of potassium metabisulfite: estimation of distributed reactivity model, J. Phys. Chem. Solids 69 (2008) 1923–1933, http://dx.doi.org/10.1016/j.jpcs.2008.01.013.

[29] M.J. Starink, Analysis of aluminum based alloys by calorimetry: quantitative analysis of reactions and reaction kinetics, Int. Mater. Rev. 49 (2004) 191–226, http://dx.doi.org/10.1179/095066004225010532.

[30] M.J. Starink, The determination of activation energy from linear heating rate experiments: a comparison of the accuracy of isoconversion methods, Thermochim. Acta 404 (2003) 163–176, http://dx.doi.org/10.1016/S0040-6031(03)00144-8.

[31] M.J. Starink, Activation energy determination for linear heating experiments: deviations due to neglecting the low temperature end of the temperature integral, J. Mater. Sci. 42 (2007) 483–489, http://dx.doi.org/10.1007/s10853-006-1067-7.

[32] J. Málek, The applicability of Johnson-Mehl-Avrami model in the thermal analysis of the crystallization kinetics of glasses, Thermochim. Acta 267 (1995) 61–73, http://dx.doi.org/10.1016/0040-6031(95)02466-2.
[33] A.A. Joraid, A.A. Abu-Sehly, S.N. Alamri, Isoconversional kinetic analysis of the crystallization phases of amorphous selenium thin films, Thin Solid Films 517 (2009) 6137–6141, http://dx.doi.org/10.1016/j.tsf.2009.05.034.
[34] H. Mostaan, F. Karimzadeh, M.H. Abbasi, Synthesis and formation mechanism of nanostructured $NbAl_3$ intermetallic during mechanical alloying and a kinetic study on its formation, Thermochim. Acta 529 (2012) 36–44, http://dx.doi.org/10.1016/j.tca.2011.11.017.

Paper IV

H. Sina, S. Iyengar, S. Lidin

Reaction behavior and evolution of phases during the sintering of Ta-Al powder mixtures

Journal of Alloys and Compounds, Vol.654, 2016, pp. 103-111
DOI:10.1016/j.jallcom.2015.09.100

Journal of Alloys and Compounds 654 (2016) 103–111

Contents lists available at ScienceDirect

Journal of Alloys and Compounds

journal homepage: http://www.elsevier.com/locate/jalcom

Reaction behavior and evolution of phases during the sintering of Ta–Al powder mixtures

Hossein Sina [a], Srinivasan Iyengar [a, *], Sven Lidin [b]

[a] Materials Engineering, Lund University, P.O. Box 118, 22100 Lund, Sweden
[b] CAS Chemical Centre, Lund University, P.O. Box 118, 22100 Lund, Sweden

ARTICLE INFO

Article history:
Received 14 July 2015
Received in revised form
7 September 2015
Accepted 12 September 2015
Available online 14 September 2015

Keywords:
Intermetallics
Powder metallurgy
Reaction synthesis
Microstructure
Thermal analysis

ABSTRACT

Intermetallic compounds based on tantalum aluminides are of considerable interest in various industrial applications. In this work, the formation of tantalum aluminides has been studied in elemental powder mixtures containing 25, 50 and 66.7 at% Ta. A differential scanning calorimeter (DSC) was used to heat the samples up to 1500 K at 15 K min^{-1}. Phase evolution was studied by heating a few samples to temperatures below and above the observed DSC peaks. The heat treated samples were analyzed using scanning electron microscopy, energy dispersive spectroscopy and X-ray diffraction. The results suggest an exothermic reaction between tantalum particles and molten aluminum, which leads to the formation of Al_3Ta compound as the initial product. This reaction reached completion for the aluminum-rich samples and the corresponding DSC peak was very broad, containing two distinct steps which indicated the effect of a diffusion barrier during the reaction. In these samples, the Al_3Ta product was stable upon further heating. A different behavior was observed for the equiatomic and tantalum-rich samples, an incomplete reaction with a considerable amount of unreacted tantalum. These samples were associated with a narrower reaction peak in the DSC plots, followed by a mildly exothermic peak at higher temperatures. The latter was found to correspond to the formation of $Al_{69}Ta_{39}$ phase in the solid state, together with minor amounts of σ (Ta-rich) and φ (near equiatomic) phases. The $Al_{69}Ta_{39}$ phase showed a tendency to disappear on prolonged heating. The σ and φ phases were observed to dominate as the major phases in tantalum-rich and equiatomic samples, respectively.

Increasing the heating rate shifted the reaction peak for Al_3Ta formation to higher temperatures and the apparent activation energies were estimated as 383 ± 13 kJ mol^{-1} and 439 ± 22 kJ mol^{-1} for the initial and final stages of this reaction. The heat of formation of Al_3Ta was also estimated as −36 ± 7 kJ mol^{-1} in the interval 1050–1350 K. Studies on the effect of particle sizes of the reactants showed that, in most cases, the reaction peak shifted to lower temperatures on decreasing the tantalum particle size. A similar behavior was observed for aluminum in the tantalum-rich samples, while an inverse effect was seen in equiatomic and aluminum-rich samples.

1. Introduction

Intermetallic compounds based on transition metal aluminides have been regarded as suitable candidates for advanced structural applications. These compounds exhibit an attractive combination of properties such as high melting points and enhanced resistance against corrosion and oxidation at elevated temperatures. This group of materials, including Al–Ta compounds, offers a variety of applications in different fields such as thin films and coatings [1,2], microelectronics, resistors and capacitors [3,4], diffusion barriers [5,6] and structural materials which can serve at high temperatures [7,8]. Amorphous Al–Ta alloys have been employed in applications requiring high thermal and chemical stability [1,4]. However, low ductilities of intermetallic compounds, particularly at ambient temperatures, may limit their use in some applications.

Despite extensive studies on the Al–Ta system [3,4,7–12], uncertainties are still associated with some phase relations and the binary phase diagram is not yet fully established. However, there is agreement in literature on the existence, stabilities and

* Corresponding author.
E-mail addresses: Hossein.Sina@material.lth.se (H. Sina), Srinivasan.Iyengar@material.lth.se (S. Iyengar), Sven.Lidin@chem.lu.se (S. Lidin).

http://dx.doi.org/10.1016/j.jallcom.2015.09.100
0925-8388/

compositions of several phases in the system. For example, it is generally agreed that the compound Al_3Ta, which has shown good potential for advanced applications at elevated temperatures [2,7,13], is an almost stoichiometric (24–25 at %Ta) phase [7,11,12] with a tetragonal $D0_{22}$ structure and melts incongruently at 1814 K [8]. This compound has been reported as the first phase to form in Al–Ta diffusion experiments [5,6].

In addition to Al_3Ta, a non-stoichiometric σ-phase has also been identified in the Al–Ta system [4,7,8,10–12]. According to a recent experimental and thermodynamic study performed by Witusiewicz et al. [8], the σ-phase has a homogeneity range of 65–81 at % Ta [12]. This phase has a topologically close packed structure with a tetragonal unit cell [8,10], and has been mainly designated as $AlTa_2$ [3,4,7,10,11]. However, deviations in the phase composition and the stability range for this phase have been reported in some studies [3,4,10].

As seen in the Al–Ta phase diagram (Fig. 1), the σ-phase is in equilibrium with phase φ which is stable around the equiatomic composition (52.2–57.3 at % Ta) [12]. In some references, the phase φ has been designated as AlTa [3,9,10]. However, this phase is assumed to be a line compound at lower temperatures [8]. It has been suggested that the phase φ has a complex monoclinic unit cell representing a topologically close-packed structure [10]. According to the Al–Ta phase diagram, the Ta-rich σ-phase decomposes to φ (equiatomic) and an intermediate phase which was initially reported as Al_3Ta_2 or Al_2Ta [3,8]. However, further studies by Mahne and Harbrecht [14] revealed that this intermediate phase corresponds to the $Al_{69}Ta_{39}$ compound exhibiting a face centered cubic structure with a giant unit cell. The eutectoid transformation at 1371 K [8] leads to the decomposition of $Al_{69}Ta_{39}$ phase into Al_3Ta and φ phases.

Several researchers [5,6] have studied the formation of aluminides through solid-state diffusional reactions in the Al–Ta system. In these experiments, the Al_3Ta compound was observed to form at temperatures below the melting point of aluminum. In the temperature range 723–848 K, Howard et al. [6] reported the growth of a Al_3Ta layer with an irregular interface. They suggested a non-parabolic growth rate for the Al_3Ta compound, which was thought to be due to the selective penetration of diffusing species through the grain boundaries where the lattice diffusion was negligible. This led to the conclusion that high melting compounds like Al_3Ta exhibit a lower lattice diffusivity compared to those with relatively lower melting points such as Al_7Cr that showed parabolic growth during annealing [6]. Chung et al. [1] studied the thermal stability of Al–Ta compounds and found that it is strongly related to the composition of the mixture and increased with tantalum content.

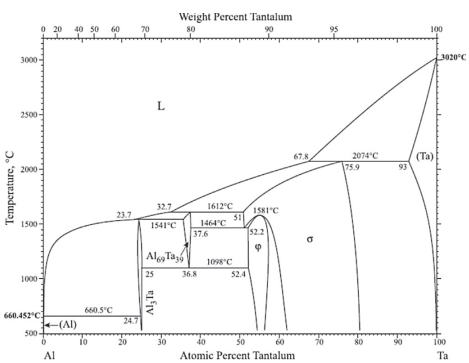

Fig. 1. Aluminum-tantalum phase diagram [12].

Intermetallic compounds can be produced using different techniques, but methods based on powder metallurgy are considered to be advantageous. Most powder metallurgical routes for synthesizing intermetallic compounds use pre-alloyed powders as starting materials. However, premixed elemental powders have been successfully used to produce high strength alloys and compounds [15,16]. Premixed powders are generally softer than pre-alloyed powders, resulting in higher compact densities and an increased die life. Reactive synthesis or combustion synthesis is a well-suited technique to produce intermetallic compounds from elemental powders. A reaction occurs between the reactant powders upon heating and such reactions are usually exothermic. A self-sustaining process is thus possible provided enough heat is generated during the reaction. This method is recognized as an efficient route through which a wide range of materials like intermetallic compounds, ceramics, functional materials and composites can be produced [17]. Compared to conventional production techniques such as melting and casting, reactive synthesis offers some advantages like simplicity, energy savings and higher productivity. Further, near-net-shape products can be fabricated through this method [6]. However, controlling the exothermic reactions and limiting porosity formation are critical in this process [18].

Tantalum aluminides have been synthesized using combustion synthesis. Yeh and Wang [19] produced tantalum aluminides through thermite-based reactions between tantalum oxide (Ta_2O_5) and aluminum powder mixtures. In their study, the effect of sample stoichiometry on the combustion behavior and the degree of phase conversion was investigated. Alumina-tantalum carbide composites have also been synthesized using a thermite-based combustion process [20].

Aydelotte et al. [21] performed a mechanistic study on impact-initiated reactions in explosively consolidated Ta + Al powder mixtures. Significant plastic deformation of both constituents was found to play a key role in decreasing the energy required for the initiation of reactions in Ta + Al samples, as compared to those observed in Ni + Al and W + Al systems.

A scan of literature shows a number of studies on the reactive synthesis of nickel, cobalt, titanium and iron aluminides [22–25], but the studies devoted to the Al–Ta system are very few. Although these studies focus on the production of tantalum aluminides, the reaction behavior and phase evolution during heating have not been investigated in detail. Information on the effect of processing parameters such as reactant particle size and heating rate on the reaction behavior in Ta–Al system is not available in literature. This has prompted the present study on the reactive synthesis of tantalum aluminides using elemental powder mixtures. In this work, binary tantalum-aluminum powder mixtures with selected Ta/Al ratios were chosen for study in a differential scanning calorimeter (DSC) in order to identify the reactions governing the process. It may be noted that calorimetric studies have been effectively employed in powder different metallurgical processes to optimize the sintering regime [26,27].

2. Materials and methods

Pure elemental powders of tantalum (<75 μm) and aluminum (<60 μm) were used as the starting materials to prepare the samples. The powders were thoroughly mixed to get three sets of specimens with nominal compositions of Ta+3Al, Ta + Al and 2Ta + Al, corresponding to the constituent phases in Al–Ta system. Compacted discs (4 mm in diameter and <1 mm in thickness) were

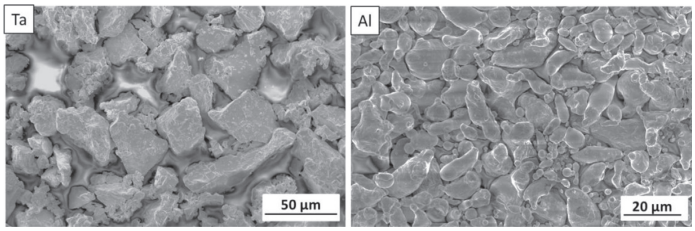

Fig. 2. SEM images of tantalum (<75 μm) and aluminum (<60 μm) powders.

prepared through uniaxial pressing of the powder mixtures. Fig. 2 shows the images of the elemental powders used in this study.

The samples were heated in a simultaneous TG-DSC unit supplied by Netzsch (STA 449-F3 Jupiter). The DSC unit was calibrated for temperature and heat sensitivity using pure metals as reference materials. Baseline correction was also done by carrying out measurements using empty alumina crucibles. To minimize the presence of air and avoid the oxidation of samples during heating, the DSC chamber was evacuated and flushed with pure argon gas at least three times prior to running the experiments and a constant flow of the gas (70 ml min^{-1}) was maintained during the measurements. The gas was dried by passing through towers containing drying agents like anhydrous calcium chloride and molecular sieve 4 Å, before entering the DSC chamber. After heating the samples to a maximum temperature of 1500 K at 15 K min^{-1}, DSC data were analyzed using Netzsch Proteus software (version 6.1). To study the phase evolution during heating, some samples were heated at temperatures below and above the observed peaks in the DSC plots. Further, the stability of the products was examined by prolonged heating at elevated temperatures. After cooling to room temperature, the samples were studied using a Philips XL-30 scanning electron microscope (SEM). Energy dispersive spectroscopy (EDS) was used to analyze the chemical composition of the phases present in the sample. For this purpose, a liquid nitrogen cooled Si(Li) detector (EDAX) was utilized. The detector had a super ultra-thin polymer window, providing a resolution of 127.4 eV (with reference to Mn-K_α). The distribution of various elements in the microstructure was checked using X-ray mapping and line scanning. Quantification analysis was made using the Genesis software (version 5.21), based on ZAF correction and standardless calibration. The results from EDS analysis were verified at different accelerating voltages and spot sizes to minimize the effect of signals from adjacent areas. In order to confirm the phases formed during the experiments, the heat treated samples were analyzed by X-ray diffraction (XRD), using a vertical Stoe Stadi MP diffractometer equipped with a copper radiation source, a Germanium monochromator (Johan geometry) and a linear PSD detector. XRD results were analyzed using Pearson's crystallography database [28].

The effect of processing parameters such as powder particle size and heating rate on the reaction behavior was also studied. Samples with different particle size combinations were prepared and heated in the DSC unit at several heating rates. The apparent activation energy of the initial reaction observed during heating has also been estimated from DSC data using the isoconversion method.

3. Results and discussion

3.1. Al-rich samples (Ta+3Al)

The DSC plot for the Ta+3Al sample heated to 1473 K at 15 K $min^{-1}$is shown in Fig. 3. An endothermic peak appears during the initial stages of heating, corresponding to the melting of aluminum. This peak is followed by a broad exothermic peak exhibiting two distinct steps representing the interaction between aluminum melt and tantalum particles. The reaction is triggered after wetting of the tantalum particles by molten aluminum. This behavior is comparable to that observed in the Nb–Al system [29], showing the occurrence of a broad exothermic DSC peak at temperatures relatively higher than the aluminum melting point. The broad peak observed is suggestive of diffusional effects governing the reaction. This is similar to the experimental data of Kofstad and Espevik [13], showing a diffusional reaction between aluminum vapor and tantalum. However, in the present case, the reaction peak exhibited an initial progress and then it showed a decrease in exothermicity for a short period after which the heat flow increased again. This behavior can be attributed to a diffusional barrier formed during the initial reaction which is surmounted with the help of extra thermal energy available at higher temperatures. For a closer study of the reaction behavior during heating, a few samples were heated in the DSC unit at 15 K min^{-1} to different temperatures below, within and above the observed exothermic peak region. After cooling to room temperature at 30 K min^{-1}, the samples were characterized using SEM, EDS and X-ray diffraction.

Fig. 4 shows the phase evolution in Ta+3Al specimens heated to different temperatures. The micrograph of the sample heated to 1100 K, which corresponds to the initiation of reaction, mainly consisted of aluminum regions surrounding the tantalum particles. A minor grey phase is also visible adjacent to the tantalum particles. Using EDS analysis, a chemical composition of 25 ± 1 at % Ta was determined for this phase, which corresponds to the Al_3Ta compound. This result confirms that the exothermic peak observed in the DSC plot represents a reaction initiated between tantalum particles and molten aluminum, and this resulted in the formation

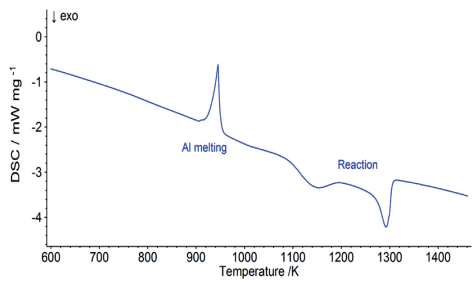

Fig. 3. DSC plot for Ta+3Al sample heated at 15 K min^{-1}.

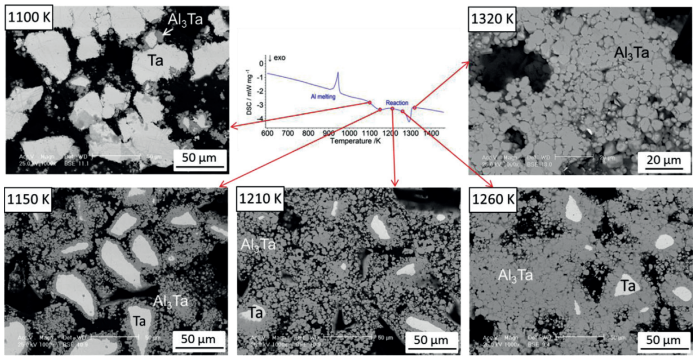

Fig. 4. Micrographs of Ta+3Al samples heated to different temperatures shown in the DSC plot.

of Al_3Ta intermetallic compound as the product. This observation is in agreement with thermodynamic data and also with previous studies indicating that Al_3Ta is the first compound to form in the Al–Ta system [5,6].

The Al_3Ta product was observed to grow with continued heating of the samples to 1150 and 1210 K. However, unreacted elemental regions were still present in the micrographs. At this stage, the Al_3Ta product has surrounded the unreacted tantalum cores and can act as a barrier against the diffusion of the reactant atoms, limiting the progress of reaction in the sample. This is seen in the DSC plot showing reduced exothermicity for the peak after the initial reaction. However, heating the sample further to higher temperatures led to an increase in reaction and heat evolution. At 1320 K, the completion of reaction in the sample is indicated by the complete coverage of the specimen surface by Al_3Ta.

In order to confirm the results obtained from EDS analysis, the heat treated samples were examined by X-ray diffraction and the resulting diffractograms are shown in Fig. 5. At 1100 K, the formation of Al_3Ta compound is quite evident. Heating the sample further to 1210 K resulted in relatively stronger peaks for Al_3Ta. This was accompanied by weaker reflections for tantalum, which were detectable up to 1260 K. After heating the sample to 1320 K which corresponds to the completion of the DSC reaction peak, XRD results confirmed the formation of a single phase product which was stable on further heating. The enthalpy of this reaction was estimated by the overall area of the corresponding peak in the DSC plot and a value of -36 ± 7 kJ mol^{-1} was obtained in the temperature interval 1050–1350 K. This result can be compared to a value of -30 kJ mol^{-1} reported by Witusiewics et al. [8].

3.2. Ta-rich samples (2Ta + Al)

The DSC plot obtained for a 2Ta + Al sample heated to 1473 K at 15 K min^{-1} is presented in Fig. 6. The peak corresponding to the melting of aluminum is observed first during heating, followed by the reaction peak. However, as the tantalum content increases in the given sample, a relatively sharper reaction peak is initiated at lower temperatures relative to that observed for the Ta+3Al specimen. This indicates that the reaction was triggered earlier between the aluminum melt and tantalum particles, which continued for a while due to lesser amount of aluminum available in the sample.

On further heating of the sample to higher temperatures, a weak and mildly exothermic peak is observed in the DSC curve, which may be due to a phase change in the sample associated with a small heat effect. In order to understand this behavior, a few 2Ta + Al samples were heated at 15 K min^{-1} to temperatures below, within and above the observed DSC peaks. Fig. 7 shows the backscattered

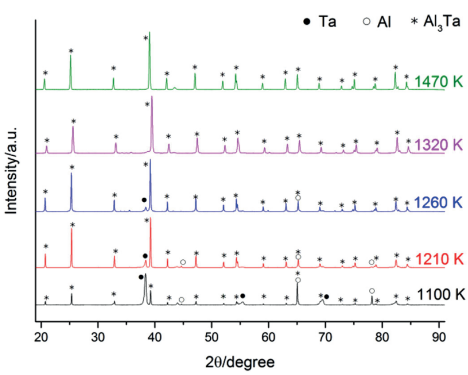

Fig. 5. Diffractograms of Ta+3Al samples heated to different temperatures.

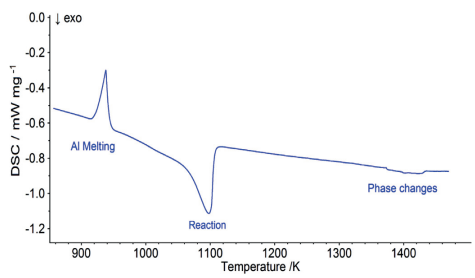

Fig. 6. DSC plot for 2Ta + Al sample heated at 15 K min^{-1}.

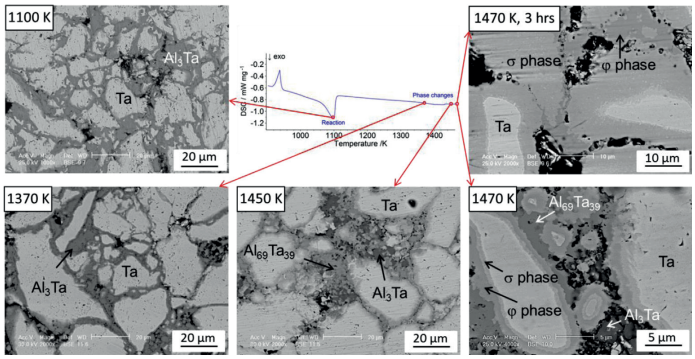

Fig. 7. Micrographs of 2Ta + Al samples heated to temperatures shown in the DSC plot.

electron images obtained for these samples. The micrograph of the sample heated to 1100 K corresponds to the peak temperature for the first reaction and is mainly covered by regions of unreacted tantalum. However, these regions are interconnected through thin layers of a minor phase which was identified as the Al_3Ta compound using EDS analysis. This result confirms the formation of Al_3Ta as the product of the reaction between aluminum melt and tantalum particles, as observed for the Al-rich samples. This reaction stops once the aluminum content in the sample is completely used up, leaving behind a lot of unreacted tantalum. Any further progress in reaction now depends on the solid state diffusional reaction between tantalum and Al_3Ta.

No changes were observed in the micrograph on heating the sample to 1370 K, which is close to the onset temperature for phase changes. However, a new phase was observed to form on heating the sample to the end temperature (1450 K) of the peak. EDS analysis of this phase showed a tantalum content of 36 ± 1 at%. According to the Al–Ta phase diagram (Fig. 1), this composition corresponds to the formation of $Al_{69}Ta_{39}$ phase (with 36.8 at % Ta) at 1371 K. This is an intermediate phase which is formed through a eutectoid reaction involving Al_3Ta and the near equiatomic phase φ. As equilibrium conditions are not completely applicable in the present study, experimental results may deviate from thermodynamic predictions.

The formation of $Al_{69}Ta_{39}$ is also seen in some areas between Al_3Ta and unreacted tantalum regions. This observation suggests that $Al_{69}Ta_{39}$ has been formed through a solid-state reaction between Al_3Ta phase and the unreacted tantalum particles, leading to a small heat evolution seen in the DSC plot. It is also interesting to note that after a slight increase in temperature from 1450 to 1470 K, significant changes were observed in the micrograph which was characterized by a multilayer product forming around the unreacted tantalum regions.

EDS analyses showed the tantalum contents of the inner and outer layers surrounding the tantalum cores were 66 ± 4 and 52 ± 2 at%, respectively. These compositions correspond to the tantalum-rich σ-phase and the near equiatomic phase φ in the phase diagram. At this stage, the two Al-rich phases $Al_{69}Ta_{39}$ and Al_3Ta were also detected in the micrograph, but were not dominant.

Prolonged heating for 3 h at 1470 K (Fig. 7) showed that the surface of the sample was mainly covered by the σ-phase which was dominant after the heat treatment. Keeping in mind the initial composition of the powder mixture (2Ta + Al), this observation is consistent with the phase diagram which shows a wide stability range for the σ-phase, including the stoichiometric $AlTa_2$ composition. However, some unreacted tantalum and φ-regions are still present in the micrograph, indicating the role of kinetic factors in the evolution of phases during heating. It may be noted that, since the interactions between the generated phases take place in the solid state, higher temperatures and longer annealing times may be needed to obtain the final single-phase product.

As described above, heating the tantalum-rich samples led to the formation of different relatively complex phases evolved at different temperatures. Therefore, it was important to reassess these results using X-ray diffraction. Fig. 8 shows the X-ray diffractograms of the samples heated to different temperatures. The samples heated to 1100 and 1370 K showed relatively similar and simple diffraction patterns. The presence of Al_3Ta and tantalum phases was also confirmed at these temperatures. A series of complex patterns were observed at higher temperatures and an effort was made to perform a reliable analysis of the X-ray diffraction patterns using Pearson's crystallography database [28]. However, getting ideally refined patterns presented difficulties due to the complexity of the crystal structures associated with some phases in the Al–Ta system and their composition ranges. Both

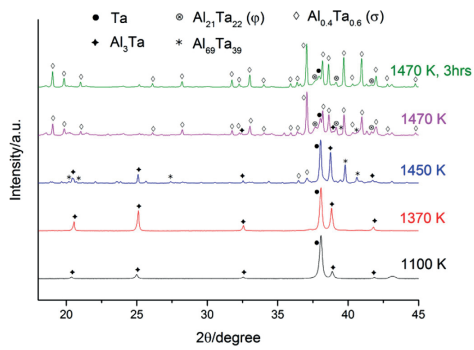

Fig. 8. Diffractograms of 2Ta + Al samples heated to various temperatures.

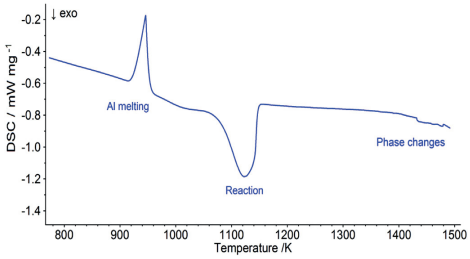

Fig. 9. DSC plot for Ta + Al sample heated at 15 K min^{-1}.

$Al_{69}Ta_{39}$ and the φ-phase show considerable phase width, and this is manifest in the crystal structures as changes in cell parameters and occupancy of mixed atomic sites. Given the non-equilibrium nature of the samples, with the complex phases present and in contact with both Ta and Al-rich phases precludes any attempts of quantitative assessment. Further, at 1450 K, it was seen that in addition to Al_3Ta and tantalum, there were strong reflections which corresponded to the $Al_{69}Ta_{39}$ phase. However, some minor reflections could also be found in the pattern, representing the $Al_{0.4}Ta_{0.6}$ compound with a tetragonal unit cell which is considered as σ-phase.

Diffractogram of the sample heated to 1470 K indicated a growth of the σ phase, while $Al_{69}Ta_{39}$ and Al_3Ta showed weaker reflections. At this stage, φ-phase with a near equiatomic composition ($Al_{21}Ta_{22}$) was also detected in the sample. After heating a sample at 1470 K for 3 h, σ-phase was identified as the major product. However, unreacted tantalum and $Al_{21}Ta_{22}$ compound were present as minor phases, consistent with previous results.

3.3. Equiatomic (Ta + Al) samples

Fig. 9 presents the DSC plot of a Ta + Al sample heated to 1500 K at 15 K min^{-1}. This sample exhibited relatively similar behavior compared to that in tantalum-rich samples, where the exothermic reaction was triggered at temperatures above the melting point of aluminum. However, the reaction peak in this case was observed to be wider, showing a longer period for reaction between tantalum particles and the aluminum melt. This is due to the relatively higher aluminum content in the initial composition of the present sample. On heating to higher temperatures, a small and diffuse exothermic peak was observed similar to that found for the tantalum-rich sample (Fig. 6). This behavior was also confirmed to be related to a phase change in the product.

Phase evolution in this group of samples was also checked during heating to temperatures below and above the observed DSC peaks. The backscattered electron images corresponding to these samples are shown in Fig. 10. Microscopic examination and EDS analyses of the sample heated to 1070 K (near the onset temperature for the initial reaction peak) confirmed the formation of Al_3Ta as the product of reaction between tantalum particles and the aluminum melt. The growth of the Al_3Ta phase which covers the unreacted tantalum particles is seen at 1140 K, which corresponds to the end temperature for the reaction peak. Heating further to 1270 K for an hour showed no appreciable change in the micrograph. However, heating to 1470 K led to the formation of different phases in the product. This temperature is within the range of the mildly exothermic peak and the observation confirms that the peak is associated with a reaction involving phase changes. As seen in the micrograph, Al_3Ta regions between unreacted tantalum particles seen at 1270 K are now replaced by another aluminum-rich phase which was identified by EDS as the $Al_{69}Ta_{39}$ compound with an average composition of 38 at% Ta. Further, a series of thin layers exhibiting different contrasts can also be observed in the peripheral regions of unreacted tantalum cores. EDS analyses revealed average compositions of 64 and 52 at% Ta for the inner and outer layers, which correspond to σ and φ-phases, respectively. This observation is comparable to that made for the tantalum-rich samples after undergoing transformation at temperatures above 1370 K, confirming a phase change in the product and in particular from Al_3Ta to $Al_{69}Ta_{39}$. This is also consistent with the phase diagram (Fig. 1) which shows that the $Al_{69}Ta_{39}$ phase is stable at temperatures above 1370 K. The multilayer pattern seen in these samples is indicative of aluminum diffusion from the aluminum-rich regions (initially Al_3Ta, and then $Al_{69}Ta_{39}$) towards the unreacted tantalum cores, which could lead to the formation of the Ta-rich and equiatomic phases, namely σ and φ around the unreacted tantalum core. These results also suggest that the

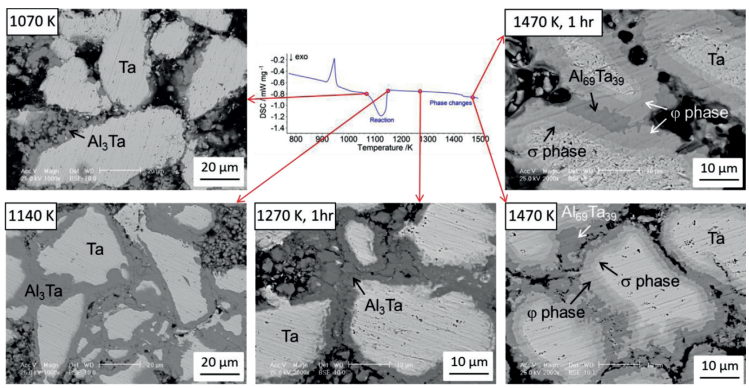

Fig. 10. Micrographs of Ta + Al samples heated to temperatures shown in the DSC plot.

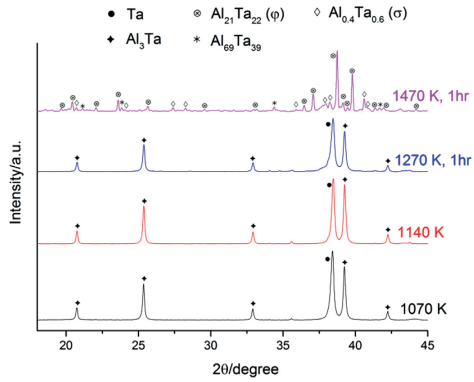

Fig. 11. Diffractograms of Ta + Al samples heated to various temperatures.

observed phase change is influenced more by the temperature to which the sample is heated than the duration of heating. The solid-state reaction can occur if the temperature is high enough for crossing the activation barrier. The φ-phase was found to grow considerably after prolonged heating at 1470 K (1 h) and the presence of σ and particularly $Al_{69}Ta_{39}$ phases had weakened. This indicates that φ is the more stable phase at this stage and is closer to the initial composition of the samples.

Fig. 11 presents the results of the phase analysis for the heated samples examined by XRD. In accordance with previous results, Al_3Ta was confirmed to form as the initial product of reaction between the aluminum melt and tantalum particles while a part of tantalum remained unreacted. XRD data also showed that Al_3Ta was stable up to temperatures above which a phase change reaction sets in. The φ-phase was dominant in the diffractogram corresponding to the sample heated to 1470 K for an hour, while σ and $Al_{69}Ta_{39}$ phases were minor components in the product.

3.4. Effect of processing parameters on reaction behavior

In order to study the parameters affecting the reaction behavior of samples with different initial compositions, powder particle size and the heating rate were chosen as the processing variables. Fine and coarse elemental powders were used to get different combinations of particle sizes in the samples.

From Table 1, it is seen that in most cases, a decrease in tantalum particle size in the sample resulted in relatively lower onset temperatures of reaction, regardless of the particle size of aluminum. This can be attributed to the relatively higher interfacial area between fine tantalum particles and molten aluminum, which can drive the reaction at relatively lower temperatures. On the other hand, an increase in heating rate generally leads to higher onset temperatures.

The effect of aluminum particle size was found to be different from that of tantalum. For aluminum-rich and equiatomic Ta–Al powder compacts, data in Table 1 show that a decrease in aluminum particle size is associated with an increase in the onset temperature of reaction. The compaction of samples containing coarse aluminum powder leads to plastic deformation and flow of aluminum which improves the Ta–Al interfacial contact. Finer aluminum particles imply a larger number of aluminum particles and more Al–Al contacts, requiring a higher temperature for establishing better Ta–Al contacts. In tantalum-rich compacts, finer aluminum particles lead to lower onset temperatures, regardless of tantalum particle size. This can be explained by the lesser amount of aluminum and more Ta–Al contacts in these samples. The upward shift of onset temperatures associated with fine aluminum particles may suggest the presence of more oxide on the particle surface. However, this may not be significant in this work, as a similar study on niobium-aluminum powder mixtures [29] showed lower onset temperatures for samples with fine aluminum particles.

The results obtained in this study show that the formation of Al_3Ta through the reaction between tantalum particles and aluminum melt, play a key role in the reactive sintering of Ta–Al powder mixtures. Therefore, the kinetics of this reaction under non-isothermal conditions has been studied. Since this reaction reached completion in aluminum-rich samples, the corresponding DSC data were evaluated at different heating rates for which the observed reaction peaks are shown in Fig. 12.

As seen in the figure, relatively sluggish and diffuse reaction peaks were observed at heating rates less than 15 K min^{-1}, higher heating rates resulted in more pronounced reaction peaks consisting of two distinct steps. Further, increasing the heating rate shifted the peak to higher temperatures, which is consistent with the general observation for thermally activated reactions. Higher heating rates are associated with larger heat transfer effects and thermal lag, and as a result, the reaction occurs at higher temperatures. The apparent activation energy of such reactions can be estimated using the model-free isoconversion methods by determining the temperatures at which a certain fraction of conversion is obtained at different heating rates. Among the isoconversion methods, the Starink equation has been reported to give relatively more accurate results [30,31] and is given below.

Table 1
Effect of particle size and heating rate on reaction temperatures in Ta–Al powder compacts.

Composition	Heating rate (K min^{-1})	Onset temperature (K)			
		Particle size combination			
		Ta (fine)[a] Al (fine)[b]	Ta (fine) Al (coarse)[c]	Ta (coarse)[d] Al (fine)	Ta (coarse) Al (coarse)
Ta+3Al	15	1138	1113	1132	1101
	7.5	1129	1091	1153	1098
Ta + Al	15	1113	1079	1119	1084
	7.5	1090	1053	1099	1093
2Ta + Al	15	1054	1071	1081	1086
	7.5	1034	1052	1083	1075

[a] 1–3 μm.
[b] <15 μm.
[c] 60 μm.
[d] <75 μm.

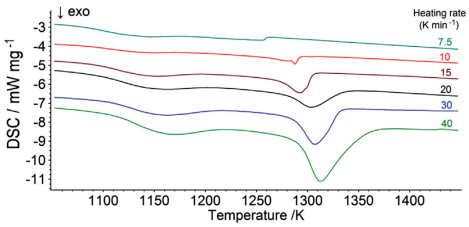

Fig. 12. DSC peaks observed during the reaction in Ta+3Al samples at different heating rates.

$$\ln\left(\beta/T_{\alpha}^{1.92}\right) = -1.0008 \times (E_a/RT_{\alpha}) + C \quad (1)$$

where β is the linear heating rate (K min^{-1}), T_{α} is the temperature corresponding to a given degree of conversion (K), R is the universal gas constant (J mol^{-1} K^{-1}), E_a is the activation energy (J mol^{-1}) for the reaction and C is a constant. In this approach, the partial area of the reaction peak in the DSC plot was considered to quantify the conversion fraction of the reaction at a given temperature. Based on this approximation, the temperatures corresponding to a series of conversion fractions from 5 to 95% were determined at different heating rates and the calculated results are plotted in Fig. 13.

This figure shows that, in most cases, the Arrhenius plots are fairly linear at various degrees of conversion. However, relatively large scatter was observed around 60% conversion where the reaction peaks exhibited reduced exothermicity in the DSC plots. Further, at 70% of conversion corresponding to the second part of the reaction peak, the slope of the line decreased initially, followed by an increase at higher conversions. These results imply that a higher energy is needed for the reaction to proceed after the initial progress observed in the DSC plots. Calculated values of activation energy vary from 383 ± 13 kJ mol^{-1} for the initial step to 439 ± 22 kJ mol^{-1} for the final stages of reaction. There is no activation energy data for the reaction to form Al_3Ta reported in literature. However, it is interesting to note that a similar activation energy has been reported in literature [32] for the self-diffusion of tantalum in the temperature interval 1523–2576 K. In the same study, the self-diffusion coefficient of tantalum was reported to be approximately 54% of the value for the self-diffusion of another transition element niobium over the same temperature range.

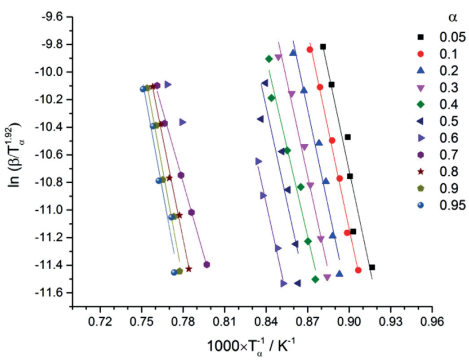

Fig. 13. Starink isoconversion plots for the determination of apparent activation energies at different degrees of conversion to Al_3Ta.

4. Conclusions

The formation of tantalum aluminides during the sintering of elemental powder mixtures with 25, 50, 66.7 at.% Ta has been investigated in this work. For all initial compositions, the results showed that a reaction was initiated between tantalum particles and molten aluminum leading to the formation of Al_3Ta phase as the product. This was observed as a broad exothermic peak in the DSC plot. The reaction was found to continue during heating, until the all the aluminum present in the mixture reacted fully with tantalum. As a result, a homogeneous and stable Al_3Ta product was formed in aluminum-rich samples, while a considerable amount of tantalum remained unreacted in equiatomic and tantalum-rich specimens. The reaction peak was relatively sharper in equiatomic and tantalum-rich samples compared to the aluminum-rich ones, which was followed by a mildly exothermic peak at higher temperatures. Phase evolution studies showed that the additional exotherm corresponded to the formation of $Al_{69}Ta_{39}$ together with minor amounts of φ (near equiatomic) and σ (Ta-rich) phases. $Al_{69}Ta_{39}$ was seen to disappear after prolonged heating, while φ and σ-phases were the major constituent products in equiatomic and tantalum-rich samples, respectively.

Powder particle size influenced the reaction behavior during heating. It was observed that by decreasing the tantalum particle size, the initial reaction between tantalum particles and aluminum melt initiated at relatively lower temperatures in the most of the samples. Aluminum particle size also showed a similar effect in tantalum-rich samples, but the behavior was different in equiatomic and aluminum-rich specimens. The data obtained for Al_3Ta formation at higher heating rates showed a shift to higher temperatures. Based on this observation, the apparent activation energy was calculated for the initial and final stages of this reaction as 383 ± 13 kJ mol^{-1} and 439 ± 22 kJ mol^{-1}, respectively. The heat of formation of Al_3Ta was also estimated as −36 ± 7 kJ mol^{-1}.

References

[1] C.K. Chung, Y.L. Chang, T.S. Chen, P.J. Su, Annealing effects on microstructure and properties of Ta–Al thin film resistors, Surf. Coatings Technol. 201 (2006) 4195–4200, http://dx.doi.org/10.1016/j.surfcoat.2006.08.059.
[2] I. Gurrappa, A. Wilson, P.K. Datta, Palladium and tantalum aluminide coatings for high-temperature oxidation resistance of titanium alloy IMI 834, J. Coatings Technol. Res. 6 (2009) 257–268, http://dx.doi.org/10.1007/s11998-008-9113-9.
[3] S. Mahne, F. Krumeich, B. Harbrecht, Phase relations in the Al-Ta system: on the translational symmetries of Al_3Ta_2 and AlTa, J. Alloys Compd. 201 (1993) 167–174, http://dx.doi.org/10.1016/0925-8388(93)90879-R.
[4] Y. Du, R. Schmid-Fetzer, Thermodynamic modeling of the Al-Ta system, J. Phase Equilibria 17 (1996) 311–324, http://dx.doi.org/10.1007/BF02665557.
[5] E.G. Colgan, J.W. Mayer, Thin-film reactions of Al with Co, Cr, Mo, Ta, Ti, and W, J. Mater Res. 4 (2011) 815–820, http://dx.doi.org/10.1557/JMR.1989.0815.
[6] J.K. Howard, R.F. Lever, P.J. Smith, Kinetics of compound formation in thin film couples of Al and transition metals, J. Vac. Sci. Technol. 13 (1976) 68, http://dx.doi.org/10.1116/1.568959.
[7] P.R. Subramanian, D.B. Miracle, S. Mazdiyasni, Phase relationships in the Al-Ta system, Metall. Trans. A 21 (1990) 539–545, http://dx.doi.org/10.1007/BF02671926.
[8] V.T. Witusiewicz, A.A. Bondar, U. Hecht, J. Zollinger, V.M. Petyukh, O.S. Fomichov, et al., Experimental study and thermodynamic re-assessment of the binary Al-Ta system, Intermetallics 18 (2010) 92–106, http://dx.doi.org/10.1016/j.intermet.2009.06.015.
[9] S. Mahne, B. Harbrecht, F. Krumeich, Phase relations in the Al-Ta system: on the translational symmetries of a triclinic structure and a new hexagonal giant cell structure, J. Alloys Compd. 218 (1995) 177–182, http://dx.doi.org/10.1016/0925-8388(94)01411-6.
[10] A. Boulineau, J.M. Joubert, R. Černý, Structural characterization of the Ta-rich part of the Ta–Al system, J. Solid State Chem. 179 (2006) 3385–3393, http://dx.doi.org/10.1016/j.jssc.2006.07.001.

[11] J.C. Schuster, Phases and Phase Relations in the System Ta-Al, Z. Fuer Met. Res. Adv. Tech. 76 (1985) 724–727.
[12] Okamoto H. Al-Ta, J. Phase Equilibria Diffus. 31 (2010) 1–2, http://dx.doi.org/10.1007/s11669-010-9786-5.
[13] P. Kofstad, S. Espevik, Oxidation of tantalum coated with aluminum and aluminum-chromium alloys, J. Less Common Met. 12 (1967) 117–138, http://dx.doi.org/10.1016/0022-5088(67)90095-1.
[14] S. Mahne, B. Harbrecht, $Al_{69}Ta_{39}$ - a new variant of a face-centred cubic giant cell structure, J. Alloys Compd. 203 (1994) 271–279, http://dx.doi.org/10.1016/0925-8388(94)90746-3.
[15] A. Gökçe, F. Findik, A.O. Kurt, Microstructural examination and properties of premixed Al-Cu-Mg powder metallurgy alloy, Mater Charact. 62 (2011) 730–735, http://dx.doi.org/10.1016/j.matchar.2011.04.021.
[16] A. Gökçe, F. Findik, A.O. Kurt, Effects of Mg content on aging behavior of Al4CuXMg PM alloy, Mater Des. 46 (2013) 524–531, http://dx.doi.org/10.1016/j.matdes.2012.10.045.
[17] J.J. Moore, H.J. Feng, Combustion synthesis of advanced materials: part I. Reaction parameters, Prog. Mater Sci. 39 (1995) 243–273.
[18] D. Dunand, Reactive Synthesis of Aluminide Intermetallics, Mater Manuf. Process 10 (1995) 373–403, http://dx.doi.org/10.1080/10426919508935033.
[19] C.L. Yeh, H.J. Wang, Formation of Ta–Al intermetallics by combustion synthesis involving Al-based thermite reactions, J. Alloys Compd. 491 (2010) 153–158, http://dx.doi.org/10.1016/j.jallcom.2009.10.203.
[20] C.L. Yeh, Y.S. Chen, Studies of Ta, Al, and Carbon Sources on Combustion Synthesis of Alumina–Tantalum Carbide Composites, Mater Manuf. Process 30 (2014) 298–302, http://dx.doi.org/10.1080/10426914.2013.852221.
[21] B.B. Aydelotte, N.N. Thadhani, Mechanistic aspects of impact initiated reactions in explosively consolidated metal+aluminum powder mixtures, Mater Sci. Eng. A 570 (2013) 164–171, http://dx.doi.org/10.1016/j.msea.2013.01.054.
[22] C. Zanotti, P. Giuliani, F. Maglia, Combustion synthesis of Co–Al and Ni–Al systems under reduced gravity, Intermetallics 14 (2006) 213–219, http://dx.doi.org/10.1016/j.intermet.2005.05.005.
[23] H. Sina, J. Corneliusson, K. Turba, S. Iyengar, A study on the formation of iron aluminide (FeAl) from elemental powders, J. Alloys Compd. 636 (2015) 261–269, http://dx.doi.org/10.1016/j.jallcom.2015.02.132.
[24] M. Adeli, S.H. Seyedein, M.R. Aboutalebi, M. Kobashi, N. Kanetake, A study on the combustion synthesis of titanium aluminide in the self-propagating mode, J. Alloys Compd. 497 (2010) 100–104, http://dx.doi.org/10.1016/j.jallcom.2010.03.050.
[25] H. Sina, S. Iyengar, Reactive synthesis and characterization of titanium aluminides produced from elemental powder mixtures, J. Therm. Anal. Calorim. (2015), http://dx.doi.org/10.1007/s10973-015-4815-6 in press.
[26] Ö. Özgün, H. Özkan Gülsoy, R. Yilmaz, F. Findik, Injection molding of nickel based 625 superalloy: sintering, heat treatment, microstructure and mechanical properties, J. Alloys Compd. 546 (2013) 192–207, http://dx.doi.org/10.1016/j.jallcom.2012.08.069.
[27] Ö. Özgün, H.O. Gulsoy, R. Yilmaz, F. Findik, Microstructural and mechanical characterization of injection molded 718 superalloy powders, J. Alloys Compd. 576 (2013) 140–153, http://dx.doi.org/10.1016/j.jallcom.2013.04.042.
[28] Villars P, Cenzual K. Pearson's Crystal Data: Crystal Structure Database for Inorganic Compounds, Release 2012/13, ASM International, Materials Park, Ohio, USA.
[29] H. Sina, S. Iyengar, Studies on the formation of aluminides in heated Nb–Al powder mixtures, J. Alloys Compd. 628 (2015) 9–19, http://dx.doi.org/10.1016/j.jallcom.2014.12.151.
[30] M.J. Starink, Analysis of aluminium based alloys by calorimetry: quantitative analysis of reactions and reaction kinetics, Int. Mater Rev. 49 (2004) 191–226, http://dx.doi.org/10.1179/095066004225010532.
[31] M.J. Starink, The determination of activation energy from linear heating rate experiments: a comparison of the accuracy of isoconversion methods, Thermochim. Acta 404 (2003) 163–176, http://dx.doi.org/10.1016/S0040-6031(03)00144-8.
[32] R.E. Pawel, T.S. Lundy, The diffusion of Nb95 and Ta182 in tantalum, J. Phys. Chem. Solids 26 (1965) 937–942, http://dx.doi.org/10.1016/0022-3697(65)90180-0.

Paper V

H. Sina, K. B. Surreddi, S. Iyengar
Phase evolution during the reactive sintering of Al-Ni-Ti powder compacts

Submitted to *Journal of Alloys and Compounds,* August 2015

Phase evolution during the reactive sintering of ternary Al-Ni-Ti powder compacts

Hossein Sina[1], Kumar Babu Surreddi[2], Srinivasan Iyengar*

Materials Engineering, Lund University, P.O. Box 118, 22100 Lund, Sweden

[1]hossein.sina@material.lth.se, [2]kumar_babu.surreddi@material.lth.se
*corresponding author: tel. +46 46 222 7984, e-mail: srinivasan.iyengar@material.lth.se

Abstract

The formation of various aluminides and intermetallic compounds in the Al-Ni-Ti ternary system offers great potential for a wide variety of applications. In the present work, reactions occurring during the heating of compacted ternary Al-Ni-Ti elemental powder mixtures were studied using differential scanning calorimetry (DSC). The effect of composition on the reaction behavior was studied by varying the aluminum addition (0 to 40 at.%) to nickel and titanium powders in equal proportions. The powder mixtures were compacted and heated in a DSC at 20°C min^{-1} up to 1200°C, using a continuous flow of pure and dry argon gas. The reaction behavior in binary Ni-Ti (1:1) powder compacts and Al-Ni-Ti samples containing 25 and 35 at.% aluminium, was studied in detail by interrupting the heating of samples at different stages of reaction. Phase evolution was followed by examining the sintered samples using X-ray diffraction technique, scanning electron microscopy and energy dispersive spectroscopy.

The DSC plots showed two main exothermic peaks corresponding to reactions taking place below and above the melting point of aluminum. For all the Al-Ni-Ti samples studied, the first exothermic peak was observed in the interval 595°-625°C, and the heat release increased with increase in the aluminum content of the samples. At 700°C, microstructural studies showed that Al_3Ni and Al_3Ni_2 were the major constituents and only a thin layer of Al_3Ti was observed around the titanium powder particles, indicating a diffusional barrier. The second exothermic peak was observed in the interval 938°-946°C which corresponds to the reaction between nickel and titanium. Titanium-rich and nickel-rich ternary compounds, in addition to some binary compounds have been observed after this reaction in all the ternary compositions studied. The formation of $AlNi_2Ti$ (τ_4) phase together with some new ternary compounds was observed in most of the Al-Ni-Ti samples heated to 1200°C. Among these, two phases correspond to compositions close to $Al_2Ni_3Ti_5$ and $Al_{36}Ni_{28}Ti_{36}$, whose structural characteristics and stabilities are yet to be confirmed in literature.

Keywords: Thermal analysis, reactive sintering, powder metallurgy, intermetallics, phase evolution, Al-Ni-Ti system.